

TR 2943 S

STELLINGEN

bij het proefschrift

The design of optimally functioning storm water settling tanks

Jeroen Kluck

Delft, 6 mei 1997

I

Het is van groot belang dat bergbezinkbassins op zodanige wijze worden vormgegeven dat een 2-dimensionale stroming door de tank kan worden verwacht. Hierbij is zowel de aanstroming als de doorstroming van belang.

II

In tegenstelling tot wat algemeen werd aangenomen, heeft de aanwezigheid van een neer in de langsdoorsnede van een bergbezinkbassin, in de meeste gevallen geen noemenswaardig effect op de bezinking.

III

Het bergen van water tijdens hevige neerslag en het behandelen daarvan in een afvalwaterzuiveringsinrichting, heeft niet altijd een positief effect op het milieu.

IV

Door lokale verschillen leidt het toepassen van landelijke normen voor het functioneren van rioolstelsels niet tot optimale investeringen.

V

Optimaal functionerende bergbezinkbassins kunnen pas worden ontworpen wanneer zowel berging als bezinking in beschouwing worden genomen.

VI

'n Dr in de riolering maakt de riolering beter.

VII

Wie structureel overwerkt doet zich slimmer voor dan hij is.

VIII

Doordat het personeelsbeleid in de gezondheidszorg zich meer richt op de kwaliteit dan de kwantiteit van het personeel, wordt de kwantiteit boven de kwaliteit van leven gesteld.

IX

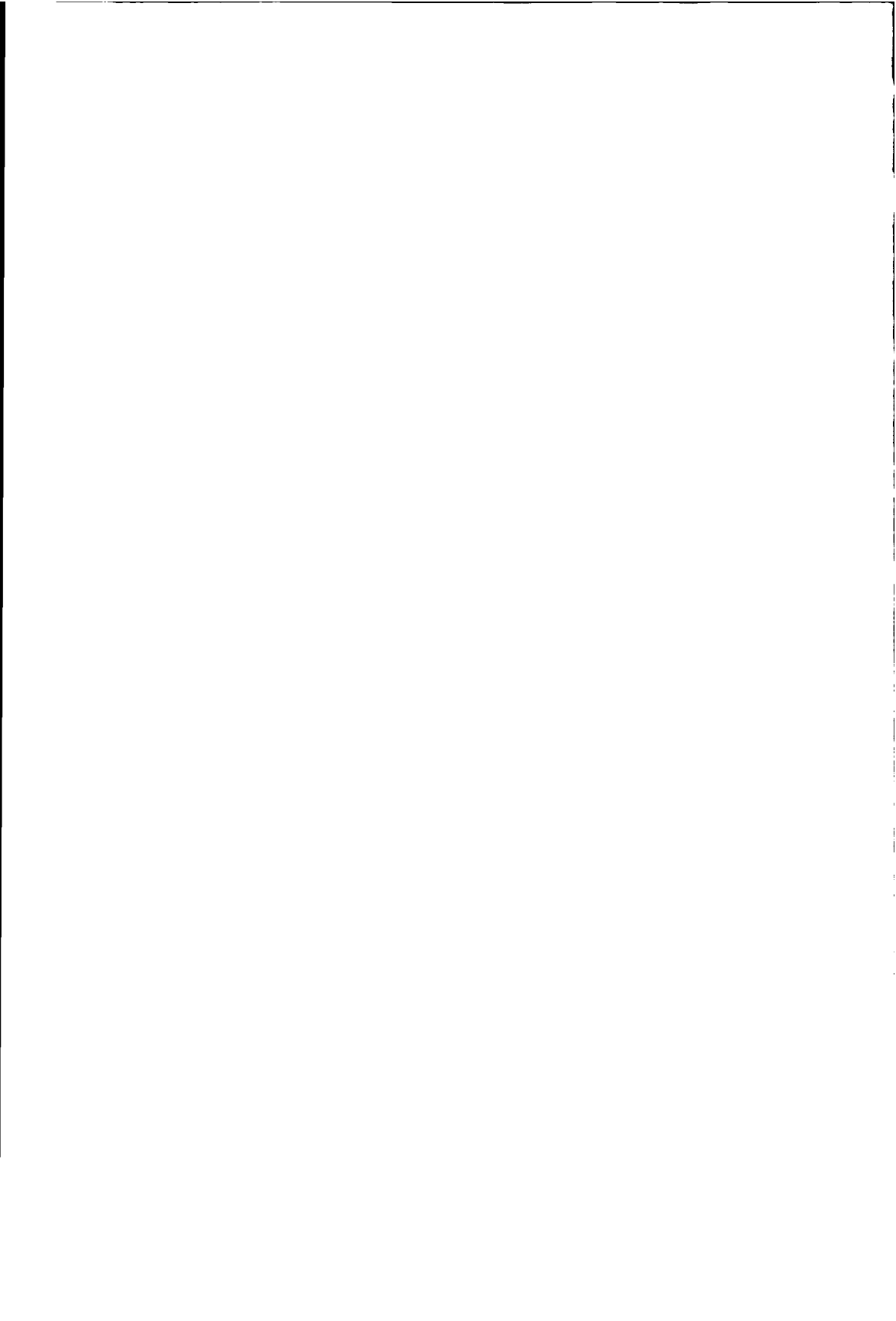
Overmatig muisgebruik leidt tot een kater.

X

Onder musici onderscheiden professionals zich van amateurs door niet terug te kijken. Dat geldt niet voor onderzoekers.

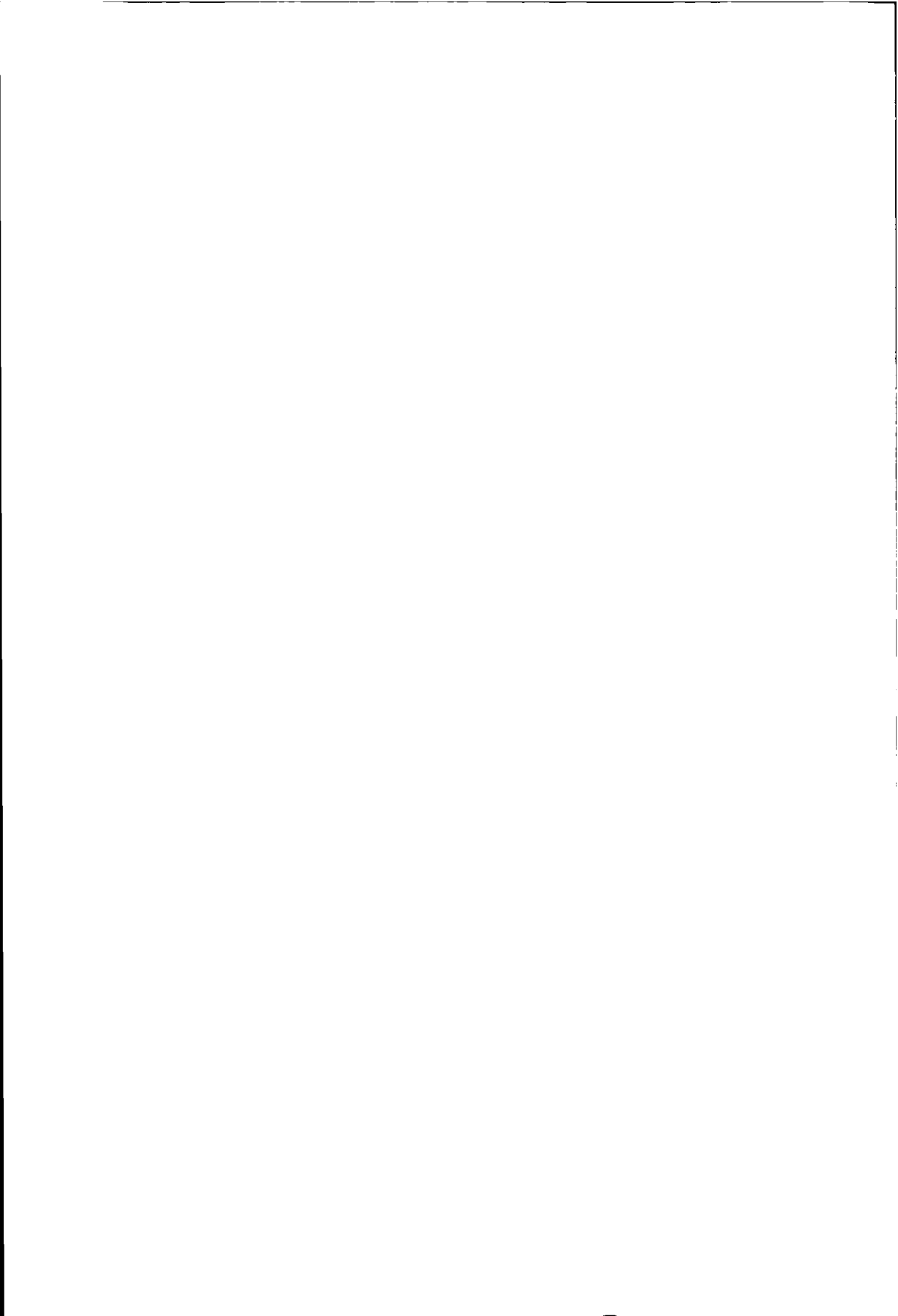
XI

Beter een goede amateur dan een slechte prof.



TR 2943

**The design of
optimally functioning
storm water settling tanks**

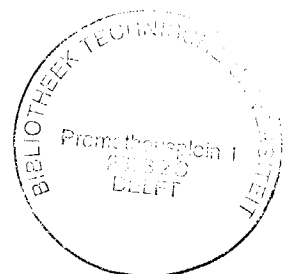


The design of optimally functioning storm water settling tanks

PROEFSCHRIFT

ter verkrijging van de graad van doctor
aan de Technische Universiteit Delft,
op gezag van de Rector Magnificus Prof.dr.ir. J. Blaauwendraad
in het openbaar te verdedigen ten overstaan van een commissie,
door het College van Dekanen aangewezen,
op dinsdag 6 mei 1997 te 16:00 uur

door Jeroen Kluck
geboren te Maastricht
civiel ingenieur



Dit proefschrift is goedgekeurd door de promotoren:

Prof. ir J.B.M. Wiggers

Prof. dr ir G.S. Stelling

Samenstelling-promotiecommissie:

Rector Magnificus, voorzitter

Prof. ir J.B.M. Wiggers,

Prof. dr ir G.S. Stelling,

Prof. dr ir J. Berlamont,

Prof. Dr.-Ing. W.F. Geiger,

Prof. Dr.-Ing. W. Rodi,

Prof. dr A.J. Saul,

Technische Universiteit Delft, promotor

Technische Universiteit Delft, promotor

Katholiek Universiteit Leuven

Universität Gesamthochschule Essen

Universität Karlsruhe

University of Sheffield

This research was partly funded by STOWA and Stichting RIONED

Published and distributed by:

Delft University Press

Mekelweg 4

2628 CD Delft

tel: (+31) 15 2783254

fax: (+31) 15 2781661

CIP-DATA KONINKLIJKE BIBLIOTHEEK, DEN HAAG

Kluck, J.

The design of optimally functioning storm water settling

tanks / Kluck J. - Delft : Delft University Press. Ill.

Thesis Delft University of Technology. - With ref. -

With summary in Dutch

ISBN 90-407-1452-5

Subject headings: Sewer systems, CSO, Settling tanks, Free surface flow, Flow simulations.

Copyright © 1997 by J. Kluck

All rights reserved.

No part of the material protected by this copyright may be reproduced or utilized in any form or by any means, electronic or mechanical, including photocopying, recording or by any information storage and retrieval system, without permission from the publisher: Delft University Press, Mekelweg 4, 2628 CD Delft, The Netherlands.

SAMENVATTING

Het ontwerp van optimaal functionerende bergbezinkbassins

Dit proefschrift beschrijft het gebruik van 2- en 3-dimensionale stromingssimulaties bij het ontwerpen van bergbezinkbassins. Dit zijn reservoirs die in gemengde rioolstelsels worden opgenomen om de vervuiling van het oppervlaktewater door overstortend rioolwater tijdens hevige neerslag te verminderen. Enerzijds verminderen deze reservoirs de hoeveelheid overstortend water door een gedeelte te bergen, anderzijds verminderen ze de concentratie aan vervuilende bestanddelen in het water doordat in de reservoirs bezinking optreedt. In Nederland wordt nu en in de toekomst een groot aantal van zulke reservoirs aangelegd. Het is echter niet zeker of de huidige Nederlandse ontwerpregels resulteren in tanks met een optimaal rendement door bezinking.

Door middel van simulaties van stroming en bezinking met bestaande stromingssimulatie-software is inzicht verkregen in de processen in de tanks. Teneinde het vullen van de bassins en de effecten van variaties in de invoer te kunnen simuleren, is een rekenmethode gebruikt waarmee de lokatie van het wateroppervlak wordt berekend. Voor het berekenen van het transport van bezinkbaar materiaal in combinatie met de berekening van het wateroppervlak is de oorspronkelijke software aangepast.

Omdat gegevens voor een goede validatie van de simulaties van het materiaaltransport ontbraken, is de opbouw van het model grondig getest en zijn veel gevoeligheidsanalyses uitgevoerd. De stromingssimulaties wezen uit dat het model geschikt is voor de evaluatie van verschillende tanks. Het gebruik van het model is echter te tijdrovend en ingewikkeld om te worden gebruikt voor het ontwerpen van elke tank. Daarom is voor de meest voorkomende gevallen (2-dimensionale stroming in rechthoekige tanks) een vergelijking afgeleid waarmee het rendement door bezinking in de evenwichtssituatie kan worden voorspeld. Hiermee kunnen op eenvoudige wijze verschillende ontwerpen worden geëvalueerd. Op basis van deze vergelijking is ten slotte een methode ontwikkeld waarmee het functioneren van een tank bij een belasting met een regenreeks van enige jaren kan worden beoordeeld, met inbegrip van het vullen en variaties in de belasting.

De stromingssimulaties lieten zien dat de bezinking binnen bepaalde grenzen ongevoelig is voor aanpassingen aan het ontwerp. De oppervlaktebelasting heeft de grootste invloed. Hoe lager deze is (dus hoe groter het oppervlak van de tank is), des te hoger is het rendement door bezinking. Daarnaast is de horizontale stroomsnelheid van belang. Wanneer deze groter wordt dan 0,15 m/s, neemt het rendement aanzienlijk af. Voor lagere snelheden is het rendement alleen een functie van de valsnelheid en de oppervlaktebelasting.

Het toevoegen van stroomgeleiders en diffusiewanden bleek slechts een beperkte invloed op het rendement te hebben. Wanneer grote 3-dimensionale structuren aanwezig zijn, is het rendement lager dan in 2-dimensionale stromingssituaties. Een diffusiewand kan helpen de stroming meer 2-dimensionaal te maken.

CONTENTS

Samenvatting

1 INTRODUCTION	1
1.1 Sewer systems in the Netherlands	2
1.2 Combined sewer overflows	3
1.3 Reduction of pollution at the overflow structures	5
1.3.1 Storage facilities	5
1.3.2 Separating facilities	5
1.3.3 Storage and separation facilities	6
1.4 Regulations	8
1.5 Design methods for storm water settling tanks	10
1.6 Conclusion	11
1.7 Setup of research	11
1.7.1 Approach	11
1.7.2 Objective	12
1.7.3 Modelling the processes	12
1.7.4 Lay-out of thesis	13
2 FLOW MODEL	15
2.1 Introduction	15
2.2 PHOENICS	16
2.3 Free surface method	18
2.3.1 Limitations	20
2.3.2 Courant number	21
2.3.3 Flow of air	21
2.4 Boundary conditions	22
2.4.1 Inflow	22
2.4.2 Wall friction: bottom and weirs	25
2.4.3 Damping of turbulence at the water surface	29
2.4.4 Outflow	30
2.4.5 Top boundary condition	32
3 CALIBRATION OF FLOW MODEL	33
3.1 Simulation results	34
3.2 Rigid lid	36
3.3 Grid dependence and numerical viscosity	37
3.4 Measurements in a scale model	41
3.4.1 Experimental setup	41
3.4.2 PHOENICS model of the experimental setup	43
3.4.3 Analysis of measurements and computations	44
3.4.4 3-dimensional effects	46

3.4.5 Conclusion of the flow modelling in the experimental setup	49
3.5 Flow over a backward facing step	49
3.5.1 Available measurements	49
3.5.2 The PHOENICS model	51
3.5.3 Discussion of the results of the computations	52
3.6 Conclusion of the modelling of the flow	55
4 QUANTITY AND COMPOSITION OF OVERFLOWING WATER	57
4.1 Flow	57
4.2 Pollutants in overflowing storm water	58
4.2.1 Measurements	58
4.2.2 Settling velocity	60
4.2.3 Relation between settling velocity and pollutants	62
4.2.4 Settling velocities in Dutch design	64
4.2.5 Simulation results	64
4.3 Conclusion	64
5 MODELLING THE SETTLING OF PARTICLES	65
5.1 Simplifications in the model	65
5.2 Particle transport equation	67
5.3 Discretisation	68
5.4 Free surface effects	70
5.4.1 Volume based concentration	70
5.4.2 Particles in the air	71
5.5 Implementing sedimentation in PHOENICS	72
5.6 Bottom boundary condition	72
6 SIMULATION OF FLOW AND SETTLING	75
6.1 Examples of flow and settling	75
6.1.1 Stationary flow situation	75
6.1.2 Filling of a tank	76
6.2 Validation on measurements	79
6.2.1 Storm water settling tank at Amersfoort	80
6.2.2 Needed future measurements	81
6.3 Sensitivity analysis	81
6.3.1 Numerical diffusion	82
6.3.2 Effect of the value for the Schmidt number in diffusion terms on the removal ratio	83
6.3.3 Sensitivity to changes in bottom boundary condition	84
6.3.4 Rigid lid computation	85
6.4 Conclusion	86
7 DESIGN RULES FOR RECTANGULAR TANKS	87
7.1 Introduction	87
7.2 2-dimensional steady	88
7.2.1 Removal ratio in relation to the shape and the flow rate	89

7.2.2 Comparison of the Camp graph and the equation found.	93
7.2.3 Conclusion	96
7.3 Time dependent 2-dimensional	97
7.3.1 Flow and settling in tanks loaded at a constant rate for a limited duration.	97
7.3.2 Step-loading	101
7.3.3 Method to predict functioning of tanks in time-varying situations	102
7.3.4 Conclusion	104
7.4 Concerning 3-dimensional effects	104
7.5 Sensitivity of found equation to variations in bottom boundary	105
7.6 Probability of short-circuiting	107
7.7 Baffle or diffuser	107
7.7.1 Baffle	108
7.7.2 Diffuser	111
7.7.3 Effect diffuser in 3-dimensional flow situations	113
7.7.4 Conclusion	113
7.8 Conclusions	113
8 CONCLUSIONS	115
List of Symbols	119
References	121
APPENDICES	
A: Point rainfall method	125
B: Present Dutch design method	129
C: Flow model	135
D: PHOENICS equations	143
E: Flow of water over a weir	147
F: Roughness parameter E	149
G: PHOENICS input file Q1	151
H: FORTRAN subroutines for settling particles	153
I: Discretisation	161
Curriculum Vitae	165

Chapter 1

INTRODUCTION

Combined sewer systems convey both storm water and waste water. In times of heavy rains, these systems cannot convey all the water to the waste water treatment plant (WTP). The excess water is discharged directly to the surface water by means of overflows. This surplus, a mixture of waste water, storm water and eroded sewer sediments, pollutes the surface water. This can result in dead fish, odour nuisance, turbid water, etc. One way to alleviate this pollution is the construction of storm water settling tanks, which store and partially clear the surplus water. Dutch water authorities have formulated regulations that actually require a large number of such tanks to be built, at costs that might add up to one billion ECU⁽¹⁾. However, no satisfactory design methods - ones that take into account the time-varying flow situations - exist for these tanks. It has not been proven that the current design practices result in tanks that will function in an optimal way.

The aim of this study is to develop design methods for optimally functioning storm water settling tanks that store and clarify overflowing water. To this end, a mathematical model has been applied, which makes it possible to simulate the most important processes in these tanks and to investigate the effects of variations in tank shape and other design parameters.

The model has been used to optimise⁽²⁾ the design of rectangular storm water settling tanks for a range of time-varying loads and then to derive 'rules of thumb' for the design of rectangular tanks in the most common cases. The mathematical model can also be applied to analyze tanks of unusual shapes. Furthermore, the mathematical model can be used to design other structures in which particles settle or float, e.g. clarifiers, etc..

⁽¹⁾ January 1996: 1 ECU = 2.06 Dutch Guilder.

⁽²⁾ With the highest removal ratio of particles in relation to the volume of a tank.

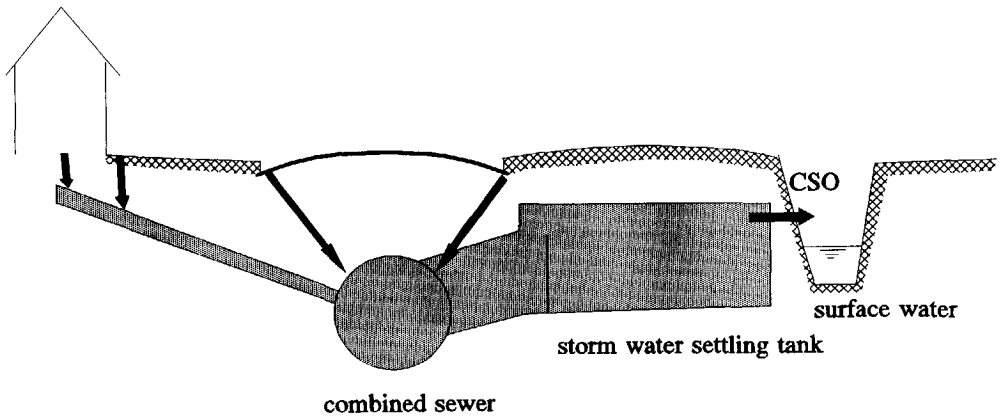


Figure 1.1: Combined sewer system with storm water settling tank.

1.1 Sewer systems in the Netherlands

In the Netherlands, as many as 93% (1990) of all houses are connected to a sewer system. Most of the existing sewers (76% of the total length) are part of combined sewer systems in which storm water and waste water are discharged together (CUWVO VI, 1992)⁽³⁾; see figure 1.1. Both rain water and waste water are pumped to the WTP. Typically, the resulting flow during rainfall can be 2 to 5 times the dry weather flow. During heavy rains, when the runoff to the system exceeds the hydraulic capacity of the sewers running to the WTP and when the in-line storage of the sewer network is fully used, a mixture of waste water, storm water and re-eroded sewer sediments is spilled to the surface water at the combined sewer overflow structures (CSOs).

The volume of the sewer network below the crest of the lowest weir of the CSOs is generally about 70 m³ per hectare of impervious area (or 7 mm of rainfall depth on the impervious area). The excess capacity of the pumps (the total capacity minus the dry weather flow) is often such that the sewer system can be emptied within 10 hours. This means that the excess capacity is in most cases 0.7 mm/h. The so called 'rational method', which is used in other countries for the design of the sewer system, is not used in the Netherlands. On the basis of years of experience, sewer systems in the Netherlands are designed on a continuous rainfall intensity of 60 l/s/ha on impervious areas. In hilly areas 90 l/s/ha is sometimes used. In terms of preventing flooding, these design rules have resulted in adequately functioning sewer systems. However, pollution from the sewer systems due to combined sewer overflows (CSOs) can be a problem.

In the Netherlands, the municipality is responsible for the construction and management of the sewer system, whereas the water boards are responsible for the control of surface water and the treatment of sewage. The water boards set the regulations concerning the quantity and quality of the overflowing water. For combined sewer systems, the regulations regarding overflows used to

⁽³⁾ Because new sewer systems are separate systems which discharge rain and waste water separately, this number declines.

be based on the frequency of overflowing (overflow frequency) only. In the 1970's, on average 10 events a year were allowed, but in the 1980's between 3 and 10 events were prescribed, depending on the type of receiving water and the insights of the particular water board.

The overflow frequency used to be determined by counting the number of rain events above the line representing the sewer system capacity in a graph with dots representing the rainfall (Dutch: 'Stippengrafiek'). Appendix A explains this easy to use method, which, due to various in-built simplifications, does not necessarily result in the actual overflow frequency. However, the method is useful for a quick insight into the operation of the system, and for estimating the effect of changes to the system on the overflow frequency without the use of more advanced computer models. In some cases it is preferable to the more accurate, but more complicated and time-consuming methods.

The rapid development of more powerful and faster computers will make it possible in the near future to accurately compute the flow through any sewer system as a result of a rainfall time series with a computer model. Such computer model can simulate time-dependent flow situations in sewer systems at the level of links and nodes. The new Dutch guidelines for evaluating the functioning of a sewer system (C2100, 1995), require the use of a rainfall time series of 10 or 25 years. To reduce the computation time, only selected storms are simulated with an accurate model of the sewer system (at the level of links and nodes). After calibrating this model to the accurate model, based on the selected storms, the long rainfall series is then simulated with a simplified model of the sewer system.

1.2 Combined sewer overflows

Combined sewer overflows (CSOs) may result in dead fish, bacteriological pollution, odour nuisances, turbid water, and oil or coarse sewer garbage spilling into the receiving waters. The stricter rules regarding the overflow frequency has not really solved these problems, because even in spite of a low overflow frequency, the water quality often did not meet the standards. It is not only the overflow frequency which plays an important role in surface water pollution, but also the pollution load per event, and the local situation are important. Reasons for this are:

- * The maximum pollution load does not decrease significantly when the number of events is reduced. One major event might contain 80% of the total yearly load (NWRW, 1989). If this major event is not avoided, then the reduction of the overflow frequency from, for example, 10 to 5 events per year will not reduce the instantaneous pollution load significantly.
- * As much as 85 percent of the current overflow structures overflow into surface water which has a low self cleansing capacity, so that the overflow has a significant detrimental effect on the water quality.
- * Pollutants accumulate due to sedimentation in the vicinity of the CSO. The accumulated pollutants in the bottom sediments can hamper life in the bottom sediments. Furthermore, during extreme discharges, pollutants built up over the years, might be eroded in a short space of time and seriously impact on aquatic life.
- * Sewer systems vary considerably (e.g. in size, slope, lay-out, etc.), therefore, the pollution load is often different for two sewer systems with the same overflow frequency.

Six possibilities present themselves to alleviate the problem:

- 1) Flushing the receiving surface water.

- 2) Preventing the accumulation of sludge in the system.
- 3) Increasing the storage capacity of the sewer system.
- 4) Increasing the excess pump capacity of the sewer system.
- 5) Preventing the inflow of huge amounts of storm water into the sewer system.
- 6) Construction of ancillary structures (like settling tanks, swirl separators, etc.) at the CSOs.

- ad 1) The first possibility is not a viable solution, as the pollution load is not reduced, but only the effects are treated. It is better to prevent than to treat the symptoms.
- ad 2) The accumulation of sludge in the sewer system can be prevented by a proper design of the sewer system, or by regular cleaning, so that during heavy rain storms, no sludge can be eroded and spilled to the surface water. As this does not reduce the pollution load from the dry weather flow and the surface runoff, the relation between those two pollution loads and the one from the sewer sludge should be known, in order to assess the effect of this measure. Such relation is unknown. Because of this, this measure is not accepted as an improvement, but each system simply must minimise the accumulation of sludge.

The other four possibilities are generally applied to reduce the pollution load.

- ad 3) Increasing the storage capacity (by enlargement of the sewers, or by means of regulation of the flow), reduces the volume and the frequency of spills. However, part of the positive effect might be lost, if as a result of the adaptations the flow conditions in the sewer systems change in such a way that more sediment is deposited at low flow conditions. This additional sediment might be washed out during heavy storms.
- ad 4) Increasing the overcapacity of the pumps also reduces the volume and the frequency of spills. The WTP, however, must be able to treat the additional flow of water. Notably, the efficiency of the treatment generally decreases with increasing loading rates (due to smaller detention times in the WTP and possible disruptions of the treatment process because of diluted sewage). Accordingly, the reduction of pollution at the CSOs is partly lost due to a greater pollution in the effluent of the WTP. This spill, though, might be located at a more favourable location than in the middle of a town where some of the CSOs are located.
- ad 5) A conceptually better solution to this problem is to prevent the inflow of huge amounts of storm water into the sewer system. This can be done by disconnecting parts of the impervious area from the sewer system. Water from roofs, quiet roads and some parking lots is believed to be clean enough to be discharged directly on the surface water or to be infiltrated directly into the ground (Stahre and Urbonas, 1990). In this way, the reasonably clean rain water is not polluted with the waste water and sewer sediments, and because of this, the flow to the sewer diminishes. Consequently, this reduces the spilled volumes and the overflow frequency.
- ad 6) Ancillary structures are constructions at the CSOs (like settling tanks, swirl separators, etc.) that reduce the pollution. The following sections present various kinds of ancillary structures.

Which solution is chosen in practice depends on the local situation. This research focuses on the application of ancillary structures.

1.3 Reduction of pollution at the overflow structures

Various types of ancillary structures have been built in the Netherlands and abroad. They aim to reduce the pollution from CSOs either by increasing storage capacity, reducing the concentration of pollutants in the overflowing water, or by a combination of the two. An elaborate description of various types of ancillary structures is given in (Sharon, et al., 1989).

1.3.1 Storage facilities

Storage facilities reduce the pollution of surface water by storing water that would otherwise overflow. After the storm, when the water level in the sewer system has dropped sufficiently, the stored water is returned to the sewer system either by pumping or by means of gravity.

In addition to concrete reservoirs, these facilities can also be constructed as part of urban green areas or as large bags below the water surface of a pond or river. Special attention must be paid to the cleaning, hygienic risk, etc.. Stahre and Urbonas (1990) give a series of examples.

1.3.2 Separating facilities

Complete treatment plants are too large and expensive to build at each overflow structure, but some primary treatment can be achieved by using the differences in the density of the particles and the water. Because of the volume needed to create flow conditions in which particles can settle, these facilities reduce the pollution both by storage and separation and are discussed below.

Teacup separators or **swirl separators** create a swirling flow in which the heavier particles move to the perimeter, from where they then flow back to the sewer system or to the WTP. The clearer water flows into the surface water from the middle of the construction. Such structures are compact, and self-cleaning. The manufacturers of vortex separators claim good separation efficiencies, which they base on steady flow conditions in laboratory situations. The separation efficiency depends on the settling velocity of the particles, the volume of the separator, and the ratio of the concentrated discharge to the WTP versus the inflow.

For high inflow rates the separation efficiency is equal to this ratio. The concentrated discharge is fixed by the design. The inflow will vary. For low inflow rates the efficiency goes to a hundred percent, see (Sharon et al., 1989; Weiß and Michelbach, 1995). NWRW (1989) reports some results of measurements on a vortex separator. These results show that a vortex separator retains 40%, 36%, 22%, and 21% more COD, BOD, N-kj, and Phosphor (respectively) than a conventional overflow structure, which consists of a chamber with a weir.

A **helical bend flow regulator** uses the secondary motion, imparted on fluids at bends. Due to this motion and the shape of the flume the heavier particles will collect at the bottom, while clearer water spills at the outer edge of the flume. Sharon et al. (1989) provide more detailed information.

Finally, a **helophyte filter** is a field of cane in which the overflowing water is spread out. Colonies of micro-organisms live around the roots on the nutrients in the water. The effect of these fields is still being investigated. Whether or not they are effective, this solution means that a part of the environment is made a part of the sewer system, and therefore the pollution of this part of the

environment is allowed. However, such a cane field still might look more pleasant than a concrete basin.

The policy in the US appears to be different to that in Europe. Whereas the ancillary structures in Europe aim at creating storage and some separation based on density differences (settling tanks, vortex flows, etc.), in the US further treatment facilities are installed after the CSOs, based on physical, biological, and chemical treatment. Systems which function automatically and are resistant to shock loads, resulting in a low suspended solids concentration in the effluent have been developed: E.g. combinations of screening and filtration or dissolved air floatation, all kinds of biological treatment, high gradient magnetic separation, and in the US inevitably, disinfection. See also (Moffa, 1990).

1.3.3 Storage and separation facilities

The most frequently applied type of structure which reduces the pollution by storing water and creating flow conditions in which particles can settle, is a **storm water settling tank**. It is only when the amount of inflow into the tank exceeds the (often large) storage capacity of the tank, that water is spilled into the surface water. The tank design is expected to ensure favourable flow conditions for settling and floating, so that a considerable amount of pollutant is retained in the tank.

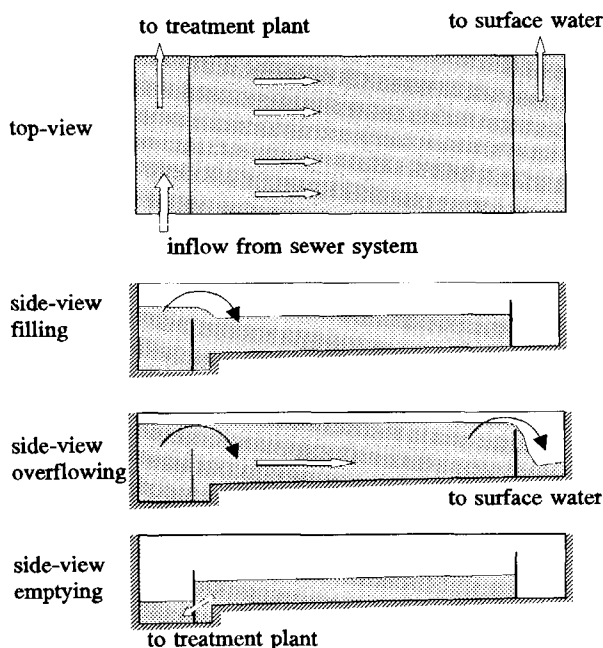


Figure 1.2: Rectangular storm water settling tank.

In the Netherlands, storm water settling tanks are generally connected off-line to the sewer system, which means that part of the sewer flow is diverted to the tanks. Usually, the tanks have an internal weir over which the water enters the tank and which ensures that water only fills the tank after heavy storms. This reduces the costs of cleaning the tank and of pumping the water out. After the storm, when the water level in the sewer system has dropped, the water in the full or partially filled tank flows back, or is pumped back, into the sewer system, see figure 1.2.

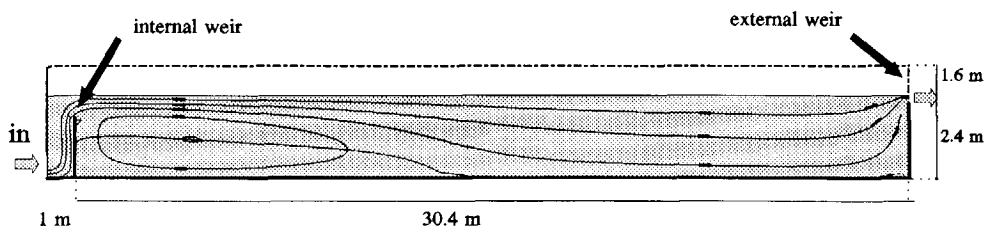


Figure 1.3: Typical flow situation in a rectangular tank.

In most rectangular tanks, the water enters over a weir and flows out over an external weir at the far end. A baffle just before the external weir is meant to retain floating particles. When the tank is full, the flow over the internal weir creates a large re-circulating eddy just behind the internal weir, as has been clarified in figure 1.3. The area containing this eddy is called the re-circulation zone. Behind the re-circulation zone the water flow is divided more evenly over the full depth. Circular tanks, for the most part, are centrally fed with the outflow at the periphery.

Veldkamp (1992)⁽⁴⁾ reports the results of measurements on two storm water settling tanks at the cities of Amersfoort and Kerkrade. For Amersfoort, the reduction of COD is 80% of the inflow. 17% can be contributed to the beneficial effect of settling. The rest is due to the reduction of the amount of the overflowing water. The storm water settling tank in Kerkrade reduced the pollution with 62%, 25% of which is due to settling.

The concept of a **parallel settling sewer** is that in a long straight sewer most of the particles will be near the bottom. It is therefore located at the end of a long straight sewer. There a separation device divides the flow in a relatively clear and concentrated flow. The concentrated flow, goes straight on to a second separation device, which again divides the flow. The clearer flow from the first separation device flows through a sewer parallel to the main sewer. Then it is joined by the clearer flow from the second separation device. Together these clearer flows, spill to the surface water. See figure 1.4.

Due to its size, the parallel sewer will also provide additional storage capacity.

Finally, **sewers with a storage and settling function** are simply so big that the flow condition becomes favourable enough to allow settling.

⁽⁴⁾ Veldkamp gives a clearer insight in the functioning of such tanks than the original source (NWRW, 1987).

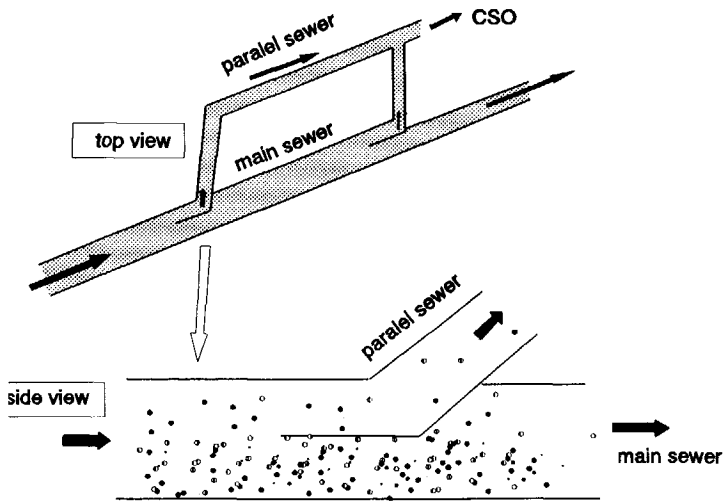


Figure 1.4: Parallel settling sewer

1.4 Regulations

In 1990, the Dutch authorities established a committee to formulate rules to reduce the pollution of the surface water by CSOs. In 1992, the committee proposed that a combined sewer system should not pollute the receiving waters more than the following reference system does (CUWVO VI, 1992). This reference system is equal to a system with a storage of 7 mm, an excess capacity of the pumps of 0.7 mm/h, and 2 mm extra storage in storm water settling tanks behind each CSO. Other measures are allowed if this results in a smaller or equal pollution load. If the measures taken do not result in water of sufficient quality, additional measures are required. The committee further proposed that the overflow frequency should still be used to assess the functioning of the sewer system.

The committee did not set regulations on the pollution load because it is still impossible to determine this load accurately. In addition, it is uncertain what the maximum shock load is for the aquatic ecosystem (without an adverse effect). Furthermore, the effect of accumulation of pollutants is not sufficiently known. Thus, an allowable emission cannot be determined. In fact, the maximum allowable overflow frequency is also unknown.

According to the laws regulating spills on the surface water, municipalities must establish a plan for the functioning of their sewer system. The sewer system must comply with the regulations of the water boards before the year 2000. Many water boards accepted the proposed reference system of the CUWVO and made it part of their regulations. In many situations, the improvement of the sewer system will only result in the construction of a settling tank, because the 7 mm in-line storage and the reference pump capacity are mostly already present. A rough estimate of the

number of tanks which have to be built in the near future shows that huge costs are involved. Assuming an impervious area per inhabitant of 60 m², a total volume of 1,800,000 m³ will be needed in the Netherlands which has 15,000,000 inhabitants. The costs of such tanks range from 500 to 1,000 ECU/m³. This means a total investment of 1 to 1.8 billion ECU. Even if only a small part of all combined sewer systems are adapted with such tanks, the required investments will be very large. However, the positive effects that such large investments will have on the environment are uncertain.

In view of the complexity of the problem, and the many uncertainties, the use of this reference system for combined sewer systems is a pragmatic choice. However, two remarks must be made. In the first place, it requires a method to assess the pollution load, either absolutely or relatively (i.e. existing or improved system versus reference system). It is still uncertain how the pollution load can be assessed. Municipalities and water boards must first agree on a method to estimate this load, or on a method to compare the existing or improved system to the reference system. There are no standardised ways to do this. Most large consulting engineering firms in the Netherlands have developed their own computational method to compute the pollution load. The uncertainties involved require that the results of such computations are examined carefully. Ruan (1995) concludes that the deterministic modelling of sewer sediments is still too complex and advocates further research into conceptual and stochastic modelling. Aalderink (1995) compared various models which compute the pollution load and he concluded that the results can differ significantly. Moreover, he concluded that the models predicted the effect on the pollution load of certain changes in the sewer system differently. In some cases, the results were even contradictory. For one alteration of the sewer system, some models predicted a decrease in the pollution load, whereas other models predicted an increase in the pollution load. In 1991, a study began in the Netherlands to furnish data on which a standard method to compute the pollution load can be based. Because of the complexity of the problem, it is unlikely that the results will be available before the year 2000, which is the year when the municipalities will have to comply with the regulations set by the water boards.

In the second place, simply fulfilling the requirements of the reference system does not guarantee surface water of adequate quality. The effect of the actions taken to meet the standard of the reference system will depend upon the sewer system and the surface water. In the best case, the water quality improves substantially towards the AMK standard⁽⁵⁾. However, it is also possible that cheaper measures might be sufficient to reach the required standard, so that the investments are not optimal. In case the AMK standard is not attained, supplementary measures will be required. This should be foreseen and plans drawn up in such a way that the measures taken at present will not conflict with future changes.

The magnitude of the problem and the high investments involved require that the water boards and the municipalities carefully consider each situation before taking action, and before following standard approaches.

⁽⁵⁾ The AMK (Algemene Milieu Kwaliteit) is the reference quality which the surface water has to meet before the year 2000.

1.5 Design methods for storm water settling tanks

The design methods for storm water settling tanks differ considerably throughout Europe. Rompaey (1991) compared several design methods. The philosophy for the design of tanks differs in various European countries. One difference stems from the fact that the occurrence of a first flush is not present as markedly in the flat sewer systems of The Netherlands as is the case abroad. Furthermore, Swiss and German design methods are based on local measurements in for example small hilly areas. The German ATV A128 guidelines (ATV A128, 1983) aim at a storage needed to catch 90% of the yearly pollution load. Furthermore, they relate the required volume to the discharge of the receiving waters and the size of the catchment. The Swiss methods of Munz, or Horler, are also based on local measurements and aim at a certain volume to retain a certain percentage of the pollution. The use of these methods in flat areas might not result in the 90% reduction of the yearly pollution. These empirical methods cannot be translated for use in the Dutch situation, because they have been set up for markedly different situations than in the Netherlands (i.e. small sewer system in hilly areas versus often large sewer systems in often flat areas).

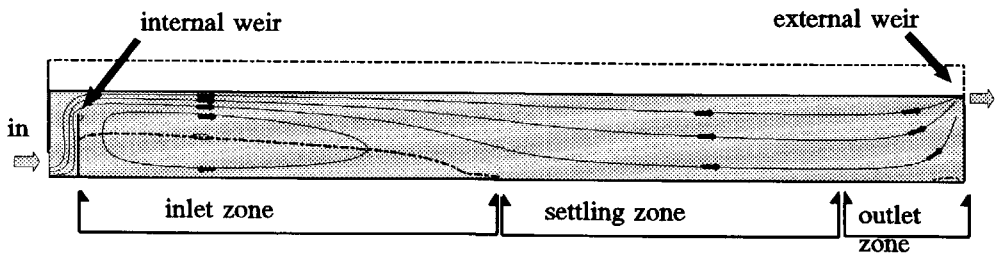


Figure 1.5: Inflow, settling and outflow zone in rectangular tank.

In the Netherlands, the volume of the tank often follows from demands like the 2 mm storage of the reference system mentioned above. The tank has to be shaped to ensure optimal removal of pollutants through settling. The design is based on stationary flow conditions, which prevail in the continuously loaded clarifiers (settling tanks) used in the drinking water and the waste water treatment. The design method further distinguishes three zones in the tank: the inlet zone, which contains the re-circulation zone, the settling zone and the outlet zone, see figure 1.5. The method assumes that particles only settle in the settling zone, in which the water is assumed to flow uniformly and the settling conditions are assumed to be optimal.

A more elaborate description of the Dutch design method for storm water settling tanks is given in Appendix B.

It is uncertain if the Dutch design method results in optimally functioning tanks, for the following reasons:

- * In reality, the steady state flow conditions on which the design is based do not occur or only occur for a part of the time. This is due to the fact that the inflow will vary in time (due to variations in the rainfall intensity and the flow towards and in the sewer system) and that the tanks will have to be filled before water flows out. Water falls into the tank and fills the tank when the water level in the sewer system rises above the internal weir crest. When the

water level in the tank rises above the external weir crest, flow conditions become more quiescent. Both the filling and the effect of variations in the flow are not taken into account in the design.

- * Next, the size of the settling zone, which is crucial in the design method, is not exactly known and must be guessed. The size depends on the lay out and will change during a rain event with changing discharges. A sudden rise in the inflow rate can temporarily increase the length of the re-circulation zone and thus temporarily reduce the settling zone size.
- * Furthermore, settling does not only occur in the settling zone, but also outside that zone.
- * In addition, the assumptions on which the settling in the settling zone is based are doubtful. See Appendix B for further information.

Other disadvantages are that the method can only be used for 2-dimensional flow situations and that the effect of baffles or diffusors can only be inferred.

1.6 Conclusion

The present design methods do not accurately describe the real processes in storm water settling tanks and hence do not guarantee a tank design with an optimal removal of pollutants. The stationary flow situation on which the tank design is based in the Netherlands, occurs only for a short period, if at all. Furthermore, the effect of filling is not taken into account, the flow is not uniform, and the length of the settling zone must be estimated.

To ascertain the design of optimally functioning tanks, design rules need to be based on the time fluctuating character of the processes (flow and sedimentation) in the tanks.

As many storm water settling tanks will be built and huge investments will be involved, a more reliable design method is required. Therefore, this study has been commissioned.

1.7 Setup of research

1.7.1 Approach

To derive reliable design rules for storm water settling tanks, insight is required into the influences that changes in the design have on the efficiency of reducing the pollution load. The in-situ process of flow and settling in real tanks is extremely difficult to study due to the fact that they are only used a few times per year, during which their flow is uncontrollable. Finally, in order to investigate the effects of changes in the design, the tank would have to be altered, which is almost impossible. Another option is to compare the functioning of different tanks, but such comparison will be extremely difficult because of the inevitable variations in the inflow.

In scale models of storm water settling tanks the flow conditions and the tank design can be controlled and changed, so that the required relations can be derived. However, such experiments are expensive and prohibitively time consuming as many experiments will be needed in order to derive generally applicable design rules. In addition, scaling down the process of settling introduces many difficulties which are not easily solved.

The chosen option is the use of a mathematical model to model the processes in the tank. Such a model can simulate the time-dependent flow and settling in storm water settling tanks and can

predict the influences of changes in the design (e.g. changes in the shape or the use of baffles), and thus can help to design optimally functioning tanks. Furthermore, such a model can be used to evaluate the functioning of a tank for a range of loading conditions.

Although this research concentrates on storm water settling tanks, generality has been built in to ensure that the resulting model it can provide insights into the processes in other ancillary structures in which particles settle and into their functioning, so that it can also be used for their design. The decision to use a mathematical model, and not measurements, has been influenced by this advantage.

The mathematical model should be validated on measurements of the flow and settling in real tanks or in scale models.

1.7.2 Objective

The aim of this research is to create design rules for optimally functioning storm water settling tanks.

1.7.3 Modelling the processes

The mathematical model should be able to handle the following:

- * 2-DV flow situations (in a vertical plane);
- * 3-D flow situations;
- * tanks of different shapes and sizes: rectangular, circular and other;
- * time dependent flow;
- * turbulent flow;
- * filling of the tank (free surface flow);
- * settling of particles with different settling velocities;
- * re-entrainment of particles from the bottom;
- * hindering of settling;
- * density currents.

In 1990, computational fluid dynamics (CFD) packages especially written to handle dynamic flow and settling, were not available (Vermeer, 1990). To set up and write a new package would require an enormous amount of time, with no guarantee of success. Therefore, a general purpose package has been used and extended. And still, in 1997, no other CFD package describing all the above mentioned aspects at the same time seems to exist.

A number of processes occur in storm water settling tanks, such as flow, settling, erosion, turbulence, density currents, free surface flow, etc.. These processes are not independent and should not be considered independently. Some of these processes can be modelled in more than one way with different demands in terms of computation time and resulting in different levels of accuracy. In order to set up a mathematical model, models for the various processes have to be combined. The selection between various models for the different processes depends on the required accuracy and allowable computation time.

Models are normally always descriptions of reality. Since these descriptions are generally incomplete or simplifications, and due to shortcomings of the theory used to describe the various processes, the results of a simulation might differ from reality. To prove that these differences are not that large, and that the results are trustworthy, the simulation results have been compared with measurements of flow and particles in experimental set-ups, and hence validated.

Use of a mathematical model requires considerable experience and is often very time consuming. It is impractical and even impossible to model each and every situation. Therefore, the mathematical model has been applied to derive a set of rules to simplify the design in most common cases; the equilibrium flow situation in rectangular tanks with 2-dimensional (length-height) flow conditions.

This research did not result in design rules for less common shapes of tanks. For these specific cases, the mathematical model can be applied.

1.7.4 Lay-out of thesis

Chapter 2 presents the required equations and the setup of the model for the simulation of the water flow. The general purpose CFD code PHOENICS has been used and adapted. Chapter 3 shows that the model describes the flow in a satisfactory way. As measurements of the flow in real storm water settling tanks were not available, those of experimental set-ups (scale models of a storm water settling tank and a flow situation from literature) have been used for the validation of the model. The consistency of pollutants in overflowing sewage will be discussed in Chapter 4. Chapter 5 presents how the mathematical model has been extended for the simulation of settling particles. Chapter 6 concerns the validation of the flow and settling simulations and Chapter 7 presents new, more realistic design rules for rectangular tanks. Finally, Chapter 8 summarizes the conclusions and recommendations of this research.

Chapter 2

FLOW MODEL

2.1 Introduction

The simulation of the transport of settling particles in running water has been divided into two parts. The first part deals with the flow of the water (in fact, the flow of the water with particles in it). The second part considers the behaviour of the particles (i.e. the settling of the particles relative to the water flow, the deposition of the particles on the bottom, and the erosion of particles from the bottom). This chapter discusses the mathematical model which describes the water flow. The model describing the behaviour of the particles will be discussed in Chapter 5.

Uncoupling the simulation of flow and settling is acceptable, because the concentrations of pollutants are so small that their effect on the density and viscosity can be neglected.

Conservation laws describe the motion of a fluid in a continuum of time and space. The equations for the conservation of mass and momentum, known as the continuity equation and the Navier Stokes equations, are solved to simulate the water flow. Appendix C gives the differential equations describing the water flow. In combination with boundary conditions for a chosen flow domain, they describe the flow situation in that domain. For the situations considered in this research, the fluids can be assumed to be incompressible. The flow situations studied are highly turbulent. Turbulence still cannot be described exactly in the studied flow situations and is therefore modeled. For that purpose, the k - ϵ turbulence model has been adopted. This model applies the eddy viscosity concept to bring into account the effect of turbulence. The eddy viscosity, ν_t , is a function of two variables; k , the kinetic energy of turbulent motion, and ϵ , the dissipation of that energy, for which transport equations are solved. Appendix C gives a description of the k - ϵ turbulence model. Besides the standard form of this turbulence model the appendix presents some adapted forms. In some cases, these adapted forms of the k - ϵ turbulence model result in more realistic flow simulations. The results obtained through the use of the standard or adapted forms will be presented in Chapter 3.

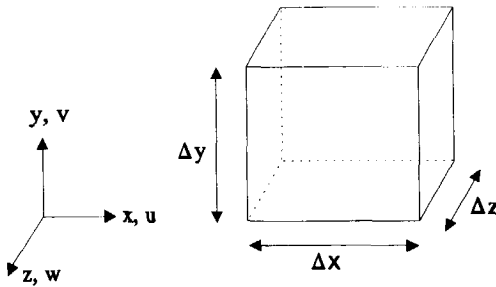


Figure 2.1: Basic element.

In order to solve the differential equations by a computer, the flow domain is divided into finite volume elements (or cells) and the equations are made discrete. For each element, transport equations for mass, momentum, and the turbulence variables k and ϵ must be solved. The equations have been set up for elements in Cartesian coordinates. See figure 2.1, in which u , v , and w are the velocities in x -, y -, and z -direction respectively. The shapes of the elements are fixed (Eulerian approach). Within the chosen CFD package the grid can also be set up in polar or body fitted coordinates. This allows virtually for all kinds of tank shapes.

The transport equations can be solved by a range of CFD (Computational Fluid Dynamics) packages. However, none could model all the wanted processes without further modifications (Vermeer, 1990). The commercially available general purpose CFD package PHOENICS of CHAM Ltd., has been selected because of the possibility to add coding, thus allowing to make it comply with specific needs.

Section 2.2 gives a description of the way the equations are solved by PHOENICS. The simulation of a flow situation with a time-varying free surface appeared troublesome. Section 2.3 presents the method which has been used in this research to simulate the time dependent free surface flow. Section 2.4 explains the boundary conditions which have been used.

2.2 PHOENICS

PHOENICS is the acronym for Parabolic Hyperbolic Or Elliptic Numerical Integration Code Series. It enables to simulate fluid flow, heat transfer, and mass transfer problems in flow situations varying from 1-dimensional, single phase, and steady to 3-dimensional, multiple phase, and transient.

PHOENICS applies a staggered grid, see figure 2.2, which means that the velocities are defined at the cell faces, whilst all the other variables are defined at the cell centres. In a non-staggered grid all variables are defined at the same points. Figure 2.2 presents the lay-out of the grid in the 2-dimensional case. The indices i and j denote the spacial steps in x - and y -direction respectively.

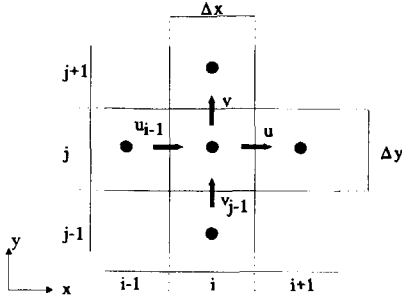


Figure 2.2: Staggered grid for the 2-dimensional case.

The transport equations are written in the same way for all variables. For the 2-dimensional situation they read:

$$\frac{\partial \rho \varphi}{\partial t} + \frac{\partial}{\partial x}(\rho u \varphi) + \frac{\partial}{\partial y}(\rho v \varphi) = \frac{\partial}{\partial x}(\Gamma_{\varphi} \frac{\partial \varphi}{\partial x}) + \frac{\partial}{\partial y}(\Gamma_{\varphi} \frac{\partial \varphi}{\partial y}) + S_{\varphi} \quad (2.1)$$

in which t denotes the time, ρ the density, and Γ_{φ} the exchange coefficient of the entity φ . S_{φ} is the source term, which contains terms like gravity and boundary conditions. PHOENICS applies the SIMPLER algorithm of Patankar (1980) to solve the transport equations. This algorithm rewrites the transport equations by fully upwind implicit discretisation⁽⁶⁾. The discrete transport equation is then rewritten as a relation between the value of a variable in a particular cell and the values of variables in the surrounding cells. In order to limit the amount of super- and subscripts, they have not always been printed. When the superscript is omitted, the new time step value is meant. When the subscript i or j has been omitted the current i or j value is meant: e.g. $c_{j-1} = c_{i,j-1}^{n+1}$. The new concentration c ($= c_{i,j}^{n+1}$) can be computed from:

$$\varphi = \frac{\varphi^n A_t + \varphi_{i-1} A_{x(i-1)} + \varphi_{i+1} A_{x(i)} + \varphi_{j-1} A_{y(j-1)} + \varphi_{j+1} A_{y(j)} + \varphi_s A_s}{A_t + A_{x(i-1)} + A_{x(i)} + A_{y(j-1)} + A_{y(j)} + A_s} \quad (2.2)$$

- With $\varphi^n = \varphi$ value at old time step (all other values are of the new time step, i.e. $n+1$);
- $A_t = (\Delta x \Delta y \rho)^n / \Delta t =$ time coefficient;
- $A_{x(i-1)} = \max(0, (\rho \Delta y u)_{i-1}) + \text{Dif}_{i-1};$
 $=$ coefficient of inflow and diffusion in x -direction at the $i-1$ cell face;
- $A_{x(i)} = \max(0, -(\rho \Delta y u)_i) + \text{Dif}_i;$
 $=$ coefficient of inflow and diffusion in x -direction at the i cell face;
- $A_{y(j-1)} = \max(0, (\rho \Delta x v)_{j-1}) + \text{Dif}_{j-1};$
 $=$ coefficient of inflow and diffusion in y -direction at the $j-1$ cell face;
- $A_{y(j)} = \max(0, -(\rho \Delta x v)_j) + \text{Dif}_j;$
 $=$ coefficient of inflow and diffusion in y -direction at the j cell face;

⁽⁶⁾ For scalar variables, also more accurate but more complex higher order discretisation schemes can be used, such as QUICK (POLIS).

Dif_i , Dif_{i-1} , Dif_j , and Dif_{j-1} represent the diffusion terms. More information is given in Appendix D. The source term S_φ of equation 2.1 has been introduced as a function of the local φ value:

$$S_\varphi = A_s(\varphi_s - \varphi) \quad (2.3)$$

A_s and φ_s are the coefficient and the value for the variable used to impose the source term. This allows for imposing different kinds of boundary conditions. When A_s is very large, all other terms of equation 2.2 will be negligible and φ will be fixed to φ_s , so a variable can be given a certain value. It is also possible to dictate a fixed flux. This is done by assigning A_s equal to $1 \cdot 10^{-10}$, which flags PHOENICS to multiply the φ_s value by $1 \cdot 10^{+10}$. Consequently, the source is

$$S_\varphi = 1 \cdot 10^{-10}(1 \cdot 10^{+10}\varphi_s - \varphi) \approx \varphi_s \quad (2.4)$$

Intermediate values of A_s are also possible. Finally, when no boundary condition is given, mirroring conditions apply ($d\varphi/dx = 0$ perpendicular to the wall). Each boundary condition is given for a group of named cells. Thus, not only at the borders, but also anywhere in the flow domain, sources can be introduced. By means of self-written subroutines, the PHOENICS-user can introduce time-varying boundary conditions and sources, depending on local flow variables.

See Appendix D for a more elaborate description of the equations. For 3-dimensional situations, similar terms are present for the z-direction.

2.3 Free surface method

When the tank is full and the inflow rate is constant, the flow conditions will eventually become steady. For such flow situations, the water level is virtually horizontal and the free water surface can be represented by a rigid lid, which means that the top edge of the mathematical model is chosen just at the water surface. However, at the start of a storm the tank is empty. To simulate the process of filling of the tank, the movement of the rising water level must be computed. Also after the tank has been filled, the water level varies, because the inflow changes in time. These minor fluctuations of the water level have to be simulated to correctly take into account the effects of the time-varying inflow.

There are several methods to simulate a free surface flow (i.e. the moving of the interface between different fluids). One option is to apply a moving body fitted grid. The top of the grid then follows the water surface. Its position is based on the fact that the pressure at the water surface should be zero. See for example (Blom, 1994). Within PHOENICS, this method can also be applied by changing the porosities of the cells above the interface. Such methods are not suitable to model the flow over a weir. Furthermore, the computation of a moving water level by such methods, is expected to be extremely time-consuming.

PHOENICS provides two methods to simulate free surface flows. Both methods employ a single phase treatment. The different fluids have only one value for each velocity component, concentration, etc. for each cell. The differences between the fluids are incorporated in the fluid characteristics such as density and viscosity. The methods use different means to determine the position of the interface between the two fluids. One method deduces the interface position from

the solution of a conservation equation for a scalar variable, which is the fluid marker. This method was rejected because it appeared to require more computation time than the other method. Furthermore, to restrict the smearing of the interface due to numerical diffusion, the use of a fluid marker requires a fine grid.

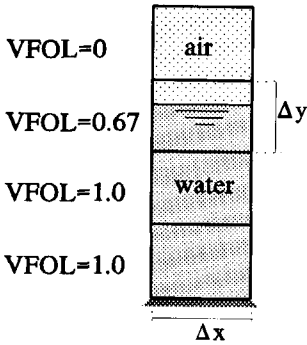


Figure 2.3: Free surface method HOL.

The other method, which is the PHOENICS Height Of Liquid (HOL) method (CHAM, 1992), does not suffer from smearing of the interface by numerical diffusion, and has been used to simulate the flow of water with a varying water surface. The flow of both water and air is simulated. Although these are two different fluids, in this model they are treated as one. A variable VFOL (=Volume Fraction Of Liquid) is defined, representing the filling of a cell with water. See figure 2.3. For VFOL equals 1.0, the cell is completely filled with water. If VFOL is 0.0, then the cell only contains air. Cells with a VFOL value between zero and one contain both water and air. The fluid properties in these cells vary between those of water and air. The density, ρ , and kinematic viscosity, ν , are:

$$\rho_m = \rho_l \text{VFOL} + \rho_g(1-\text{VFOL}) \quad (2.5)$$

$$\nu_m = \nu_l \text{VFOL} + \nu_g(1-\text{VFOL}) \quad (2.6)$$

The subscripts denote either mixture (m), liquid (l), or gas (g). The method is based on the balance of water in a column of cells. The amount of water flowing in and out is in equilibrium with the change of water level in the column. All water entering above the water surface in a column is instantly transported to the water surface.

The HOL method efficiently simulates steady state and transient free surface flows for grids set up in cartesian, polar and body fitted coordinates. However, there are some limitations.

2.3.1 Limitations

Steep water levels

The fact that all the water is instantly transported to the water surface means that the water surface should not be steep. In this research, steep water surfaces occur during the filling of the tank, when the water falls over the internal weir⁽⁷⁾. As no other adequate method to simulate the free surface was available, it has been used nevertheless. Appendix E investigates the simulation of water falling over a weir for various grids. The results appeared to be grid dependent. For a coarse grid, less potential energy appeared to be converted into kinetic energy than for a fine grid. The use of a fine grid for the filling of a whole tank is prohibitive for computational reasons. To limit the computation time to an acceptable level, the filling of a tank has only been computed for a coarse grid. For that reason, the results of the filling of a tank need further calibration. The exact computation of the flow over a weir was considered to be outside the scope of this research, which aimed at deriving design rules for the storm water settling tanks. Because the mass balance during filling is correct, the results have been assumed to be adequate. The margins of the error reduce as the height of falling reduces. From the moment that the water level reaches the internal weir crest, the results can be assumed to be correct.

In fact, the HOL method is not suitable for correctly simulating the falling of water correctly. Possibly, in the future a new more realistic method will be offered in one of the CFD packages.

Overturning fluids

One restriction resulting from the assumption that all water is in the lower part of the column, is that the lighter fluid is always on top of the heavier fluid. Thus, flow situations with overturning fluids and enclosures of air cannot be computed correctly.

Surface tension

The surface tension effects at the water-air interface have not been included in the HOL method. This has a negligible effect on the water flow.

Buoyancy term in k-equation

The use of the k - ϵ turbulence model involves the solution of a transport equation for k , the kinetic energy of turbulent motion. The buoyancy term in this equation damps the turbulence when a lighter fluid is situated on top of a heavier fluid and creates turbulence when the heavier fluid is on top. PHOENICS provides the proper terms to bring this buoyancy effect into account. However, in combination with the free surface method this term gives incorrect results, because of the following two reasons.

Firstly, the density differences between water and air are so large that the buoyancy term damps all the turbulence at the water surface. This is not in accordance with reality. In reality, eddies in the vertical plane are restricted more by the water surface than eddies in the horizontal plane. The turbulence will therefore be an-isotropic. The k - ϵ turbulence model assumes isotropic turbulence, and all turbulence is damped in the cell containing the water surface.

Secondly, another discrepancy with reality is introduced if the cell containing the water surface occupies an important part of the water depth. This is the case during filling and for the flow over the internal weir. When the turbulence in the cell containing the water surface is completely

⁽⁷⁾ The falling of water over the external weir is not completely modelled. The outflow boundary condition has been chosen just on top of the external weir so that no steep water levels occur there. See section 2.4.4.

damped, the overall turbulence will be underestimated. To bring the damping correctly into account, the grid near the water surface should be very fine. This would result in too large computation times.

For these reasons, the buoyancy term has been omitted in combination with the free surface method, while the damping of the turbulence at the water surface is taken into account separately (see section 2.4). Omitting the buoyancy term in the water means that density currents cannot be correctly computed by the program in combination with a free water surface. The error is believed to be acceptable because the density differences are so small that density currents are assumed to be negligible (see Chapter 4). However, further research into this is required.

In order to incorporate the buoyancy term in combination with the free surface method, the flow simulation program would have to be adapted. The program for that purpose would have to compute the term based on the density differences in the water only (and not on the differences of the density in cells filled with water and cells without or partially filled with water). Due to lack of time, it was not possible to take this into account.

In flow simulations without a free surface, the buoyancy term of course can be used because there is no water-air interface at which the buoyancy term can become too large.

2.3.2 Courant number

Free surface computations as implemented in PHOENICS are far more time consuming than rigid lid computations. In the time dependent computations the time step has to be small to prevent numerical instability. The Courant number, which is the ratio of the velocity multiplied by the time step and the cell length, has to be smaller than 1:

$$N_c = \frac{u\Delta t}{\Delta L} \leq 1 \quad (2.7)$$

For the horizontal direction, this means that the displacement of a fluid parcel in one time step is less than the cell length, so that the fluid parcel does not jump over a cell. This means that the time step should be smaller than $\Delta L/u$. On top of the weir, the horizontal velocity at the water air interface can become significantly higher than the average water velocity. For this reason the time step must be small. See figure 2.4, which presents velocity vectors in the water and the air for the flow over a weir. In computing practice, a time step equal to the cell length divided by 5 times the average horizontal velocity could be applied without problems.

2.3.3 Flow of air

The HOL method computes the flow of both air and water, as can be seen in figure 2.4. Because the density of the water is a thousand times higher than that of the air, the water flow causes the air to flow, while the air flow has a negligible effect on the water flow. In the scope of this research the air flow is of no interest. The air flow in the results of the simulations, has only been assessed in a very rough manner, in order to detect potentially incorrect results. Because of the above mentioned, the air flow will not be presented in the simulation results.

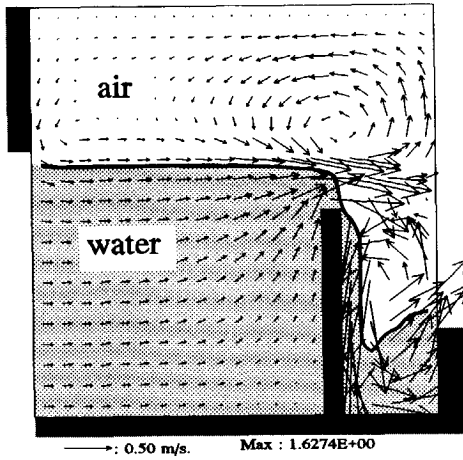


Figure 2.4: Velocity vectors in water and air for flow over a weir.

2.4 Boundary conditions

This section explains the boundary conditions for the 2-dimensional flow situation in a rectangular tank, as seen in figure 2.5.

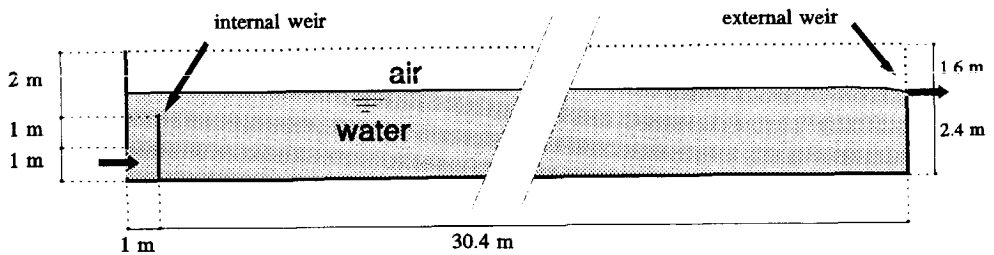


Figure 2.5: Set up of a 2-dimensional model of a rectangular tank.

2.4.1 Inflow

The inflowing flux and velocity are imposed at the inflow. Also values for k and ϵ must be given. No values for k and ϵ are known from measurements in storm water settling tanks. However, the values for the situation of a free surface flow with a logarithmic velocity distribution can provide some understanding of the possible values. For such a flow situation, the values can be estimated with the following equation presented by Booi (1992):

$$k = \frac{1}{\sqrt{C_{\mu D}}} u^2 \quad (2.8)$$

with $C_{\mu D}$ as a constant of the turbulence model and u_* as the shear velocity, which in turn can be estimated with

$$u_* = \frac{u}{15} \quad (2.9)$$

$$\epsilon = C_{\mu D} \frac{k^2}{\nu_t} \quad \text{with } \nu_t = \frac{1}{6} \kappa u_* h \quad (2.10)$$

in which h denotes the water depth, and κ the von Kármán constant (≈ 0.4). The actual values will depend on the inflow construction. The following two examples give an indication of possible values for k and ϵ : For these examples, a tank of 8 m wide and a flow rate of 1.0 m³/s has been chosen. An inflow opening of 2 m high over the full width of the tank results in $k = 6 \cdot 10^5 \text{ m}^2/\text{s}^2$ and $\epsilon = 5 \cdot 10^{-7} \text{ m}^2/\text{s}^3$. When the water flows in via a sewer with a diameter of 1.5 m, the velocity is much higher, and consequently, k and ϵ are also higher.

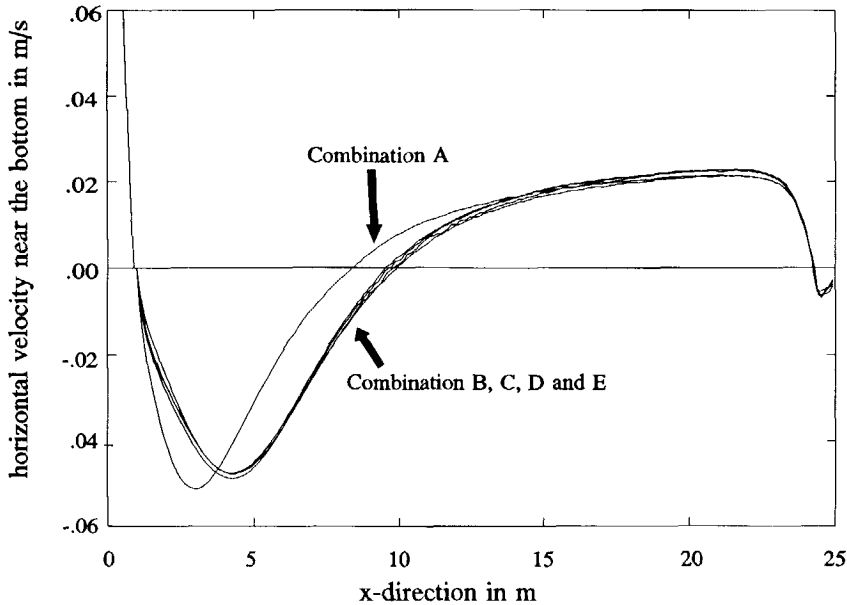


Figure 2.6: Horizontal velocity near the bottom for various values of k and ϵ at the inflow.

To test the effect of the inflow values of these turbulence variables, several simulations of the flow in a storm water settling tank have been executed with different inflow values for k and ϵ . The layout of the tank resembles that of figure 2.5. The total length of the tank is 25 m. The internal weir is at 1 m from the inlet and is 1.2 m high. The water flows in via the bottom 0.60 m at the left. Table 2.1 presents the 5 combinations of inlet values for k and ϵ , for which the flow has been computed. The length of the re-circulation zone, L_r , should be about 8 times the height of the internal weir, H (see Chapter 3).

Table 2.1: Effect of inflow values of k and ϵ .

$\log(k)$ m^2/s^2	$\log(\epsilon)$ m^2/s^3	$\log(\nu_i)$ m^2/s	L_r/H_i	combination
10^{-4}	10^{-6}	$9 \cdot 10^{-4}$	6.1	A
10^{-4}	10^{-5}	$9 \cdot 10^{-5}$	7.1	B
10^{-5}	10^{-6}	$9 \cdot 10^{-6}$	7.3	C
10^{-5}	10^{-5}	$9 \cdot 10^{-7}$	7.3	D
0	0	-	7.3	E

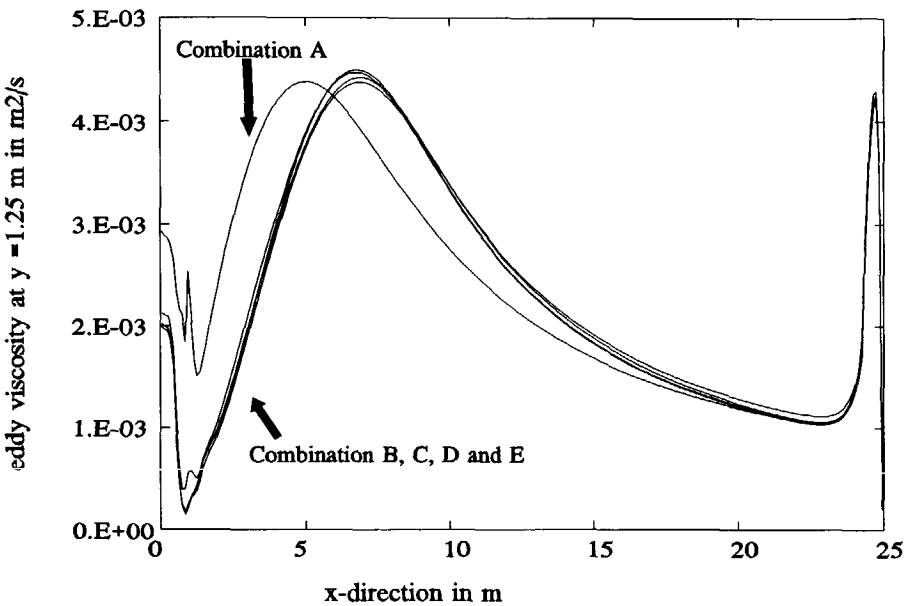
Figure 2.7: Eddy viscosity at $y = 1.25$ m from the bottom for 5 combinations of k and ϵ at the inflow.

Figure 2.6 presents the horizontal velocity near the bottom for these five combinations. Combination A, with the highest resulting value of ν_i at the inflow, clearly results in a smaller re-circulation zone, but the differences are not so important. For the other four combinations the results are almost identical. Even for combination E, in which k and ϵ were zero at the inlet, the results are almost the same as for the other combinations. Apparently, the development of k and ϵ (and thus the development of ν_i) before, and in the re-circulation zone, is more important than the inflow values. The conclusion is that the effect of these different inflow values can be neglected.

Figure 2.7 presents the values of the eddy viscosity for the five combinations at 1.25 m from the bottom. Behind the re-circulation zone the differences are negligible.

In the flow simulations presented later, the value of k at the inflow was $1 \cdot 10^{-5}$ and the value of ϵ at the inflow was $1 \cdot 10^{-6}$.

2.4.2 Wall friction: bottom and weirs

Close to the wall, viscous forces dominate over the turbulent forces and dissipate energy. To accurately simulate this dissipation of energy, a very fine grid should be applied, as well as a model to relate the mean velocity and the turbulence parameters to this dissipation. However, it is more convenient to choose the first grid node in the fully turbulent fluid, outside the viscous sub-layer, and to apply empirical equations, called wall functions, to bridge the viscous sub-layer. The wall functions provide the boundary conditions for the transport equations of the mean flow and the turbulence transport variables.

The dissipation of energy due to wall friction is introduced by adding the wall stress as a momentum source to the momentum equation in the grid cells bordering the walls. The wall stress, τ , is equal to

$$\tau = -u_* |u_*| \rho \quad (2.11)$$

Logarithmic wall functions

The wall functions depart from the assumption that the velocity parallel to the wall is a logarithmic function of the distance to the wall (i.e. logarithmic velocity distribution). For the bottom, this means that the shear velocity, u_* , is the following function of the local horizontal velocity, u :

$$u_* = \frac{u \kappa}{\ln(E y^+)} \quad (2.12)$$

in which y^+ denotes the dimensionless wall distance:

$$y^+ = \frac{y u_*}{\nu_1} \quad (2.13)$$

y is the distance to the wall. For smooth walls the roughness parameter E equals 9.0 (POLIS). Otherwise E is a function of the wall Reynolds number. This has been explained further in Appendix F.

Next to the momentum source for the velocity parallel to the wall, boundary conditions for k and ϵ are imposed. The boundary condition for k is based on the assumption that the turbulence is in local equilibrium, which means that the production of k in the cell near the wall is equal to the dissipation of kinetic energy ϵ . This is valid if the velocity gradient perpendicular to the wall is much larger than the gradient parallel to the wall. The production of kinetic energy of turbulent motion can then be computed with:

$$\text{prod } k = \nu_1 \frac{\partial u}{\partial y} * \frac{\partial u}{\partial y} = \epsilon \quad (2.14)$$

With

$$\tau = \rho \nu_t \left| \frac{\partial u}{\partial y} \right|, \quad \tau = u_* u_* \rho, \quad \text{and } \nu_t = C_{\mu D} \frac{k^2}{\epsilon} \quad (2.15)$$

this results in the following boundary condition for k .

$$k = \frac{u_*^2}{\sqrt{C_{\mu D}}} \quad (2.16)$$

The boundary condition for ϵ follows after differentiating the following equation.

$$u = \frac{u_*}{\kappa} \ln(Ey^+) = \frac{u_*}{\kappa} \ln\left(\frac{Eu_*}{\nu_t} y\right) \quad (2.17)$$

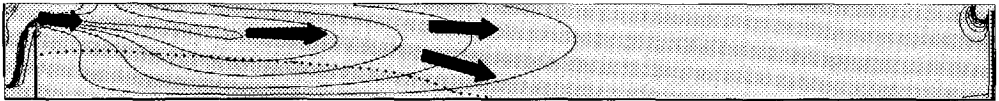
This gives:

$$\frac{\partial u}{\partial y} = \frac{u_*}{\kappa y} \quad (2.18)$$

Consequently,

$$\epsilon = \frac{u_*^3}{\kappa y} \quad (2.19)$$

In PHOENICS the boundary conditions impose the values of k and ϵ obtained from these equations to the grid points along the walls.



$L*B*H_e = 32.0*8.0*3.28, Q=0.8\text{m}^3/\text{s}$
Indicated values of k range from zero to $0.003 \text{ m}^2/\text{s}^2$

Figure 2.8: Convection of k towards the bottom at the end of the re-circulation zone.

At the end of the re-circulation zone the velocity goes down. Consequently, u_* and the shear stress become small. According to the boundary condition for k given above, k then also becomes small. However, this is probably incorrect, because the convection of k (transport from the shear layer towards the bottom, see figure 2.8) is important and creates a larger k -value near the bottom. See for example (Hoffmans and Booij, 1994). The dashed lines in figure 2.8 indicate where the horizontal velocity is zero. Below the dashed line, at the right-hand side of the internal weir, the water flows back to the left. The point where the dashed line touches the bottom indicates the end of the re-circulation zone.

Non-equilibrium logarithmic wall functions

The assumption that the production of kinetic energy of turbulent motion is equal to its dissipation is not really valid under flow conditions with a re-circulation zone (like in storm water settling tanks). Launder and Spalding (1972) proposed logarithmic wall functions for non-equilibrium flow situations, which have been implemented into PHOENICS. The wall shear stress τ now is computed as $u_{*1}u_{*2}\rho$, in which u_{*1} is computed almost in the same way as u_* above (the difference is that in the y^+ computation u_{*2} is used) and u_{*2} is based on the local value of k :

$$u_{*2} = \sqrt{k\sqrt{C_{\mu D}}} \quad (2.20)$$

For the equilibrium situation u_{*2} equals u_{*1} . Now, the boundary condition for k does not fix k to the earlier presented equation, but solves the full transport equation for k in such a way so that the convective terms influence the result. Additionally, the boundary condition applies special conditions for the diffusion, dissipation, and production terms. The term representing the diffusion of energy to the wall in the k equation is set to zero. The production rate of k is computed with:

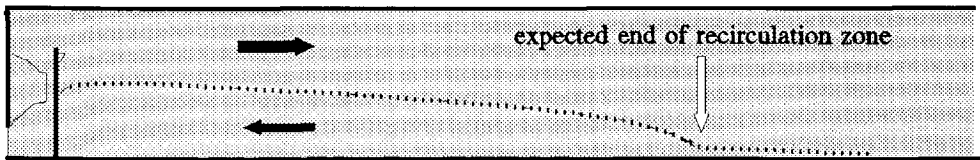
$$\text{Prod}(k) = u_{*2} \frac{u}{2y} \quad (2.21)$$

Furthermore, the boundary condition increases the dissipation by fixing it to:

$$\epsilon = \frac{C_{\mu D}^{\frac{3}{4}} k^{\frac{3}{2}} \ln(Ey^+)}{\kappa y} \quad (2.22)$$

To compensate for the convection of energy to the wall, this is a factor $\ln(Ey^+)/2$ larger than the dissipation in the equilibrium log wall boundary condition. For more information on this boundary condition, see (Launder and Spalding, 1972).

As the flow situation near the reattachment point is not in equilibrium, the non-equilibrium boundary conditions were expected to perform better. And indeed, the simulation results with this non-equilibrium boundary condition were better than those with the equilibrium boundary condition.



Negative horizontal velocities below the dotted line

$$L \cdot B \cdot He = 32.0 \cdot 8.0 \cdot 3.28, Q = 0.8 \text{ m}^3/\text{s}$$

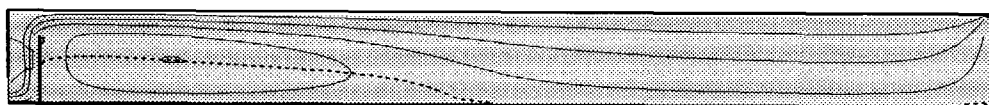
Figure 2.9: Non-realistic negative horizontal velocities near the bottom beyond the expected end of the re-circulation zone for the equilibrium boundary condition.

E.g., when the equilibrium boundary condition was used, some simulations resulted in a negative horizontal velocity in the cells near the bottom for a much longer part of the tank than when the non-equilibrium boundary condition was used. The re-circulation zone appeared much too long. See figure 2.9, in which the dotted line shows where the horizontal velocity is zero. At the right hand side of the expected end of the re-circulation zone (indicated by an arrow in the figure), the horizontal velocities in the cells bordering the bottom appeared directed to the left for some length. This is incorrect. The use of the non-equilibrium boundary conditions resulted in positive horizontal velocities beyond the expected end of the re-circulation zone.

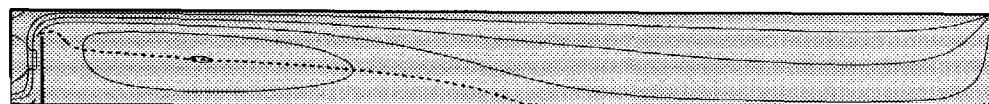
Restriction on logarithmic boundary condition

The first cell must be at a small distance from the wall to model the friction correctly. The cells near the wall have to be so small that at least some cells lie within the turbulent inner area. According to (POLIS), this means that the value of the dimensionless parameter y^+ (see page -25-) has to be between 30 and 130.

COARSE



FINE



$$L*B*He = 32.0*8.0*3.28, Q=0.8m^3/s$$

Figure 2.10: Streamlines for coarse and fine grid.

To comply with the requirement for y^+ the cells must be very small, which results in large computation times. To restrict the computation time to an acceptable level, a grid has been chosen that is so coarse that the value of y^+ was higher than 130. This means that the prescribed requirement (y^+ between 30 and 130) was not met. However, this seemed not to have a bad effect on the flow simulations. The difference between computations with a coarse and a fine grid (resulting in y^+ values within the required range) appeared to be only small. See, for example, figure 2.10, which shows the streamlines and indicates the recirculation zone for a flow simulation with a coarse and a fine grid. In addition also the values of the eddy viscosity were almost the same for simulations with a coarse and a fine grid (not shown in a graph).

When applying the non-equilibrium logarithmic wall functions, PHOENICS computes y^+ based on $u_{\tau 2}$. This choice is disputable. It could also be based on $u_{\tau 1}$. Since $u_{\tau 1}$ is smaller than $u_{\tau 2}$, this results in lower values of y^+ . The disadvantage of $y^+ = f(u_{\tau 1})$ is that it results in y^+ equal to zero at the end of the re-circulation zone because there the horizontal velocity and thus the values of $u_{\tau 1}$ go to zero. $y^+ = f(u_{\tau 2})$ does not have this disadvantage, see also figure 2.11, which shows the values of y^+

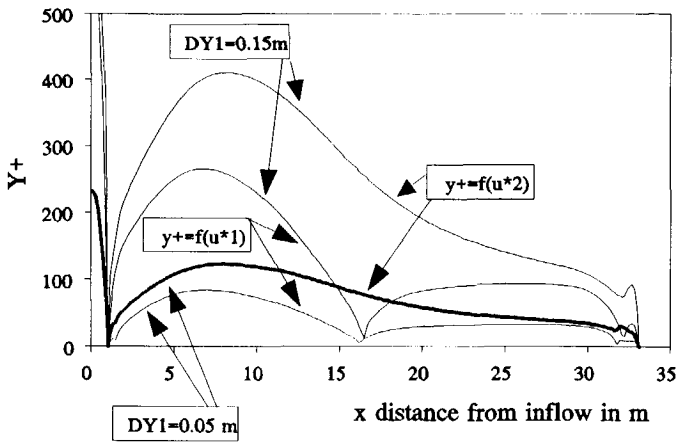


Figure 2.11: Values of y^+ for cells near the bottom of 5 and 15 cm high, computed in two ways.

computed with the coarse and the fine grid. The coarse grid consisted of cells of 0.15 m near the bottom. The values of y^+ are too high (> 130) for both $y^+ = f(u_{*1})$ and $y^+ = f(u_{*2})$. Consequently, the y^+ requirement is not met. The use of a finer grid near the bottom (with cells of 5 cm high) resulted in y^+ values within the required range for $y^+ = f(u_{*2})$.

Because the results of the simulations are so much similar for the case in which the requirement for y^+ was and was not met, it is assumed to be unnecessary to comply with the requirement for y^+ in these flow situations. The cells near the bottom can be coarser, like in the given computations.

2.4.3 Damping of turbulence at the water surface

Both the free surface computations and the rigid lid computations (see section 2.3) need a boundary condition to bring into account the damping of the eddies by the free surface. The size of the turbulent eddy's is restricted near the surface. In fact the size of the eddies in the vertical plane is restricted more than those the size of those in the horizontal plane, which makes the turbulence anisotropic. However, the turbulence has been assumed to be isotropic in the k - ϵ turbulence model. Consequently, no distinction is made between horizontal or vertical eddies. To take this damping into account the dissipation of turbulent kinetic energy ϵ is given a minimum value, so that ν_t cannot become too high. Rodi (1980) proposed the following boundary condition for ϵ near the water surface.

$$\epsilon = \frac{(\sqrt{C_{\mu D}} k)^3}{\kappa(y + ah)} = \frac{C_{\mu D}^{\frac{3}{4}} k^{\frac{3}{2}}}{\kappa ha} \cdot \frac{1}{1 + \frac{y}{ah}} \quad (2.23)$$

y = distance to surface

$a = 0.07$

For a boundary condition at the water surface ($y=0$), this equation fixes ϵ to a value of $1/a$ times the equilibrium value: u^3/kh . For a boundary condition at a small distance from the water surface, it fixes ϵ to a smaller value. Computations with and without this boundary condition resulted in important differences in the values of the eddy viscosity near the water surface. A correct value for the eddy viscosity is expected to be important to predict the distribution of settling particles in the water, because the eddy viscosity determines the diffusion (Reynolds analogy).

This boundary condition has been derived for a uniform free surface flow. Only the flow behind the re-circulation zone is comparable to such an equilibrium flow situation. In the complex flow situation, as occurring during filling of the tank and in the jet flow on top of the re-circulation zone, this boundary condition might not be valid. However, no other relation was found. In order to take into account at least some damping of the turbulence due to the water surface, this boundary condition has been applied nevertheless. During filling, the water depth will be small, and the minimal damping will be larger than for a full tank.

The boundary condition is only activated when the local ϵ value is below the value according to the given equation⁽⁸⁾. Consequently, the equation gives the minimum ϵ value. As this boundary condition was not available in PHOENICS, software coding has been added. See Appendices G and H. In combination with the HOL method the boundary condition is slightly different. The extra ϵ boundary condition is implemented at the water surface, of which the position is computed. The boundary condition concerns the values in the middle of the cell. However, in the computations, the water surface is not always in the middle of the cell. The distance between the middle of the cell and the water surface would even be negative if the cell filling is less than 50%. In the computations of the ϵ boundary condition, the y value was assumed to be zero, as if the water-air interface is always in the middle of the cell.

2.4.4 Outflow

Initially, the model extended for some cells downstream of the external weir. However, for time-varying flow situations (i.e. with a free water surface), this induced problems with the outflow of water and air (Kluck, 1993). To obtain reliable results with the free surface method (HOL-method), the outflow boundary condition was moved to the cells on top of the external weir. At that point the outflow could successfully be given using a relation between the water depth on top of the weir and the outflow rate.

To that purpose, the outflow boundary stretches out over a few cells located above one another, as in figure 2.12. The water level at this vertical is computed by the free surface method. The amount of water flowing out is fixed to the following equation:

$$Q = C * B * h_d^{\frac{3}{2}} \quad (2.24)$$

with

h_d = difference between the upstream water level and the weir crest. See figure 2.13.

B = width.

C = constant.

⁽⁸⁾ When no boundary condition is given mirroring conditions apply.

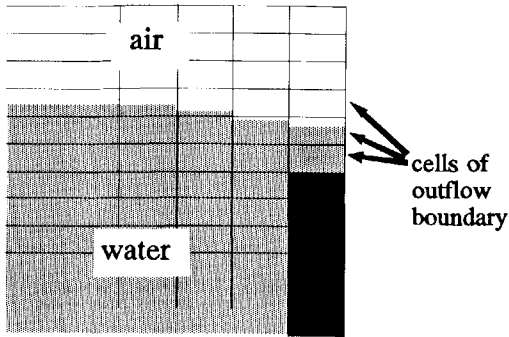


Figure 2.12: Location of outflow boundary on top of weir.

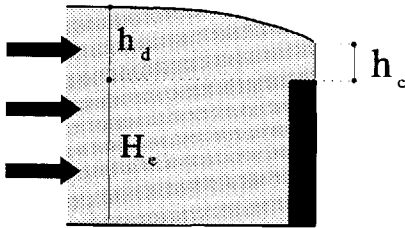


Figure 2.13: External weir.

For a sharp crested weir the constant is equal to 1.86. According to Franke (1980) the water level just above the weir crest h_c is 85% of the upstream water level h_d (in case that $h_d \ll H_e$). In practice, in storm water settling tanks this restriction is sufficiently met. Consequently, the flow rate will be:

$$Q = 2.3 * B * h_c^{\frac{3}{2}} \quad (2.25)$$

The shape of the weir crest influences the value of C. For a weir with a flat top the constant has to be increased by the following empirical factor (Franke, 1980):

$$f = 0.70 + 0.85h_d/w,$$

with w representing the width of the crest of the weir. In practice, this width in storm water settling tanks is 10 to 20 cm. Consequently, the factor f will be about 1.0. Therefore, the value 2.3 has been chosen for the constant C.

The boundary condition is imposed iteratively. The flow rate of the outflowing water is based on the water level and the water level is based on the inflow and the outflow of the column. Within the available iterations per time step, these variables reach a final value.

Next, the outflow velocity is fixed at $Q/(B.h)$, in which h is the water depth above the weir. This boundary condition for the velocity applies for the full height of the outflow boundary. The water level does not reach the top of the outflow boundary⁽⁹⁾, like in figure 2.12. For the remainder of the height, air will also flow out with the water.

For a rigid lid computation the outflow is implemented by giving a fixed pressure in the cells above the external weir, so that the water can flow out freely. All the pressures are computed relative to this pressure. It is emphasised that all rigid lid computations will be steady computations. In order to correctly bring into account the effect of variations in the flow, the free surface method must be used.

The relation between Q and h (equation 2.24) is valid for the steady state. In the way it is implemented as a boundary condition, it is however also applicable for transient situations.

2.4.5 Top boundary condition

If the free surface computation is simplified to a rigid lid computation, then the rigid lid is the top of the model. The boundary condition for ϵ has been explained in section 2.4.3. For the other variables, mirroring boundary conditions apply, which means that there is no exchange. For the HOL computations the top of the whole flow domain is used to impose a fixed pressure, so that the air can flow in and out freely.

⁽⁹⁾ In fact, the relation between Q and h is valid for free overflow situations, so the boundary condition is only valid if the water level falls within the cells of the boundary condition.

Chapter 3

CALIBRATION OF FLOW MODEL

With the elements of Chapter 2, the flow in storm water settling tanks can be computed. Section 3.1 presents an example of the flow in the equilibrium situation and an example of the filling of a tank. The flow model has to be validated to ensure that the model works properly for the flow problems under consideration. This is important because of the many assumptions made in setting up the model. In general, a model is a simplification of reality. Some of the processes are not, or only partly, incorporated in the model. This might be due to lack of data and knowledge or because of computational reasons. Even though for the simulations an existing CFD package has been used, and flow simulations are not new, the proper functioning of the model in this specific case needs validation.

Reasons why the flow according to the simulations might differ from reality are:

- * For computational reasons, the cells have been taken large, which makes numerical viscosity important.
- * The eddy viscosity is assumed to be isotropic, resulting in isotropic turbulence. However, in reality turbulence is not isotropic.
- * The boundary condition for ϵ at the water surface has been set up for equilibrium flows in a channel. Only downstream of the re-circulation zone flow conditions are similar to such flow situations. Nevertheless, the boundary condition has been applied in the whole tank and also during filling.
- * In simulations of the steady state, the location of the water level has been fixed at the top of the flow domain (rigid lid computation).

To investigate whether these simplifications are allowed and the flow simulations sufficiently accurately describe reality, the effects of the simplifications have been studied and the simulation results have been compared with measurements.

Section 3.2 presents the effect of the simulation of the water surface by a rigid lid for steady state situations. To study the effect numerical viscosity due to the use of a coarse grid, also simulations

with a finer grid have been carried out. As a very fine grid is not feasible for the whole research, only some specific cases have been worked out more accurately. See section 3.3.

The comparison of the simulation results with measurements can prove that the simulations sufficiently represent reality. In theory, different kind of measurements might be used; measurements of the real flow in real tanks and measurements in scale models of storm water settling tanks. No measurements of the flow in real storm water settling tanks are available. Such measurements are expensive, and for that reason, have not been carried out. One of the problems is that it's uncertain when an overflow will occur, which means that measuring devices will have to be operational permanently for an extended period. In case of an overflow the measurements have to be carried out in a short period. This, in practice, results in failure of the devices at critical moments. And even if such measurements were available, it's still extremely difficult to calibrate the model on a time dependent flow situation.

For the calibration of the flow model set up with PHOENICS, measurements from a scale model of a storm water settling tank are available (Kluck, 1994). See section 3.4 The use of modified forms of the $k-\epsilon$ turbulence model appeared to affect the simulations results. See section 3.4.3. The flow in the experimental setup appeared to be a 3-dimensional one (section 3.4.4), which makes it less suitable for calibration purposes. To investigate the pros and the cons of the different forms of the $k-\epsilon$ turbulence model (provided within PHOENICS), also additional measurements have been used. The measurements on a backward facing step carried out by Tropea with a Laser Doppler Anemometer (Tropea, 1982) are suitable and have been used to calibrate the flow model (section 3.5).

3.1 Simulation results

As examples of flow simulations, this section presents both simulation results of the steady state, and the filling of a rectangular storm water settling tank. In these simulations, the flow situation is assumed to be a 2-dimensional one. The 3-dimensional effects will be discussed in section 3.4.4. The tank dimensions and the loading have been arbitrarily chosen from the wide range of possibilities in the Netherlands: a rectangular tank of 30 m, with an internal weir of 2.46 m high and an external weir of 3.30 m. The flow domain has been divided into 221×22 cells of about $15 \times 15 \text{ cm}^2$, see figure 3.1.

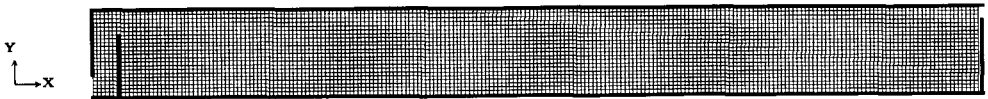


Figure 3.1: Grid of cells of about $15 \times 15 \text{ cm}^2$.

The results of the simulations seem realistic for the steady state flow situation. See figure 3.2, which presents the flow in the equilibrium stage. Just before the external weir a second recirculation is computed. In this free surface computation the flow of both water and air has been simulated. The horizontal line just above the crest of the external weir, indicates the water surface. The figure presents the flow of water by means of stream lines. The flow of the air is not presented in the graph.

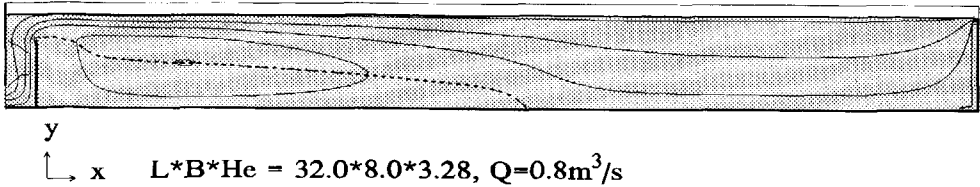


Figure 3.2: Streamlines in water. The dashed line indicates the re-circulation zone.

This computed flow situation is as expected. Only the length of the re-circulation zone is a bit short; 6.7 times the height of the internal weir. According to Tropea (1982), Booij (1992), and observations in a scale model, this should be between 7 and 9. Reasons for this difference are the grid size and the turbulence modelling, which are discussed in the next chapter. The computations showed that the value of y^+ in the cell bordering the wall is not small enough. In section 2.4.2 it has been explained that this is acceptable.

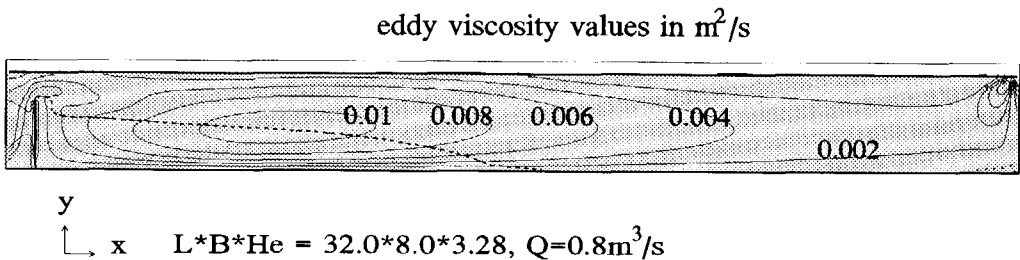


Figure 3.3: Eddy viscosity in stationary flow situation.

Figure 3.3 presents the values of the eddy viscosity. The highest values appear in the mixing layer of the re-circulation zone and at the inflow. Subsequently they are transported in the downstream direction. Without the ϵ boundary condition at the water surface (see section 2.4.3), the highest values would appear along the water surface.

Figure 3.4 gives the streamlines, the zero-line for the horizontal velocity, and water levels for the filling of the tank with a lay-out as presented in figure 2.5. The water falling over the internal weir creates a re-circulating flow turning anti-clockwise. When the internal weir becomes drowned, the re-circulating flow turns to clockwise. Next, the length of the re-circulation zone grows to a length of almost 6 times the height of the internal weir, which is the equilibrium situation.

In order to determine if the results are trustworthy they have to be validated by means of comparison to measurements.

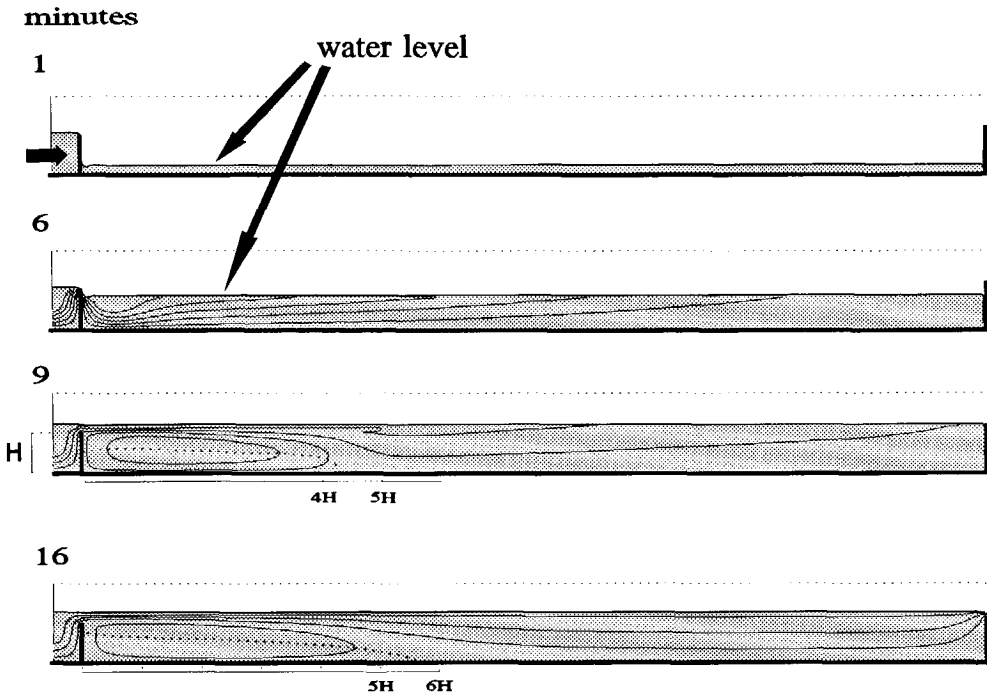


Figure 3.4: The filling of a rectangular tank.

3.2 Rigid lid

The use of the rigid lid to represent the water surface for flows in the equilibrium stage, gives a 10 fold reduction of the computation time⁽¹⁰⁾. The results are almost the same as for the simulation with the computation of the location of the water-air interface. Compare figure 3.5 (rigid lid simulation) to figure 3.2 (free surface simulation).

⁽¹⁰⁾ The reduction is so much because with the free surface simulation the time dependent flow is computed until an equilibrium flow situation is reached, whereas with the rigid lid computation the final situation is computed within one time step (steady computation).

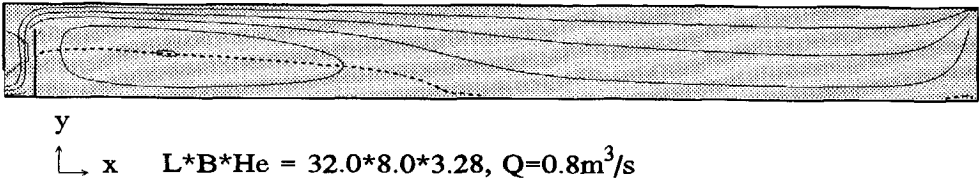


Figure 3.5: Stream lines according to simulation with rigid lid.

The length of the re-circulation zone computed in the rigid lid computation is a bit shorter than for the free surface simulation: 6.2 times the height of the internal weir instead of 6.7 times the height. Also the values of the eddy viscosity are almost equal. Compare figure 3.6 (rigid lid simulation) to figure 3.3 (free surface simulation). As the results are almost equal, the time consuming free surface simulation is concluded not to be necessary if only the final steady-state flow situation is of interest. However, to simulate the filling of a tank and to bring into account the effect of changes in the flow rate, a free surface computation must be made.

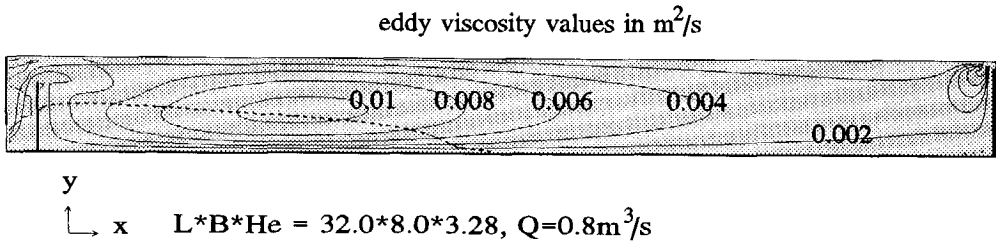


Figure 3.6: eddy viscosity in rigid lid computation.

3.3 Grid dependence and numerical viscosity

In order to solve the transport equations, PHOENICS makes the equations discrete by means of an implicit hybrid upwind scheme (see Appendix I). This scheme is for the most part a fully upwind scheme. The discretisation is an approximation of the transport equations and introduces errors in the solution. Appendix I shows that the error is for the most part similar to a diffusion term, since it can be written as coefficient times the second derivative to space of the velocity. The coefficient of this term, the so called numerical viscosity coefficient ν_N is:

$$\nu_N = \frac{1}{2} u (\Delta L + u \Delta t)$$

in which u denotes a velocity, ΔL the distance between two cell centres in the direction of the velocity, and Δt the time step. For steady state situations the term with Δt is not present. The value of the coefficient ν_N depends on the direction considered. In the flow simulations, the largest velocities occur in the x -direction, which is the main flow direction. For uniform grids this coefficient will therefore be largest in this direction. However, the error introduced by the numerical viscosity is more important in the transverse direction than in the main flow direction.

This is due to the following: the transport due to numerical viscosity in the main flow direction is small compared to the convective transport, which is of course largest in the main flow direction. In the transverse direction the transport due to numerical viscosity is smaller, but the convective transport might even be absent, so that the transport due to viscosity might be very important.

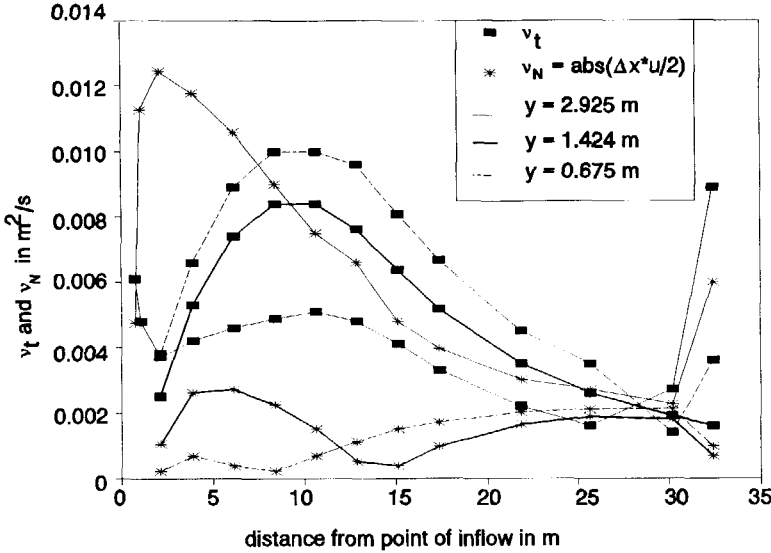


Figure 3.7: Coefficients of numerical and turbulent viscosity for coarse grid.

When ν_N is much smaller than the eddy viscosity, the effect of numerical viscosity is negligible. To obtain some insight into the importance of the numerical viscosity, ν_t has been compared to ν_N for the x-direction. It is noted that the eddy viscosity as computed by the $k-\epsilon$ turbulence model is isotropic, whereas ν_N is not. ν_N is largest in the direction of the velocity vector and zero perpendicular to it. Since the x-direction is the main flow direction, ν_N will be largest in that direction, and comparing ν_N in that direction with the eddy viscosity will provide some insight in the importance of the numerical viscosity. With cells of 0.15 m and a velocity of 0.05 m/s this coefficient is 0.0038 m^2/s . This is significant compared to the viscosity due to turbulence, because in the prototype the value of the eddy viscosity, which represents this viscosity, is between 0.001 and 0.01 m^2/s . Figure 3.7 shows that values of the coefficient of the numerical viscosity, ν_N , can be important compared to ν_t . The figure presents ν_t and ν_N at 3 different heights in the tank (for the same flow situation as in Chapter 2). The tank is 3.3 m deep.

The largest values of ν_t occur in the middle of the re-circulation zone (dashed line). The values of ν_N are considerably smaller than ν_t for the bottom and the middle (heavy and dashed lines) in the left side half of the tank. Behind the re-circulation zone, ν_N and ν_t become equally important. Near the water surface (solid line), ν_N is even larger than ν_t . The use of a finer grid will reduce the numerical viscosity. When the cell lengths and heights are halved, ν_N halves as well. Computations with a finer grid resulted in a more or less similar flow situation. This has already been shown in Chapter 2 (figure 2.10) which presents the streamlines and the re-circulations zone for the coarse

and the fine grid). The coarse grid consists of 221×22 almost uniform cells of $0.15 \times 0.15 \text{ m}^2$. The fine grid consists of 442×44 cells of $0.075 \times 0.075 \text{ m}^2$.

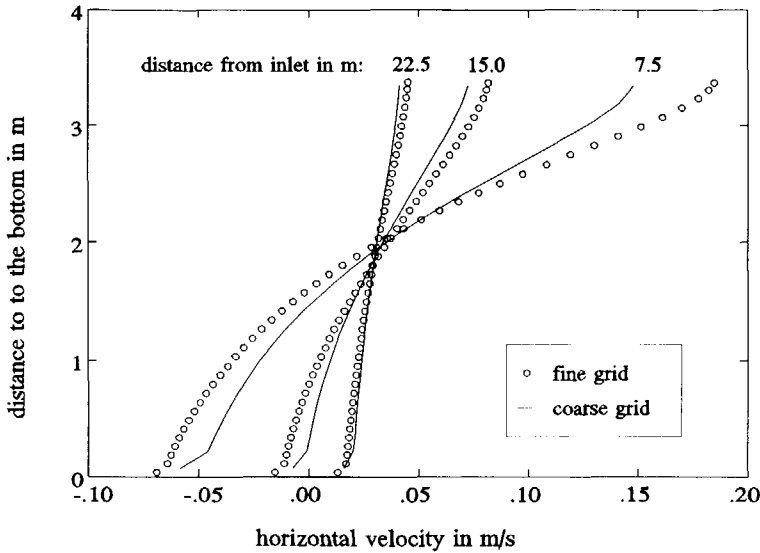


Figure 3.8: Horizontal velocities at three cross sections computed with a coarse and a fine grid.

To reach a sufficiently converged flow situation, the computation times were 40 minutes and 300 minutes at the workstation for the coarse and the fine grid respectively. To carry out many computations the very fine grid is of course prohibitively time consuming.

The length of the re-circulation zones are $6.2 \cdot H$ and $7 \cdot H$ for the coarse and the fine grid respectively. This length has been computed as the distance between the internal weir and the position of the zero velocity in bottom row of cells. Because the first cell in the fine grid is closer to the bottom than in the coarse grid (0.0375 m versus 0.075 m), the difference in the length of the re-circulation zone might be flattered compared to the results obtained with the coarse grid. Therefore, for the fine grid, the length of the re-circulation zone based on the horizontal velocity in the second cell from the bottom has also been computed. In the second cell (at 0.0875 cm from the bottom), the horizontal velocity is zero at about 6.5 times the height of the internal weir. Thus, at 0.075 m from the bottom (which is equal to the height of the first cell centre in the coarse grid), the horizontal velocity will be zero somewhere between 6.5 and 7 times H behind the internal weir. The difference in the length of the re-circulation zone is acceptable for the purpose of the flow simulations in this research (i.e. comparing the functioning of different storm water settling tanks).

Figure 3.8 presents the horizontal velocities at a distance of 7.5, 15 and 22,5 m from the inlet for the coarse and the fine grid. The y-axis denotes the distance to the bottom. The differences are considerable, but small enough for the purpose of this research. This decision was influenced by the fact that the particle settling is not very sensitive to variations in the flow, as will be shown in the following chapters. Figure 3.9 gives the values of v_1 for the same cross sections. The values of v_1 computed with the fine grid are higher than for the coarse grid. The importance of the

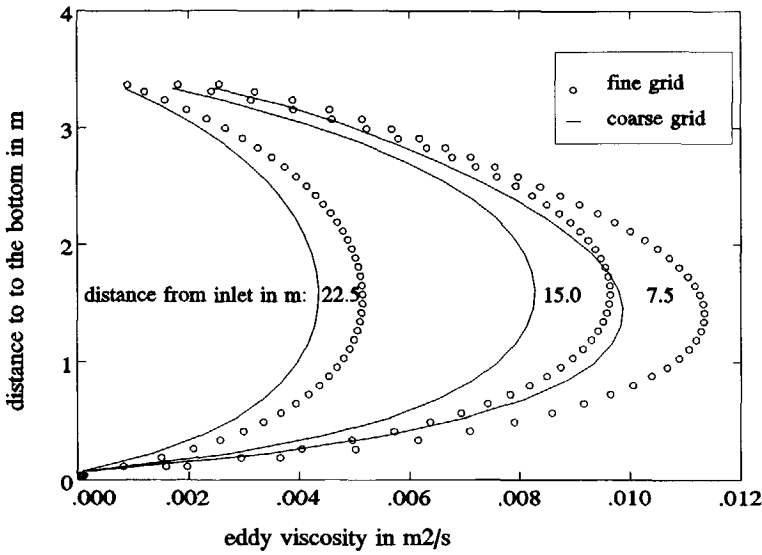


Figure 3.9: Values of the eddy viscosity at three cross sections computed with a coarse and a fine grid.

numerical viscosity can be represented by the ratio of the coefficient of the numerical viscosity ν_N and ν_t . A high value of this ratio indicates that numerical viscosity is important compared to viscosity due to turbulence. For two reasons, this ratio is smaller for the fine grid. ν_N is half of that in the coarse grid, and the values of ν_t are higher than those for the coarse grid.

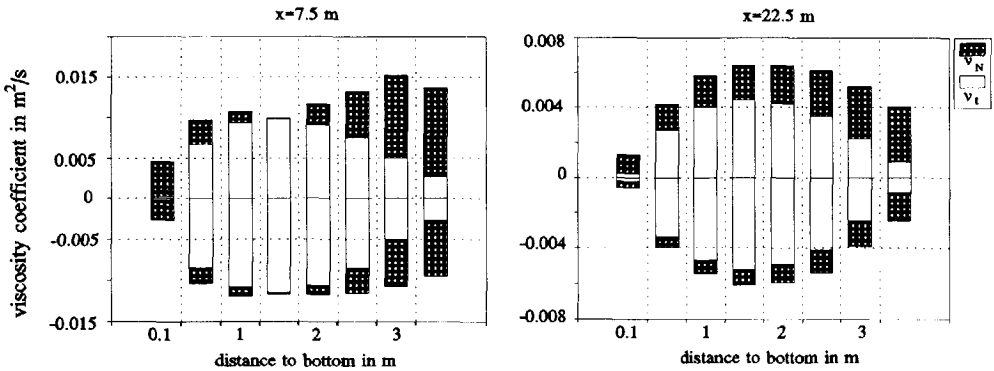


Figure 3.10: Viscosity coefficients ν_N and ν_t at $x = 7.5$ and 22.5 m, for the coarse grid, and the values of those variables multiplied by -1.0 for the fine grid.

The viscosity is based on the summation of ν_N and ν_t . Figure 3.10 shows that the values of the total effective viscosity, i.e. $\nu_N + \nu_t$, are almost equal for the coarse and the fine grid. Behind the re-

circulation zone the flow is almost completely in the x-direction. The viscosity terms will be only small, because the second derivatives to space of the horizontal velocities will be small.

The fact that the results of the simulations with the coarse and the fine grid are so similar could also indicate that the viscosity is insignificant compared to the convective transport.

3.4 Measurements in a scale model

A scale model of a storm water settling tank is useful to study in detail the flow in a storm water settling tank. The inflow is known and can be regulated, so that the effect of certain changes can be investigated. Measurements of the flow can be used to validate the flow simulations. For that purpose, the flows in the scale model have been simulated. It is expected that if the flow in the scale model can be simulated correctly with PHOENICS, then also the flow in real tanks can be predicted.

Only steady state flow conditions have been considered. It is not feasible to validate the model for a time dependent flow. Such a flow requires the handling of very much data. At several time intervals the flow velocity and the turbulence parameters would have to be observed at representative points in the whole flow field. The validation of simulation results with such measurements is far more complicated than the validation on an equilibrium flow situation. Next, because only one probe was available to measure the velocities in the required directions, it was impossible to measure at more than one point at the same time.

3.4.1 Experimental setup

Figure 3.11. presents the scale model as set up in the Hydromechanics Laboratory (Hydraulics Department of the Delft University of Technology). It represents a tank of $30.4 * 8 * 2.5 \text{ m}^3$ at a scale of approximately 1:8. The width of the flume is 1.02 m. The other dimensions are given in the figure. The water enters the flume near the bottom on the left. To facilitate the validation of the model and to limit the amount of data to be processed, a 2-dimensional flow situation was desirable. To that end, damping material was placed near the inlet, so that the inflow was as uniform as possible, and consequently, the flow conditions in the tank as 2-dimensional as possible. Jandard (1994) gives a more elaborate description of the experiments.

In this flume, five flow situations with various flow rates and heights of the weirs have been investigated. See table 3.1. Situation 5 is the flow with a diffusor just behind the internal weir, for an inflow of 30 l/s and weirs as in Situation 1.

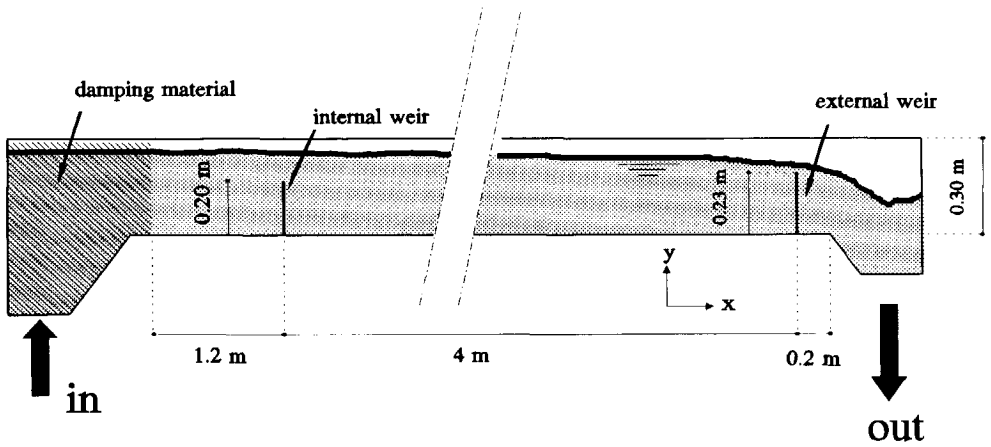


Figure 3.11: Experimental setup.

Table 3.1: Comparison of flow situations in flume and prototype.

	investigated conditions				Example for prototype
	1 & 5	2	3	4	
H_i (m)	0.20	0.20	0.14	0.14	2.0
H_c (m)	0.23	0.23	0.17	0.17	2.4
Q (m^3/s)	0.030	0.015	0.030	0.015	1.0
h (m)	0.30	0.27	0.24	0.21	2.6
u_{avg} (m/s)	0.10	0.06	0.13	0.07	0.05
L/H_i (-)	20	20	29	29	16
Re (-)	20,000	10,000	20,000	10,000	80,000
Fr (-)	0.005	0.002	0.009	0.003	0.0002

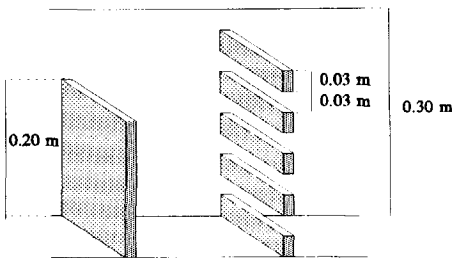


Figure 3.12: Diffusor behind internal weir in experimental setup.

The weirs consisted of 1.8 cm thick wooden plates. The diffuser consisted of horizontal bars of 3 cm high and 1.8 cm thick and was located 20 cm downstream of the internal weir, perpendicular to the main flow direction. Between the bars the gaps were 3 cm high. The first 3 cm from the bottom were closed. See figure 3.12.

The flow situations have been chosen in such a way that:

- * the Reynolds number and the Froude number are of the same order of magnitude as in the prototype (full scale tank). It is emphasized that the exact value is of no importance. Definitions of these numbers have been given in Appendix B;
- * the ratio of the height of the internal weir and the length of the flume is about the same as in the prototype;
- * the measuring device can measure the velocities sufficiently accurately.

The flow conditions in the flume have been compared with a flow through the prototype with an inflow of $1 \text{ m}^3/\text{s}$. As can be seen in table 3.1 the flow situations in the flume correspond reasonably well to the flow in the prototype.

Kluck (1994) gives an elaborate description of the experiments and the measurements carried out.

An Electromagnetic velocity meter (EMS) has been used to measure the velocities in the main flow and in the vertical direction. From the (turbulent) fluctuations in time of these velocities the turbulent kinetic energy could be estimated. To measure in the horizontal-vertical plane, only one EMS was available. Consequently, to get a complete picture of the flow, in each flow situation, measurements had to be carried out in many different places, one after another. At each location, the velocities were recorded for 10 minutes with a sample frequency of 10 Hz. This frequency appeared to be high enough to record the turbulent fluctuations of the velocities. In fact, to level out the slow flow fluctuations, a duration of 10 minutes appeared slightly short in order, but longer durations of the measurements would have taken too much time.

At five different heights in the middle and at both sides, measurements have been carried out in the centre plane (halfway the width). The inflow was measured at 47 cm before the internal weir. The velocity appeared to be higher near the surface. This can be explained by the shape of the damping material before the internal weir, which was thinner near the surface. This, unfortunately, might influence the flow behind the internal weir. At five or seven different distances from the internal weir, and at five or seven different heights, the velocities in the flume were recorded. In the following sections, some of the results are presented together with the computational results. To check if the flow was indeed 2-dimensional some extra measurements over the cross-section have been made, see section 3.4.4.

3.4.2 PHOENICS model of the experimental setup

Using PHOENICS, the five measured flow situations in the flume (see table 3.1) were simulated. The mathematical model is 2-dimensional. The water level is represented by a rigid lid⁽¹⁾.

⁽¹⁾ As presented in section 3.2, computations with and without a free-surface resulted in almost the same flow situations for the steady state situation.

3.4.3 Analysis of measurements and computations

For situation 1, figure 3.13 presents the measured and computed velocities at eight cross sections in the middle of the tank. The figure gives the horizontal velocities relative to the dashed vertical lines, which represent the zero values and the locations where the measurements were undertaken. The results show that the computations predict the flow reasonably well. The largest deviations between simulations and measurements appear in the mixing layer between the re-circulation zone and the main flow. The length of this zone is computed too short and the computed vertical gradient of the horizontal velocities (du/dy) is too small in the mixing layer. This indicates that the exchange rate of impulse is too high and thus that too much viscosity is computed. With the exception of the re-circulation zone the computations match the measurements reasonably well.

The k values have been calculated from the measured velocities. The turbulent kinetic energy is a function of the turbulent fluctuations in the velocities of the x -, y -, and z -direction (respectively u' , v' , and w').

$$k = \frac{1}{2}(\overline{u'u'} + \overline{v'v'} + \overline{w'w'}) \quad (3.1)$$

Because velocities in the z -direction (horizontal, perpendicular to the main flow direction) were not available, $w'w'$ had to be estimated. According to Nezu (1993):

$$\frac{\overline{u'u'}}{2k} \approx 0.55, \quad \frac{\overline{v'v'}}{2k} \approx 0.17, \quad \frac{\overline{w'w'}}{2k} \approx 0.28 \quad (3.2)$$

Consequently,

$$\overline{w'w'} \approx \frac{1}{2.6}(\overline{u'u'} + \overline{v'v'}) \quad (3.3)$$

Figure 3.14 gives the turbulent kinetic energy in the same way as the velocities have been given in figure 3.13. In the shear layer on top of the re-circulation zone the computed values of k are far too high. This corresponds to a high turbulence intensity and therefore a high eddy viscosity and much viscosity by turbulence. As a result of this, the velocity profiles are rather smooth. After the re-circulation zone the measurements and the computations better correspond.

Kluck (1994) gives similar figures for the other flow situations. For situations 2 through 4, the computed re-circulation zone is also always shorter than the measured one. As in situation 1, the computed viscosity is too high in the shear layer on top of the re-circulation zone.

For situation 5, the situation in which a diffusor wall was present, computations have been carried out with both a coarse and a fine grid. In both computations, the differences between the results of the computations and those of the measurements are large near the diffusor. The results correspond better downstream of the diffusor. The diffusor destroys the re-circulation zone, both in the measurements and in the simulations. The conclusion is that the mathematical model can satisfactorily simulate such flow situations.

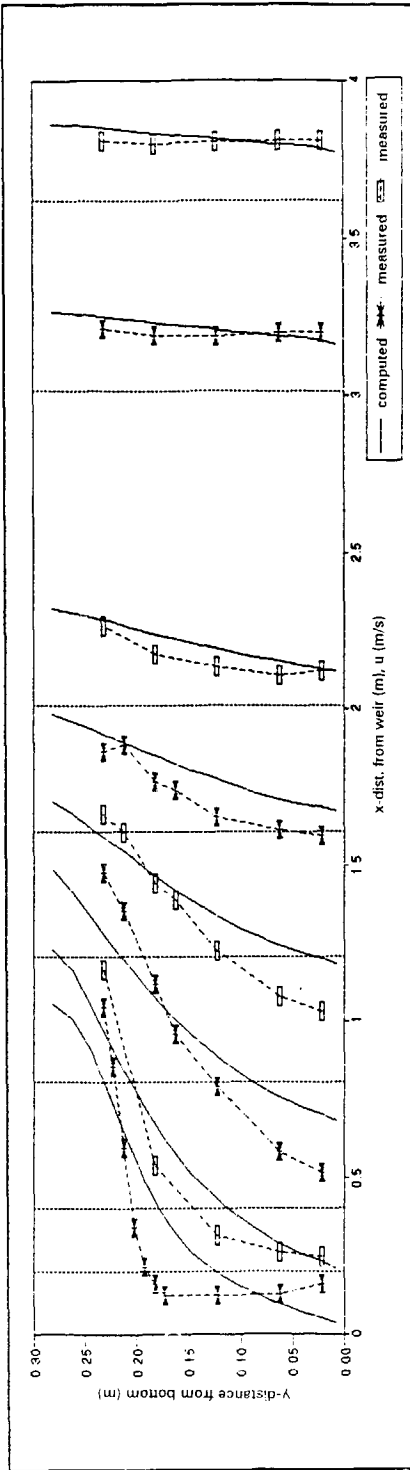


Figure 3.13: Computed versus measured horizontal velocities for situation 1.

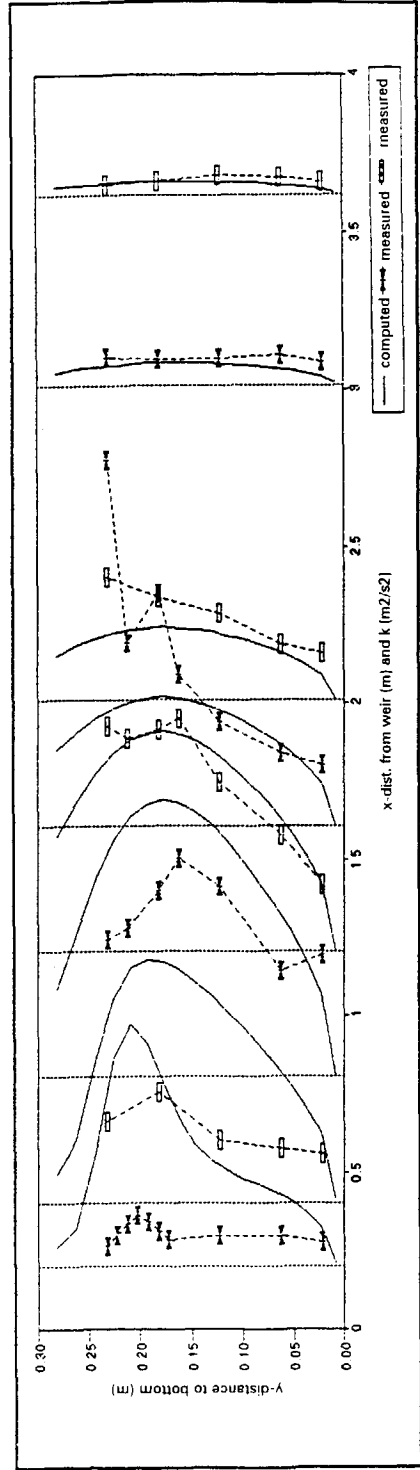


Figure 3.14: Computed versus measured turbulent kinetic energies for situation 1.

Reasons for the differences between the results of the measurements and the simulations are amongst others the deficiencies of the $k-\epsilon$ turbulence model. It causes too high eddy viscosities in the shear layer. Next to the standard $k-\epsilon$ model, a modified form of the $k-\epsilon$ model (provided in PHOENICS) has been used (see Appendix C). The Chen $k-\epsilon$ model was expected to better model the turbulence. For situation 2, figures 3.15 and 3.16 compare the measured data to two computations. The thin lines are the results of computations with the standard $k-\epsilon$ turbulence model, while the bold lines are the results of computations with the modified $k-\epsilon$ model (Chen). Just behind the internal weir in the re-circulation zone, the velocities computed with the modified form of the turbulence model are somewhat better. The turbulent kinetic energy in that area is also more consistent with the measurements. However, at the end of the re-circulation zone, the adapted model produces worse predictions than the standard $k-\epsilon$ model. The re-circulation zone becomes too long. Section 3.5 further discusses the effects of using a modified form of the turbulence model.

Differences between the 2-dimensional simulations and the measurements might also be caused by 3-dimensional effects of the flow.

3.4.4 3-dimensional effects

To simplify the mathematical model, and to save computational time the flow situations have been simulated with a 2-dimensional model. It was hoped for that the flow situation in the flume would be sufficiently 2-dimensional to allow a 2-dimensional simulation. It became clear from the measurements that this was not the case.

As can be seen in figure 3.13, all measured values at the centre are smaller than the computed values for $x = 1.6$ m (the fifth cross section from the left). This means that, according to the measurements, less water is passing through the centre-line than according to the computations. However, the mass balance of the computations is correct, because for an inflow of 30 l/(s.m), exactly 30 l/(s.m), passes. Near the inflow and the outflow the measured velocities in the mid of a cross section do result in an average flow of 30 l/(s.m), which was the flow rate in the model. This indicates that at $x = 1.6$ m more water is passing at the sides than in the middle, thus the flow is 3-dimensional. The measurements for situations 2, 3 and 4 show this same effect. Kluck (1994) gives a more elaborate description of the 3-dimensional flows.

PHOENICS model

A 3-dimensional flow simulation of flow situation 3 has been made. The main circulations of the flow in the experimental setup are in the vertical plane in the flow direction. For computational reasons it is advantageous to choose the z -direction perpendicular to this plane (i.e. horizontal). The x -direction has been chosen as the main flow direction and the y -direction is used for the vertical direction.

As the lay-out is symmetrical for the middle vertical plane of the flume, the flow domain can be restricted to one half (of the width) of the tank and is divided into $58*8*8$ cells (x - y - z). Friction was computed for all walls. In approximately 440 sec, 1000 sweeps (series of iterations over the whole flow domain) were carried out and convergence was reached.

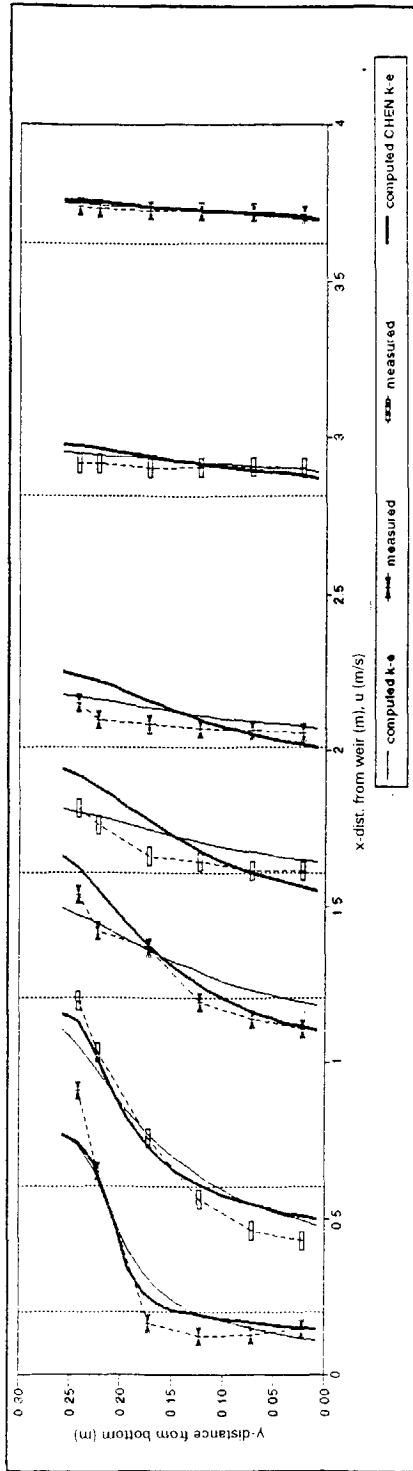


Figure 3.15: Computed versus measured horizontal velocities for situation 2.

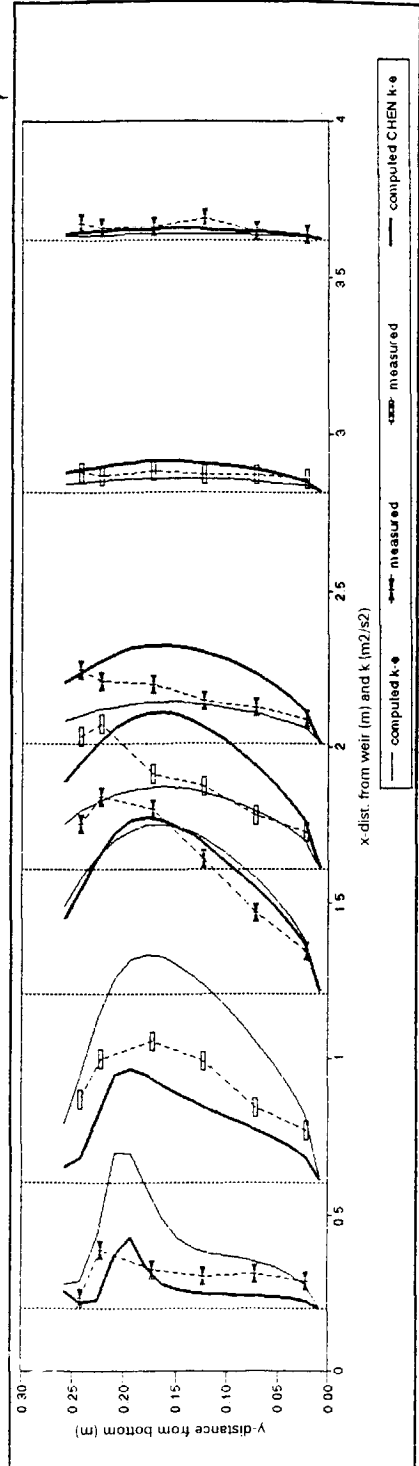


Figure 3.16: Computed versus measured turbulent kinetic energies for situation 2.

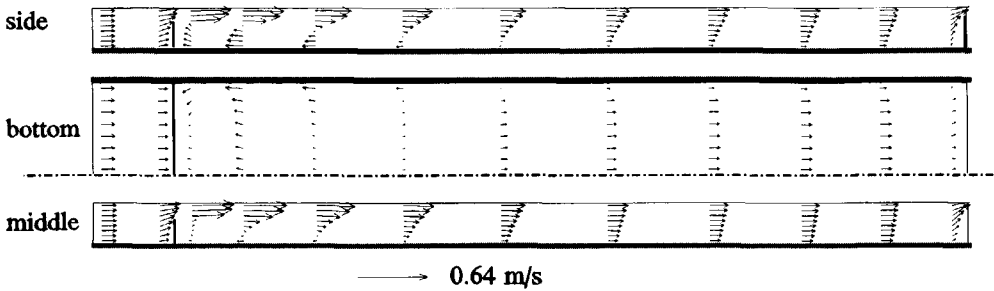


Figure 3.17: Top view of 3-D flow vectors in experimental setup as computed with a coarse grid and the Chen $k-\epsilon$ turbulence model.

The computations show a clear 3-dimensional flow situation. This flow is induced by the friction at the side wall, bottom and weirs. In figure 3.17 the flow in the experimental setup, as computed with a coarse grid and the Chen $k-\epsilon$ turbulence model, is visualized from above. The vectors of the middle plane are presented upside down. The re-circulation zone is shorter in the middle of the tank than at the side.

To check if the simulated 3-dimensional flow in one half of the tank has been computed correctly and is not merely a result of the computing methods, some extra simulations have been carried out. Firstly, the simulation of the flow in the 3-dimensional grid, without friction along the side walls, resulted in a correct 2-dimensional flow. Secondly, the simulation of the second half of the tank showed the expected mirrored result of the first half. Finally, the simulation of the flow in the full tank resulted in the expected flow situations.

Consequently, the 3-dimensional flow appeared not to be induced by means of the computing methods.

To check if the result was independent of the grid size, a model with a finer grid has been set up: $136 \times 12 \times 15$ cells in x -, y -, and z -direction. The velocities computed with a fine grid differ only slightly from those computed with model with a coarse grid. Thus, the coarse grid is fine enough.

Comparison with measurements

Outside of the centre plane of the experimental setup, an insufficient amount of measurements are available, and the results are too scattered to draw firm conclusions. Compared with the measurements, the computed flow in the re-circulation zone is too smooth: the vertical gradients of the horizontal velocities as computed with the coarse grid and the standard $k-\epsilon$ turbulence model are smaller than measured (like for the 2-dimensional simulations). See figure 3.18, which gives the computed and measured horizontal velocities at 60 cm after the weir. However at 120 and 160 cm behind the weir, the computations result in larger gradients than the measurements (also figure 3.18).

Conclusion

The 3-dimensional modelling of the flow in the experimental setup resulted in somewhat different horizontal velocities in the middle of the width than the 2-dimensional modelling of the flow. The measurements are too scarce to conclude if the simulated 3-dimensional flow is correct. The obvious 3-dimensionality of the flow in the computations is less obvious in the measurements. However, the velocities can be predicted fairly well. The turbulence variables could not be validated in this flow field, because the measurements were too scarce in the z-direction.

3.4.5 Conclusion of the flow modelling in the experimental setup

The flow in the experimental setup can be predicted quite accurately. However, the measurements are unsuitable for drawing firm conclusions. More accurate validation has been carried out based on more extensive measurements of the flow over a backward facing step.

It is expected (and hoped for) that the mathematical modelling of the flow in a real storm water settling tank can be predicted as well as these validated flow situations. This expectation is based upon the fact that the mathematical model consists of generally applicable transport equations. PHOENICS is widely used and tested for all kinds of flow situations. Furthermore, to obtain good resemblance with the measurements in these computations, only a few flow parameters and modelling options have been changed: turbulence model, grid size and level of k and ϵ at the inflow. The use of a modified form of the k - ϵ turbulence model resulted in an improvement of the simulations, but the general flow field is also predicted well by the standard k - ϵ model.

3.5 Flow over a backward facing step

Some extra data was required to validate the flow simulations. The flow over a backward facing step is appropriate. Although it's of a much simpler nature than the flow through a storm water settling tank, it shows two important flow characteristics also present in the flow in a storm water settling tank. These are the separated flow and the reattached flow. The separating point is fixed by the lay-out at either the top of the step or the top of the weir. The location of the reattachment point is undefined in both situations and has to be computed by the model.

3.5.1 Available measurements

The measurements on a backward facing step carried out by Tropea with a Laser Doppler Anemometer (Tropea, 1982) have been used to calibrate the flow model. A highly turbulent flow situation with a free water surface (situation II from (Tropea, 1982)) has been chosen, because it was most similar to the actual flow in storm water settling tanks. The height of the step, H , is 4 cm. The total depth is 33 cm. The average inflow velocity is 0.37 m/s. Measurements have only been carried out at the lower 12 cm of the flume. The following variables were measured:

- u = average horizontal velocity in the main flow direction,
- v = average vertical velocity,
- u'^2 = turbulent fluctuation of horizontal velocity,
- v'^2 = turbulent fluctuation of vertical velocity,
- $u'v'$ = turbulent shear stress.

This data has been used to discover which form of the k - ϵ model should be used to predict the flow with PHOENICS.

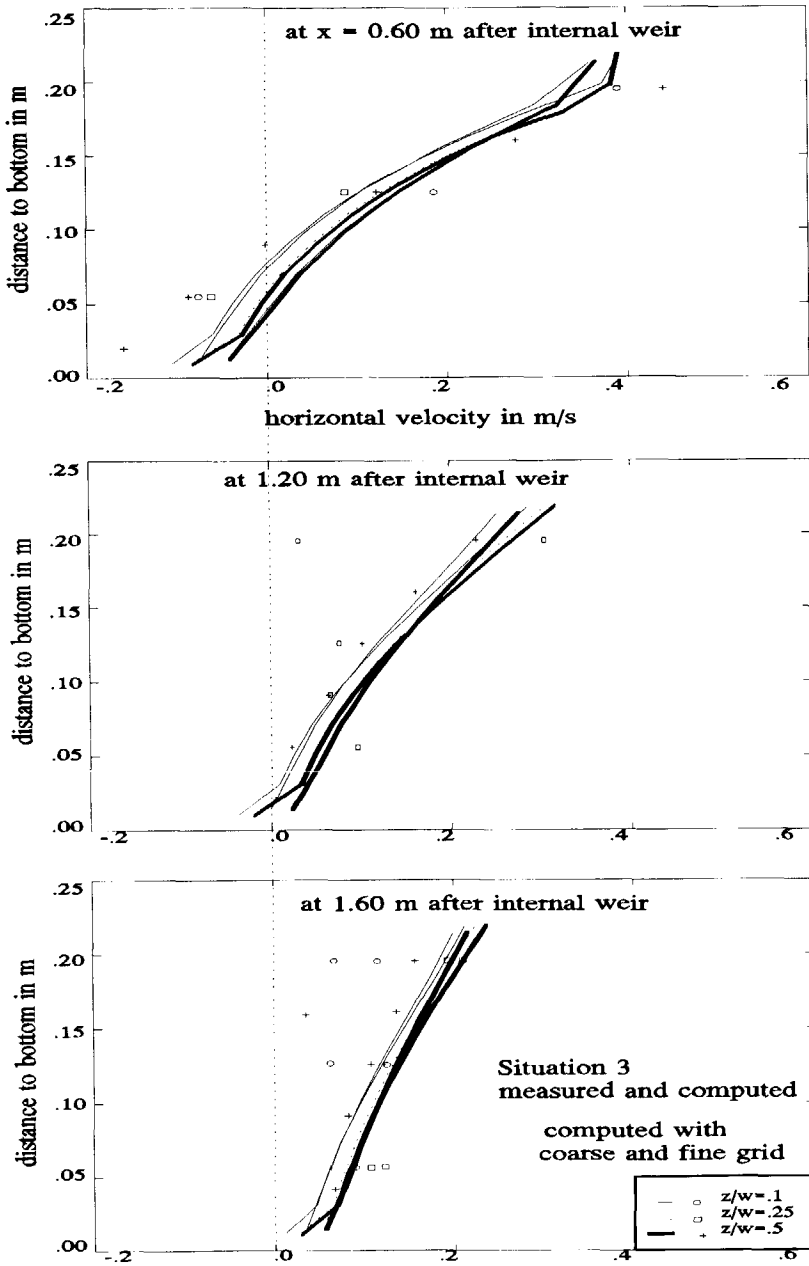


Figure 3.18: Measured and computed horizontal velocities for situation 3.

This flow situation is much smaller than that in a storm water settling tank. Because of this the largest structures of turbulence (eddies), will be a smaller than those in real tanks, whereas the smallest eddies are of the same size. Nevertheless this flow situation was used for the validation of the mathematical model.

3.5.2 The PHOENICS model

The flow situation over a backward facing step has been modelled with PHOENICS. The flow domain has been divided into 110*34 cells (horizontally*vertically). The left-side border of the flow domain is at 14 cm left of the step. The flow domain stretches for 160 cm after the step, so the total length is 174 cm. See figure 3.19. The upper boundary is a rigid lid, with the required boundary condition to simulate a free water surface (see section 2.5), at 0.33 cm above the bottom level after the step.

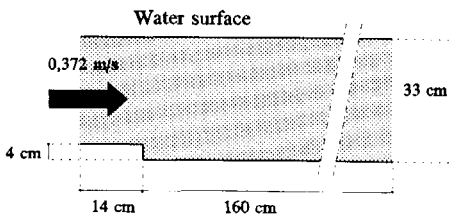


Figure 3.19: Flow over backward facing step.

The inflow is at the left (14 cm before the step) over the full depth. The mass and momentum inflow is the same as measured at $x = -4$ cm. This difference in location is allowable because the flow before the step is a free surface flow in equilibrium. The vertical velocity equals zero. The values of k at the inflow have been computed from the measured turbulent fluctuations of the velocities⁽¹²⁾ as $k = \frac{3}{4}(u'^2 + v'^2)$. For the values of the dissipation of turbulent kinetic energy at the inlet, Tropea (1982) proposes:

$$\epsilon = \frac{k^{\frac{3}{2}} C_{\mu D}^{\frac{3}{4}}}{\frac{h}{2} (0.14 - 0.08 \left(1 - 2\frac{y}{h}\right)^2 - 0.06 \left(1 - \frac{y}{h}\right)^4)} \quad (3.4)$$

This equation estimates a length scale of the eddies (the nominator in equation 3.4) out of the distance to the bottom y and the depth h , and uses this length scale to estimate ϵ at the inflow via

⁽¹²⁾ Which implies that $w'w' = 1/2(u'^2 + v'^2)$. This is almost the same as promoted by Nezu, see section 3.4.3.

$$\epsilon = \frac{k^{\frac{3}{2}} C_{\mu D}^{\frac{3}{4}}}{L} \quad (3.5)$$

The outflow boundary at the right over the full depth is a hydrostatic pressure. The water can flow out freely. At the bottom the standard PHOENICS wall functions have been used (non-equilibrium log wall function).

Next to the standard $k-\epsilon$ model, some modified forms of the $k-\epsilon$ model have been used to compute the turbulence: Chen, and RNG, as discussed in Chapter 2.

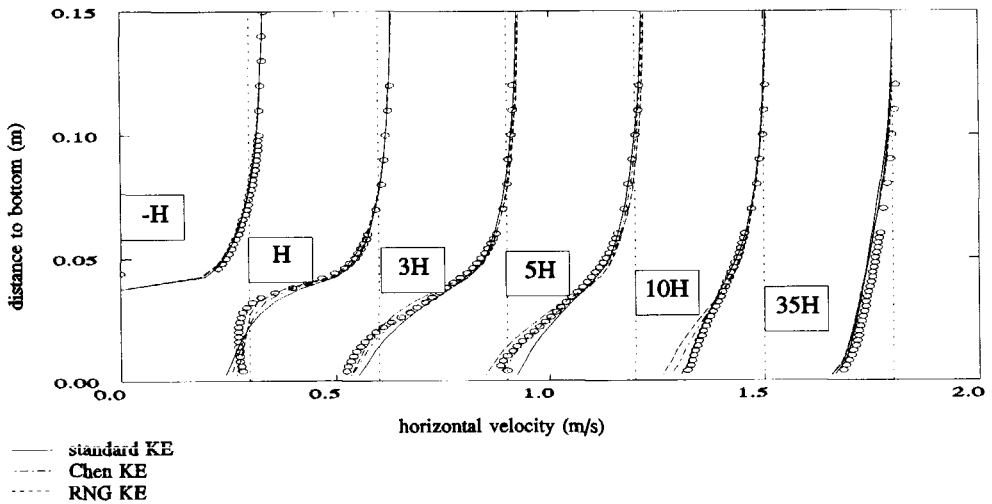


Figure 3.20: Horizontal velocities in a flow over a backward facing step as measured by Tropea and computed with different turbulence models.

3.5.3 Discussion of the results of the computations

The computed length of the re-circulation zone is shorter than the measured length, which is between 5^*H and 6^*H . The flow fields are in reasonably good agreement with the measurements for all computations with the different forms of the $k-\epsilon$ turbulence model. See figure 3.20. The simulation with the standard $k-\epsilon$ model computes the shortest re-circulation zone: 4.3^*H , which is shorter than the measured length. The model with the RNG $k-\epsilon$ version overestimates the length of the re-circulation zone: 8.2^*H . The Chen modification resulted in a length of 5.4^*H .

It is just behind the step that the velocities of the RNG model fit the measurements best. It is after the re-circulation zone that the velocities computed with the standard $k-\epsilon$ model are closest to the measurements. However, this is not so important because there the differences in velocities computed with the different models are negligible. The Chen modifications result in intermediate values.

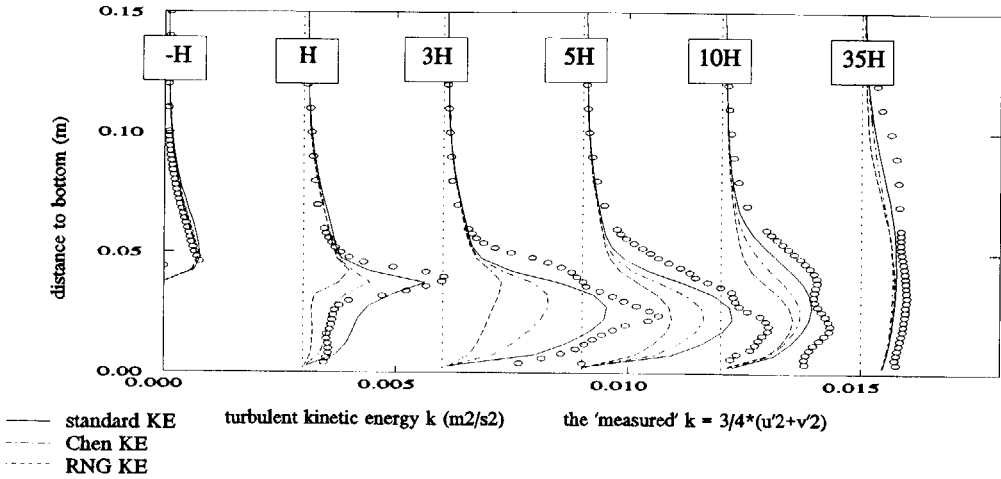


Figure 3.21: Values for k in backward facing step as measured by Tropea and computational results with different turbulence models.

Based on the velocities and the length of the re-circulation zone, the model with the Chen modifications can be selected as the most suitable form of the $k-\epsilon$ model. However, this choice should not be based on the velocities and the length of the re-circulation zone only. Also the values of the kinetic energy of turbulent motion, k , and the eddy viscosity have to be observed. Figure 3.21 presents the computed values of the turbulent kinetic energy k together with the measured values. The measured values have been derived from the turbulent fluctuations of the velocities.

$$k = \frac{3}{4}(u'^2+v'^2) \tag{3.6}$$

Figure 3.22 shows important differences in the values for k computed with the three different forms of the $k-\epsilon$ model. The k values computed with the standard $k-\epsilon$ model are the highest, the k values of the RNG model the smallest. The peaks of the measured values are always higher, but would have been between the peak of the standard $k-\epsilon$ and the Chen model if k had been computed from the measurements as $k = 1/2(u'^2+v'^2)$, which is, however, less realistic. The k -equation presented in section 3.4.3 gives lower k values for the measurements:

$$k = 0,69(u'^2+v'^2) \tag{3.7}$$

The large differences in the k values in the mixing layer on top of the re-circulation zone create doubts about the correct functioning of the different turbulence models. A closer look is required.

The measure for the length of the turbulent vortexes is $L = k^{3/2}/\epsilon$. The value of L is within reasonable ranges for all three models. At 0.15 m from the bottom and higher, L equals about 0.11 m for all models. In the re-circulation zone the standard $k-\epsilon$ model results in a peak of 4 cm, which grows to 7.5 cm at $x = 25*H$. The RNG model computes a smaller peak in the re-circulation zone (3 cm), and only 6.5 cm at $x = 25*H$. The Chen model results in intermediate values.

Another variable to study is the eddy viscosity ν_t . The value of ν_t is important because it is used to compute the diffusion of momentum and suspended matter by turbulence. The measured value of ν_t can be computed from the shear stresses obtained from the turbulent fluctuations of the velocities and the average velocity gradients:

$$\nu_t = \frac{-\overline{u'v'}}{\frac{du}{dy} + \frac{dv}{dx}} \tag{3.8}$$

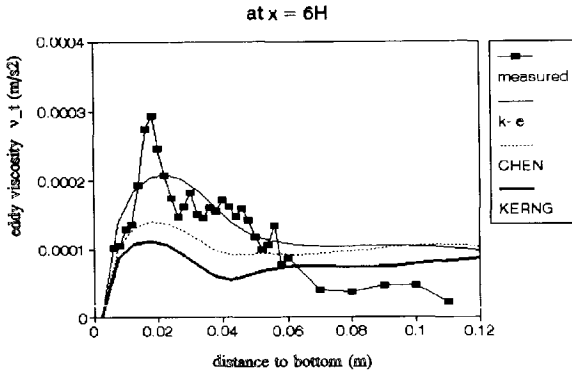


Figure 3.22: Measured and computed eddy viscosity at $x = 6*H$ in the flow over a backward facing step.

Figures 3.22 and 3.22 present the resulting values of the eddy viscosity. The curves based on the measurements show large fluctuations. These fluctuations are due to the way these values have been obtained: Δx is much larger than Δy , and the recorded accuracy of u and v is only 0.01 m/s, which is not enough to compute $\Delta u/\Delta y$ and $\Delta v/\Delta x$ accurately. The standard $k-\epsilon$ model appears to simulate the peak of the ν_t in the re-circulation zone best. However, the simulation with the Chen modifications also shows reasonable results. The RNG model clearly predicts values of the eddy viscosity below the values based on the measurements.

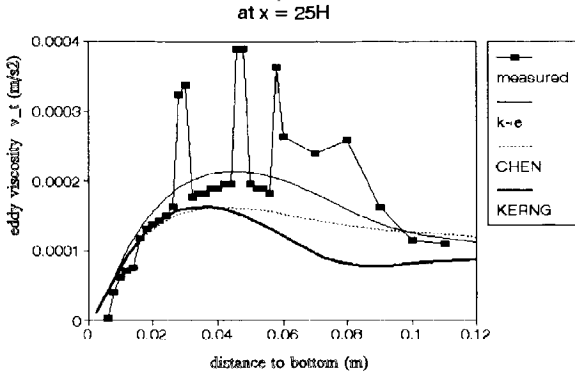


Figure 3.23: Measured and computed eddy viscosity at $x = 25 \cdot H$ in the flow over a backward facing step.

3.6 Conclusion of the modelling of the flow

The flow model built with PHOENICS can simulate the water flow in storm water settling tanks in a satisfactory way. The use of a finer grid did not really affect the results of the flow simulations. The coarse grid with cells of 0.15 m and $\Delta x/u = 3$ s is therefore concluded to be appropriate. The use of a modified form of the $k-\epsilon$ turbulence model can lengthen the re-circulation zone, but does not give an overall improvement of the simulations. Because a convincing improvement is absent, the standard $k-\epsilon$ turbulence model has been adopted.

Chapter 4

QUANTITY AND COMPOSITION OF OVERFLOWING WATER

The pollution load of CSOs is highly variable in time and space. The variation is due to:

- * the characteristics of the sewer system, such as size, shape, slope, etc.;
- * the type and size of the ancillary structure;
- * the characteristics of a storm (intensity and duration);
- * the slope, the type of soil, vegetation, etc..

The concentration of pollutants also depends on the amount of solids accumulated on the ground. This amount is related to the length of the preceding dry weather period, as well as other aspects such as type of pavement, traffic density, climate, etc..

For the design of a storm water settling tank, both the variation in the flow, and the composition of the overflowing water, are important.

4.1 Flow

The characteristics of the flow, such as the average flow rate, the distribution of the flow rate, the overflow frequency, etc., differ per sewer system. Several studies have been carried out in order to measure the discharge during overflows. The results of investigations carried out in the Netherlands are presented in (NWRW, 1989). Between 1982 and 1989, the NWRW⁽¹³⁾ managed a research into the functioning of sewer systems and overflow structures in the Netherlands. Amongst other things, the water flowing in and out of the storm water settling tanks of two combined sewer systems was sampled and analyzed. Furthermore, the outflowing water for four

⁽¹³⁾ NWRW is the acronym for Nationale Werkgroep Riolering en Waterkwaliteit (National Task Group on Sewerage and Water Quality).

combined sewer systems without storm water settling tanks was sampled and analyzed. The data collected at these four systems can also be regarded as representing the inflow into tanks, if these tanks would have been constructed behind the external weirs.

Generally, the results of surveys are not used in the design of storm water settling tanks. The design is mostly based on experience or rules of thumb, and seldom on calculations of the discharge from the sewer system. It is possible to apply sewer flow simulation programs to obtain distributions of overflow rates for a rainfall time series (for example, over a period of 10 years). Such results could be used instead of measurements. It should be noted that the flow simulations can result in a realistic prediction of the average flow rate and overflow frequency for most rain events, but for some distinctive storms, the results may differ dramatically from measurements.

4.2 Pollutants in overflowing storm water

Pollutants in overflowing storm water originate from domestic and industrial waste water and from surface runoff. Sewer solids (stemming from waste water and runoff) deposit in the sewer system during dry weather. The resulting sediments might be eroded by heavy rain and washed out of the sewer system.

4.2.1 Measurements

In several surveys CSOs were analyzed. In the Netherlands the results of the NWRW research are the most extensive and readily accessible. For several combined sewer systems with one overflow structure, the overflowing water was gauged and sampled. Table 4.1 presents some average pollutant concentrations in CSOs, as measured during the NWRW investigations, as well as concentration provided by Moffa (1990). He compiled 8 sources from the USA.

Table 4.1: Average concentration of pollutants in the overflowing water for 4 combined sewer systems (NWRW, 1989) and 8 source from the USA (Moffa, 1990).

	NWRW mg/l	Moffa mg/l
BOD	40-124	59-222
COD	148-389	264-481
Kjeldahl Nitrogen	10- 15	2.6-4.9
DSC	105-320	-
TSS	-	273-551
VSS	-	109-182
Lead	0.042-0.162	0.14-0.6
Zinc	0.357-0.472	-

The highest concentration of the NWRW data has been measured for the sewer system of Oosterhout, where some houses discharged their waste water directly to the main to the overflow structure. During dry weather flow, the flow conditions in this main allowed settling. Therefore, in a storm situation more sediment was washed out.

structure. During dry weather flow, the flow conditions in this main allowed settling. Therefore, in a storm situation more sediment was washed out.

The data of the NRW research also consists of the concentration of COD and DSC (dry solid contents) in the in- and outflowing water of the sewer systems in the cities of Amersfoort and Kerkrade (systems with one CSO and a tank behind that overflow structure). According to the registered data, in 3.7 years, 17 storms resulted in an overflow of the tank in Amersfoort. The average COD concentration of the inflowing water was 225 mg/l. The average COD concentration of the outflowing water was 124 mg/l. For the DSC the concentrations were 164 and 71 mg/l respectively (NRW, 1987).

Wiggers (1991) and Veldkamp (1996) evaluated the NRW data and concluded that the pollution load in BOD per hectare of impervious area for the four combined sewer systems with one CSOS appeared to be almost equal for these sewer systems: 2.7 kg BOD/ha. For other pollutants, the results were less unambiguous, but also point to an approximately constant pollution load per hectare impervious area, independent of the sewer system.

Furthermore, the composition of the sediments in sewer systems provides some information on the pollution load, as this material might partly be discharged during an overflow. The characteristics of sewer sediments vary per sewer system, and even within a system they may vary considerably. Kleywegt (1992) reports (from several sources) that the average organic content by mass in sewer deposits is between 4 and 18%. Further, he gives the following distributions of particle sizes in sewer deposits.

Table 4.2: Particle size in sewer deposits (after Kleywegt (1992)).

range mm	mean value mm	Location
0.1-25	2.43	Several in UK
0.06-2.0	0.36	Hamburg
0.34-2.94	1.18	Bratislava
0.8-1.8	-	Moscow
0.2-4.0	-	-

These sewer sediments consist of coarse materials. Storm water samples also consist of finer materials. In fact, in many cases, the heavier particles are expected to stay in the sewer system (caught before the internal weir which divides the tank from the system). According to Verbanck et al. (1990), on average 75% or more of the total mass passes through a 0.1 mm sieve. CIRIA (1987) reports particle sizes between 0.001 to 0.05 mm at the outlet of a storm water sewer. Crabtree (1988) reports on one sample of storm water overflow. It consisted of 44% (in dry mass in ashed residual) gravel (2-50 mm), of 54% sand (0.063-2 mm), and of only 2% silt and clay (< 0.063 mm).

By estimating the settling velocities for these particle sizes, it is possible to estimate the probability that they will be retained by settling in a storm water settling tank.

4.2.2 Settling velocity

For the removal of particles by settling, the settling velocity is the most important quality of the particles. The settling velocity depends on the density, the diameter, and the shape of a particle. Consequently, all these properties are needed to compute the settling velocity v_s . The settling velocity for round spheres in quiescent water can be computed with the following equations.

$$v_s = \sqrt{\frac{4}{3C_D} \frac{\rho_s - \rho_w}{\rho_w} gd} \quad (4.1)$$

d denotes the diameter of the particles. The drag coefficient C_D , depends on the magnitude of the Reynolds number for settling, which is

$$Re_s = \frac{dv_s}{\nu} \quad (4.2)$$

The relation between C_D and Re_s has been thoroughly investigated by several researchers. Huisman (1989) presents the results. For Re_s values below 10,000 the relation can be approximated with

$$C_D = \frac{24}{Re_s} + \frac{3}{\sqrt{Re_s}} + 0.34 \quad (4.3)$$

For Re_s values less than 1.0, the friction is entirely due to viscous forces. The flow of the upward moving water along the downward moving particle occurs under viscous flow conditions. For Re_s values greater than 2,000, turbulent forces (owing to irregular water movements) dominate the friction. For intermediate values both viscous and turbulent forces are important. Because the drag coefficient depends on the Reynolds number for settling, which in turn, depends on the settling velocity, the right value of the settling velocity has to be obtained iteratively.

Table 4.3 presents the values of Re_s and the settling velocities for round spheres with a density of 2,650 kg/m³ (like sand) in water of 10°C.

Table 4.3: Settling velocity and Re_s for spheres with a density of $2,650 \text{ kg/m}^3$ (as for sand) in water of 10°C .

d mm	v_s m/h	Re_s
2	1,018	432
1	592	125
0.5	290	30.8
0.2	77.6	3.3
0.1	24.7	0.52
0.063	9.8	0.13
0.05	6.2	0.07
0.02	1.0	<0.01

Most particles in CSOs (according to Verbanck et al. (1990) 75% has $d < 0.1 \text{ mm}$) have a settling velocity resulting in laminar flow conditions around the particle. The relation between C_D and Re_s can then be approximated with $C_D = 24/Re_s$. This results in the equation of Stokes for the settling velocity.

$$v_s = \frac{(\rho_s - \rho_w) g d^2}{\rho_s 18\nu} \quad (4.4)$$

The settling velocity increases with increasing diameter, which is directly incorporated in the equation for v_s and hidden in the drag coefficient. Equations 4.1 through 4.4 show that the settling velocity increases quadratically with the diameter for the laminar range, but only linearly for settling under turbulent settling conditions. This is due to the fact that the turbulent eddies increase the drag around the sphere and accordingly reduce the settling velocity.

The following remark needs to be made on the computation of the settling velocity: The relation between Re_s and C_D as presented above, has been derived for settling in quiescent water. It must be stressed that the Reynolds number applied in determining whether the settling is laminar or turbulent is Re_s , the Reynolds number for settling. In storm water settling tanks, however, the flow conditions will generally be turbulent. This turbulence is expressed in the Reynolds number for the flow: $Re = uR/\nu$. The settling of particles whose settling velocity in quiescent water can be computed with Stokes, equation 4.4, (i.e. settling under laminar conditions), will be influenced by the turbulent eddies of the main flow. In the first place, the relatively large eddies (as compared to a particle diameter) will decrease concentration differences and thus have an adverse effect on the settling. In the simulations, this influence is accounted for via the diffusion terms in the equations. In the current design of settling tanks, the effect of the turbulence is taken into account separately (see Chapter 1 and Appendix APDNLDES).

In the second place, relatively small eddies (as compared to a particle diameter) might influence the drag around the particle. The effect is unclear, but for particles with a diameter of less than 0.1 mm , this second effect will be absent. The relatively small eddies would have to be smaller than the Kolmogorov scale (0.1 mm), and thus can't exist.

In the field of water and waste water engineering it is common practice to neglect the fact that the flow conditions in the settling tanks can be turbulent, and to apply the settling velocity for settling in quiescent water. For CSOs this is a right assumption since most particles have a diameter less than 0.1 mm. Furthermore, because of uncertainties in diameter, shape, density, likelihood of flocculation, etc., the settling velocity cannot be known accurately at all. Consequently, even in turbulent flowing water the settling velocity for settling under laminar flow conditions can be applied for small particles.

When all the right characteristics of the particles (such as size distribution, densities, shapes) properties are known, it is possible to compute the settling velocity. Combining this with the information on the relation between the different pollutants and the different particle sizes, would give a good indication of the efficiency of tanks. However, such relations do not abound. In addition, it is impossible to get to know all the characteristics. Moreover, even knowing all these characteristics does not result in the required settling velocities when particles flocculate or fall apart, because this changes the settling velocity.

Chebo et al. (1990) report that the measured settling velocity is higher than the one following from Stokes, equation 4.4. This indicates flocculation and coagulation. However, the literature is unclear on this subject. According to Kleywegt (1992), several researches indicate that the behaviour of sediment in sewers is less cohesive than expected.

Instead of computing the settling velocity and applying the relation between particle size and pollutant, it is much more straightforward and convenient to directly measure the settling velocity distribution and relations between settling velocity and adherent pollutants and to use these relations. This conclusion has also been drawn by Verbanck (1994).

4.2.3 Relation between settling velocity and pollutants

Sharon et al. (1989) give some information on the distribution of the settling velocity. The following conclusions stem from curves of the mass distribution of settling solids. These curves have been compiled from various sewer systems and discharges: 30 to 40% of the solids in dry weather flow has a settling velocity below 0.036 to 0.36 m/h. Several measurements of overflowing sewage show a settling velocity starting between 0.1 and 1 m/h. 50% of the solids have a settling velocity below 4 m/h and 70% have a settling velocity below 22 m/h.

Pollutants are partly solved in the water and partly connected to suspended solids. Different pollutants might be connected to different particles. Verbanck (1994) reports that heavy metals and organic matter are associated with the finest size fractions of particulate solids, but the research of Michelbach and Wörle (1992) give different results. Contradictory to Verbanck (1994), they found that the heavy metals and organic matter are for the most part associated to the mediate particle size fraction. The information is not abundant enough to be used.

For the design of storm water settling tanks and other ancillary structures in which particles have to settle, a relation between the incoming pollutants and a settling velocity should be known for several kinds of pollutants.

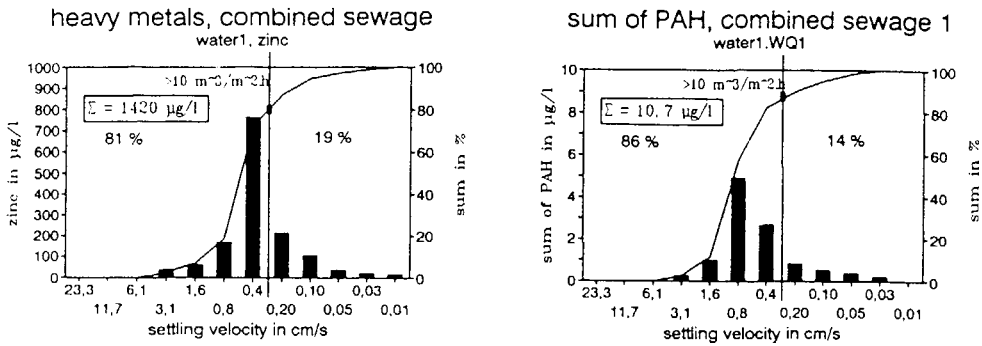


Figure 4.1: Settling velocity distributions for zinc and PAH, in combined sewage (Michelbach and Wörle, 1994).

Studies into such relations have started only recently. Michelbach and Wörle (1992) describe a method to determine such relations and present settling curves for the dry weight of pollutants in overflowing water. For the specific case they studied, about 80% of the settled material has a settling velocity of more than 10 m/h. Figure 4.1 gives examples of settling distributions for zinc and PAH in combined sewage (not CSO!). The heavy metals were expected to be associated with the finest particles, and therefore with the smallest settling velocities. Unexpectedly, the fraction with a settling velocity of 14.4 to 28.8 m/h (respectively 0.4 to 0.8 cm/s) showed the highest loads. This indicates that storm water settling tanks can retain an important part of these kinds of pollutants.

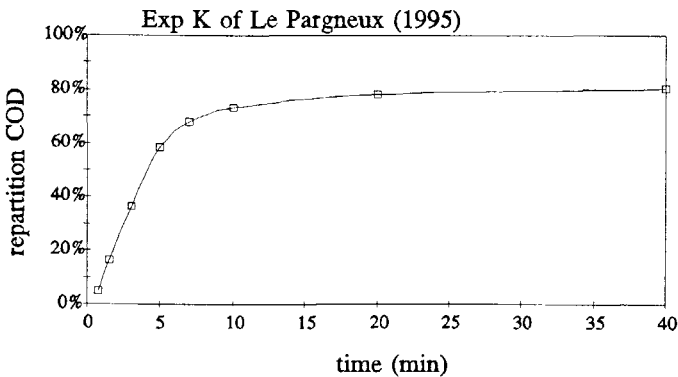


Figure 4.2: Settling distribution for sludge of Delft sewer system.

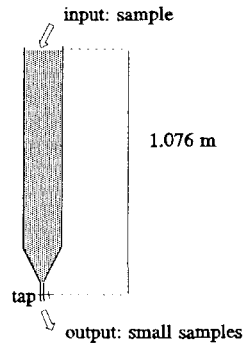


Figure 4.3: Settling tube.

Le Pargneux (1995) carried out experiments similar to those of Michelbach and Wörle (1994) with sludge from the Delft sewer system and he found similar lines. See figure 4.2. He fed the raw sample of sludge at $t = 0$ s into the top of a tube with length h and gathered small samples from the bottom at several timed intervals and analyzed them. The settling velocity of the particles in the first small sample (taken at $t = t_1$) was greater than h/t_1 m/s, see figure 4.3. The settling velocity of the particles in the second small sample (taken at $t = t_2$) was between h/t_1 and h/t_2 m/s,

etc. This resulted in the relation between BOD or COD and the settling velocity, as presented in figure 4.3. 72% of the organic matter appeared to have a settling velocity greater than 5 m/h, and 62% had a settling velocity greater than 10 m/h. For COD, this is 80% and 70% respectively.

Because of differences in slope, ground material, sewer system, etc., it is expected that such relations will differ for each location. More research into such distributions of several pollutants is required to design optimally functioning tanks. With the aid of such distributions, it is possible to determine which particles, i.e. with what settling velocity, should be retained. For example, if there is a sharp jump in the distribution, this can be taken into account in the design.

To derive design rules for storm water settling tanks, such settling velocity distribution curves are not indispensable. It is possible to make the best design for a range of settling velocities. The simulation of the flow and settling as presented in the coming chapters showed that the best design for one settling velocity also resulted in the best removal ratio for the other settling velocities. But to relate the volume or the costs of the tank to the removal ratio due to settling, knowledge of such distributions is needed because the costs of creating a larger volume has to be compared to catching a certain extra percentage by settling.

4.2.4 Settling velocities in Dutch design

Because of lack of data, in Dutch design practice, generally the functioning of a tank is evaluated for particles with a settling velocity of 5 or 10 m/h. These values for the settling velocity are related to the historical choice that a tank should have a surface loading of about 5 to 10 m/h. Such tanks are most suitable for particles with the above settling velocities. See also Appendix B.

4.2.5 Simulation results

Unlike the overflow rate, it is still impossible to compute the time-varying concentration of pollutants resulting from a chosen rainfall event, or a rainfall time series. The process of inflow of pollutants into the sewer system and the processes inside the sewer system (e.g. particle transport, sedimentation, and re-entrainment) are not yet sufficiently understood to create a reliable model (Ruan, 1995). The existing models only give a rough estimate of the pollution load and should only be used in a relative manner, i.e. to investigate the effect of certain measures. Consequently, simulation results cannot be used for the design of tanks.

4.3 Conclusion

The amount of water and the flow rate of the water flowing into tanks is sufficiently known. It has been measured and can be computed.

The constitution of the overflowing water is much less known. Measurements are scarce and insufficient for the design of tanks. Results of pollution load simulations are not realistic enough to be used in the design of tanks. Besides inflow concentrations, the design of optimally functioning tanks requires a relation between settling velocity and pollution parameters. Such relations are not sufficiently available. Because of the major importance of the settling velocity on the functioning of a tank, overflows should be sampled and analyzed, in order to derive such relations.

Chapter 5

MODELLING THE SETTLING OF PARTICLES

This chapter describes the extension of the flow model with a model describing the transport of settling particles in water. It presents the equations of which the settling model consists and the way they are solved. PHOENICS provides a method to compute the behaviour of settling particles⁽¹⁴⁾, but it appeared to conflict with the method for computing the free surface. For that reason another method has been developed.

Settling particles move with the water flow, and due to gravity, they move downward relative to the water flow. Many phenomena are associated with the behaviour of particles in water. They influence the water movement through the density and viscosity. Particles might flocculate when they collide, or they might fall apart due to turbulent forces. At the bottom, particles might deposit or stay in suspension. Deposited particles might coagulate or be compressed by the weight of other particles on top. They also might be eroded from the bottom into the water flow. Another phenomenon is the reduction of the settling rate due to upflow of water between the settling particles when the volumetric concentration of the settling particles increases. Not all of these phenomena need to be taken into account.

5.1 Simplifications in the model

It is impossible to exactly model all the phenomena in a storm water settling tank. Some phenomena must be simplified, in order to keep the computational time within an acceptable range and because of limitations on the data characterizing the inflowing material. The behaviour of particles has been simplified in the following ways.

* Flocculation is not taken into account.

⁽¹⁴⁾ ASM method, (*POLIS*).

In reality, particles might flocculate and fall apart. The model does not incorporate this. It simulates the flow and settling of discrete particles. For the following reasons, the simulations can be used to draw reliable conclusions, even without taking flocculation into account. Firstly, due to the highly turbulent nature of the flow, flocculating particles will also fall apart. Secondly, the conclusions will be based on the comparison of simulated flow situations. Such comparisons will show the effect of changes in the design even if flocculation is not incorporated.

A further reason for not taking it into account is the lack of information on the consistency of the inflowing water.

* Hindered settling is not taken into account.

When the volumetric concentration of the settling particles increases, the settling rate is reduced because the water has to flow upwards between the settling particles. Huisman (1989) gives the following equation for the reduced settling velocity.

$$v_s' = v_s (1 - f c_v^{2/3}), \text{ with}$$

f = factor depending on particle shape and Reynolds number for settling. For laminar settling of spheres $f = 2.0$;

c_v = volumetric concentration l/l;

v_s = settling velocity according to equations 4.1 and 4.4.

For $f = 2.0$, this equation predicts the following reduced settling velocities:

$$\begin{aligned} \text{For } c_v = 0.1: & \quad v_s' = 0.57 * v_s \\ c_v = 0.01: & \quad v_s' = 0.907 * v_s \\ c_v = 0.004: & \quad v_s' = 0.95 * v_s \end{aligned}$$

According to Crabtree (1988), the concentration of settling particles in the CSOs is in the range of 2-1,550 mg/l. According to NWRW (1989), the average pollution concentration out of combined sewers is 105-320 mg/l (dry rest). The maximum is almost 4,000 mg/l, see table 5.1.

Table 5.1: concentration of dry rest in overflowing sewage from four combined sewer systems (NWRW, 1989).

dryrest mg/l	Loenen		Oosterhout		Bodegraven		Kerkrade	
	avg.	max.	avg.	max.	avg.	max.	avg.	max.
	303	1,201	260	3,943	105	429	320	1,081

Assuming a density of the particles $\rho_s = 2,000 \text{ kg/m}^3$, an inflow concentration of 4,000 mg/l would correspond to a volumetric volume of 2 ml/l.

For $f=2$, this would mean a reduction by about 3% of the slip velocity due to the hindering of settling. Near the bottom the concentrations will be higher. Assuming a two times higher concentration near the bottom gives $c_v = 4 \text{ ml/l}$. The reduction in settling velocity by hindering of settling would then be 5%. Usually, the concentrations will be much lower. Consequently it is assumed to be acceptable to neglect this hindering of settling. This is in

accordance with (Toornman, 1993). He reports that hindered settling is noticeable for $c > 10$ g/l. For $\rho_s = 2,000$ kg/m³ this complies with $c_v = 5$ ml/l.

* Density differences are neglected.

This means that density currents are not taken into account and that the fluid density is assumed to be independent of the particle concentration. For a concentration of particles at the inflow of 4,000 mg/l (the maximum concentration in the overflowing water measured in (NWRW, 1989)) the density of the mixture flow would be 1,004 kg/m³ if the particles have a density of 2,000 kg/m³. Generally, the concentrations will be lower. Consequently, the density differences are not that important. Furthermore, the flow in the tanks is usually so turbulent, and the detention time so brief, that density differences have only a small effect. Only for small discharges through the tank, density currents are important. But in such flow situations the detention time of water in the tank is so long, that the removal ratios will be high anyway, so that the design of tanks is based on the high discharges. The model can easily be adapted to make the density dependent on the concentration, and to take the effect of density currents into account.

* The viscosity is assumed to be independent of the particle concentration.

The concentration is assumed to be so low that it does not significantly change the viscosity of the mixture fluid. The model can easily be adapted to make the viscosity dependent on the concentration.

With these simplifications the model will be as given in the following section.

5.2 Particle transport equation

The settling model takes the following into account:

- Convective transport
- Diffusive transport
- Changes in time
- Transport due to settling
- Deposition and erosion depending on local flow characteristics.

Due to gravity, the particles move downward relative to the water with a velocity called the slip velocity, v_s . This slip velocity is equal to the settling velocity in quiescent water as presented in the former chapter. The transport due to the turbulent eddies is accounted for by means of a diffusion term (Reynolds analogy). In order to compute the free water surface, the y-direction has been chosen as the upward direction. Consequently, the settling only occurs in the y-direction.

The settling model does not compute the transport of distinctive particles, but that of concentrations of particles, characterized by their slip velocity. The particle concentration, c , applied in the model, is dimensionless. The total mass of particles in a cell is $\rho * c * V$, with V denoting the volume of a cell. In literature the concentration is usually defined in kg/m³, which is more convenient. Because of the way in which PHOENICS computes the scalar variables, the concentrations could not be defined in kg/m³ in combination with the method for the computation of the free water surface. See subsection 5.4.1.

The previous chapter explained that the particles are only characterized by their slip velocity. The model can simulate the flow and settling of a range⁽¹⁵⁾ of slip velocities simultaneously, but the concentrations of the particles with different slip velocities do not influence each other. For the low concentrations which occur in storm water settling tanks, the influence of the presence of other particles can be neglected in most cases. To take such effects into account, the coding has to be changed. The set up of the equations is such that this can easily be accomplished.

The resulting transport equation of the concentration in 2 dimensions is:

$$\frac{\partial \rho c}{\partial t} + \frac{\partial \rho u c}{\partial x} + \frac{\partial \rho (v + v_s) c}{\partial y} + \frac{\partial}{\partial x} \left[\frac{\nu_1 + \nu_t}{\sigma} \frac{\partial \rho c}{\partial x} \right] + \frac{\partial}{\partial y} \left[\frac{\nu_1 + \nu_t}{\sigma} \frac{\partial \rho c}{\partial y} \right] = 0 \quad (5.1)$$

with σ representing the Schmidt number which has a value between 0.5 and 1.0 and which has been assumed to be isotropic. It is noted that in the $k-\epsilon$ turbulence model ν_t is assumed to be isotropic, and that also the kinematic viscosity ν_1 is isotropic.

The description of the turbulent transport as a diffusion process might underestimate this transport. Relative large coherent parcels of water that move from the bottom upward, might transport particles from the bottom directly over large distances (Booij, 1995). In the diffusion model, this can only be achieved by a (non realistic) low value for the Schmidt number. In case particles are present throughout the whole flow domain, such effects are much less pronounced. The effect of the value of the Schmidt number is discussed in the next chapter.

5.3 Discretisation

In order to solve the particle transport equation in PHOENICS, fully upwind discretisation has been applied⁽¹⁶⁾. To minimize the numerical diffusion, the particle flux in vertical direction is computed at once, based on the final vertical particle velocity, which is the sum of the vertical mixture velocity (v) and the slip velocity (v_s). Therefore, the upwind direction of $v + v_s$ is determined before the flux is computed. This is not always the same as the upwind direction of the mixture fluid, but is based on the sum of the mixture velocity and the slip velocity. Only the inflowing fluxes (i.e. upwind) are taken into account (see figure 5.1).

The discretisation of the diffusion terms is straightforward, and does not contribute to the following explanation of the way the concentrations are computed. These discretisations have been given in Appendix D. In this chapter the diffusion terms are assumed to be zero. The particle transport equation then becomes:

⁽¹⁵⁾ The FORTRAN coding has been written to compute the distribution for up to five different settling velocities. This number can easily be increased to ten.

⁽¹⁶⁾ and not the standard scheme within PHOENICS, the hybrid upwind scheme, which is used for the water flow.

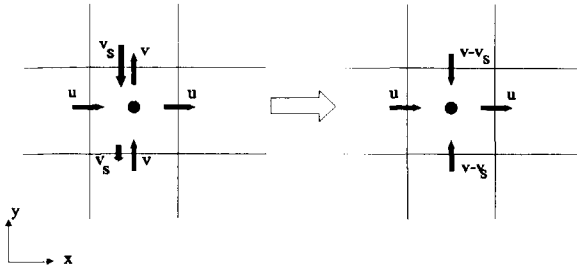


Figure 5.1: Example of upwind.

$$\frac{\partial \rho c}{\partial t} + \frac{\partial \rho u c}{\partial x} + \frac{\partial \rho(v+v_s)c}{\partial y} = 0 \tag{5.2}$$

For a horizontal velocity in the direction from cells $i-1$ to cells i , and a vertical flux due to $v-v_s$ from $j-1$ to j , fully upwind discretisation of the time-dependent and convective terms of the particle transport equation gives:

$$\frac{(\Delta x \Delta y c \rho)^n - (\Delta x \Delta y c \rho)^{n+1}}{\Delta t} + (\Delta y \rho u c)_{i-1} - (\Delta y \rho u c)_i + (\Delta x \rho(v+v_s)c)_{j-1} - (\Delta x \rho(v+v_s)c)_j = 0 \tag{5.3}$$

When the superscript is omitted, the new time step value is meant. When the subscripts i or j has been omitted the current i or j value is meant, e.g. $c_{j-1} = c_{i,j-1}^{n+1}$. The new concentration $c (= c_{i,j}^{n+1})$ can be computed from:

$$c = \frac{\frac{(\Delta x \Delta y \rho)^n}{\Delta t} c^n + (c u \rho \Delta y)_{i-1} + (c(v+v_s) \rho \Delta x)_{j-1}}{\frac{(\Delta x \Delta y \rho)^{n+1}}{\Delta t} + (u \rho \Delta y)_i + ((v+v_s) \rho \Delta x)_j} \tag{5.4}$$

In general, so also for the horizontal or vertical fluxes in the opposite directions, this equation reads

$$c = \frac{\frac{(\Delta x \Delta y \rho)^n}{\Delta t} c^n + CF_x + CF_y}{\frac{(\Delta x \Delta y \rho)^{n+1}}{\Delta t} + F_x + F_y} \tag{5.5}$$

With

- $CF_x =$ inflowing flux in x-direction of concentration c
- $= \max(0, u_{i-1}) \Delta y_{i-1} (c \rho)_{i-1} + \max(0, -u_i) \Delta y_i (c \rho)_{i+1}$
- $CF_y =$ inflowing flux in y-direction of concentration c
- $= \max(0, (v-v_s)_{j-1}) \Delta x_{j-1} (c \rho)_{j-1} + \max(0, -(v-v_s)_j) \Delta x_j (c \rho)_{j+1}$

$$\begin{aligned}
 F_x &= \text{outflowing volume flux in } x\text{-direction} \\
 &= \max(0, -u_{i-1})\Delta y_{i-1}\rho_i + \max(0, u_i)\Delta y_i\rho_i \\
 F_y &= \text{outflowing volume flux in } y\text{-direction} \\
 &= \max(0, -(v-v_s)_{j-1})\Delta x_{j-1}\rho_j + \max(0, (v-v_s)_j)\Delta x_j\rho_j
 \end{aligned}$$

The grid is staggered. This means that the value of the velocities and the cell faces apply for the cell borders, e.g. u_i is the velocity between cell i and cell $i+1$.

Since the upwind direction can change when the slip velocity is added to the vertical velocity, this equation cannot be simplified to the same extent as the equations for the standard PHOENICS variables by substitution of the mass conservation equations. See Appendix D, which gives this simplification for the standard PHOENICS variables.

To solve this equation, FORTRAN coding has been added to PHOENICS, using the setup of PHOENICS. The coding computes the fully upwind particle transport for flow situations with and without free surface. The coding has been presented in Appendix H. In order to prevent specific problems in combination with the computation of a free surface, measures have been taken. These have been presented in the following section.

5.4 Free surface effects

5.4.1 Volume based concentration

In computations with a free water surface (using the PHOENICS HOL-method presented in Chapter 2), equations could not be solved in the standard way of PHOENICS, because the simultaneous computation of a free water surface, and the particle settling, caused serious problems with the particle balance; it resulted in a loss or production of material at the water surface. This is due to the following. In the free surface method the density is omitted and the continuity equation of the fluid is based on the volume fluxes, even though the density is not constant (water-air interface!). This means that the sum of the densities multiplied by the velocities and the appropriate cell faces is not zero⁽¹⁷⁾:

$$(\rho^n - \rho^{n+1}) \frac{\Delta x \Delta y}{\Delta t} + (u\rho\Delta y)_{i-1} - (u\rho\Delta y)_i + (v\rho\Delta x)_{j-1} - (v\rho\Delta x)_j \neq 0 \quad (5.6)$$

but that for each cell the sum of the horizontal and vertical velocities multiplied by the appropriate cell faces equals zero:

$$(u\Delta y)_{i-1} - (u\Delta y)_i + (v\Delta x)_{j-1} - (v\Delta x)_j = 0 \quad (5.7)$$

To prevent problems with the particle mass balance, the particles are also computed independently of the density. Thus, a volume based concentration is computed. The particle content of a cell is equal to the volume multiplied with the concentration. As the concentration is dimensionless, and the density has not been made dependent on the concentration, it can also represent a relative

⁽¹⁷⁾ The equation has been set up for the horizontal velocity from cells $i-1$ to cells i , and the vertical velocity from cells $j-1$ to cells j .

concentration. It is convenient to set the inflowing concentration to 1.0 as the reference value. Then, a relative concentration of 0.4 means that the concentration is 40% of that in the reference cell. In case the inflow concentration varies in time, the reference value equals the maximum concentration occurring at the inflow. In free surface simulations some cells will be only partly filled with water. It is noticeable that also in those cells the concentration represents the concentration in the whole cell. E.g., in a cell filled for 70% with water and $c = 0.5$, the amount of material is 0.5 times the volume of the cell, see figure 5.2.

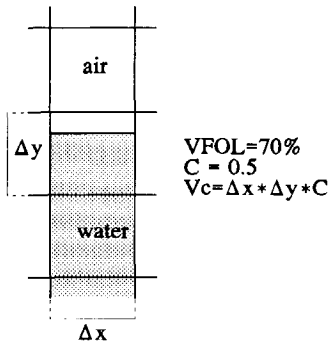


Figure 5.2: Particles in partly filled cell.

5.4.2 Particles in the air

Because in the free surface method the water and air are considered as one fluid, a part of the particles can move into the air if no precautions are taken. This is, of course, physically nonsense. To prevent this the slip velocity has been made dependent on the filling of a cell. The slip velocity in the air has arbitrarily been set to 20,000 times the slip velocity in the water. For cells without water, the air slip velocity is used, whereas for cells with only water, the water slip velocity is used. Because the water in partly filled cells is always at the lower side of the cell, the use of the air or water slip velocity for those cells depends on whether the cell face considered (top or bottom) is dry or not. This way the particles in the air drop quickly back into the water. See figure 5.3.

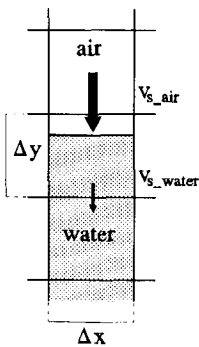


Figure 5.3: Settling velocity in air and in water.

An additional measure to keep the particles in the water stems from the following. In a partly filled cell, VFOL will be less than one. The water will be in the lower part of the cell. The concentration on the concerns the whole cell, as if the particles are spread out over the whole cell. However, the particles should be in the water, i.e. in the lower part of the cell. The concentration in the water would thus be c/VFOL . In order to take this fact into account, and to prevent problems in case that VFOL goes to zero, the flow from a cell which is only partly filled with water to the cell below has been increased by multiplying the downward fluxes by a factor FF. FF equals $1/\max(0.1, \text{VFOL}_{\text{above laying cell}})$.

And finally, to prevent diffusion of particles into the air, the diffusion has been made dependent on the filling percentage with water of the receiving cell. To that purpose the diffusion terms in Appendix H have been multiplied by the VFOL value of the receiving cell. Consequently, the diffusion to cells without water has been set to zero.

5.5 Implementing sedimentation in PHOENICS

To solve the settling particle transport equation within PHOENICS, the standard way of computing the time dependent, the convective and the diffusive terms have been switched off and the new transport terms are computed at once in FORTRAN coding written for this purpose. The following transport equation is solved for the 2-dimensional case:

$$c = \frac{\frac{\Delta x \Delta y}{\Delta t} (c\rho)^n + c_{+x} u_{+x} \rho_{+x} \Delta y_{+x} + \text{FF} c_{+y} (v+v_s)_{+y} \rho_{+y} \Delta x_{+y}}{\frac{\Delta x \Delta y}{\Delta t} \rho + u\rho \Delta y + \text{FF}(v+v_s)\rho \Delta x} \quad (5.8)$$

The subscripts $+x$ and $+y$ indicate the upwind cells in x - and y -direction respectively. It is noted that the diffusion terms have been omitted here, but are present in the equation which is finally solved. Appendix H presents the equation and the FORTRAN coding written to solve the equation.

5.6 Bottom boundary condition

Not all the particles reaching the bottom will deposit and stay there. Due to turbulence, some particles stay in suspension or particles that did deposit can be entrained from the bottom. The process of erosion and deposition of particles is still not sufficiently understood. Fundamental research into such processes is still being carried out. Turbulence structures (i.e. eddies due to turbulence) can cause particles to be picked up from the bottom and to be entrained into the fluid. The velocity of the water at which particles are entrained from the bottom into the fluid flow is influenced by the size and shape of the particles. Deposited particles might also stick together and consolidate, so that the duration that the particles are settled and the consistency of the particles becomes important.

Ashley et al. (1992) report that freshly deposited sanitary solids in sewer systems erode at the typical threshold of bed shear stress at around 1.8 N/m^2 . Due to the consolidation and cohesion of the sediments, the resistance to shear increases. According to Wotherspoon and Ashley (1992)

erosion occurs for shear stresses in the range of 0.01 to 5 N/m². These values for the shear stress are much higher than the threshold values applied in the current Dutch design method for storm water settling tanks: 0.1 to 0.25 N/m² (Noord-Brabantse waterkwaliteitsbeheerders, 1995). This threshold is therefore on the safe side. Taking into account the many uncertainties concerned, this is understandable.

The composition of the overflowing sewage is not sufficiently known. Therefore, a model is chosen without a relation between particle size, deposition, or erosion. In this model, the deposition and erosion depend upon the local shear stresses along the bottom, $\tau_b = u_*^2 \rho$.

The relation between the shear stress τ_b ; the deposition, D; and the erosion, E is as follows (Winterwerp, 1993):

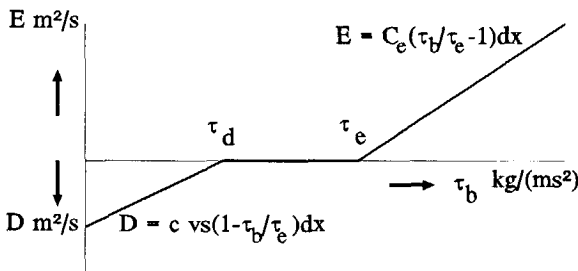


Figure 5.4: Deposition and erosion depend on the shear stress τ_b .

- For $0 < \tau_b < \tau_d$: $D = c v_s (1 - \tau_b / \tau_d) A_b$,
 $E = 0$
- For $\tau_d < \tau_b < \tau_e$: $D = 0$ and
 $E = 0$
- For $\tau_e < \tau_b$: $D = 0$ and
 $E = C_e (\tau_b / \tau_e - 1) A_b$

A_b denotes the bottom area of a cell, and c the concentration of particles in the water. The constants τ_d , τ_e , and C_e are equal to 0.15, 0.3, and $1 \cdot 10^{-6}$ respectively (Winterwerp, 1993). See figure 5.4. The values for the shear stresses have been chosen much smaller than the above presented values at which erosion occurs. Consequently, erosion and hindering of deposition will occur sooner.

The values chosen for τ_d , and τ_e will influence the simulations. Kleywegt (1992) presents the Shields curve, which is generally accepted as a criterion for incipient motion of particles in rivers (as a function of the particle diameter). Because of no other information is available, it is also applied for particle transport in sewer systems. However, the values according to Shields, do not provide a sharp value for incipient motion, but rather give an indication. Kleywegt (1992) measured particle transport for stresses at 70% of those predicted by Shields. The question of motion or no motion has furthermore a statistical character, which can not be put in one critical stress.

As in this research not the particle diameter, but the settling velocity is applied to characterize the sediments, the above presented values of τ_d , and τ_e have been chosen, which are independent of the particle diameter.

Chapter 7 presents the results of a sensitivity analysis of the simulation results to variations in the bottom boundary condition.

The process of accumulation of particles near the bottom creates a sludge blanket. This is known from the flow in clarifiers. Such tanks are fed at a continuous rate, resulting in a more or less equilibrium flow situation. The presence of a sludge blanket has not been incorporated in the model because in storm water settling tanks this is assumed to be of little importance. All particles depositing on the bottom are assumed to be out of the flow. Only by means of erosion particles can re-enter the flow. The amount of particles on the bottom is recorded. Erosion is only allowed if sediment is available.

Other fields of research where the transport of sediment is of interest, concern secondary clarifiers, or rivers, seas, and estuaries. As has been lined out before, the processes in secondary clarifiers vary too much from those present in storm water settling tanks. The measurements on which the models applied in the simulation of the sludge transport in clarifiers are based, can not be easily used for the modelling in storm water settling tanks.

The simulation of sediment transport in rivers and estuaries used to be based on depth-averaged mathematical models (1- or 2-dimensional), with supplementary equations to bring into account differences in the vertical. Most boundary conditions for the transport of sediments are therefore based on depth averaged flow parameters, e.g. see (Rijn, 1989). The boundary conditions in the storm water settling tanks need to be based on local flow parameters. In the future more and more simulations for rivers and estuary will be 3-dimensional.

Chapter 6

SIMULATION OF FLOW AND SETTLING

With the equations and the boundary conditions as described in the former chapter added to the mathematical model, the settling of particles in the water flow can be computed. Section 6.1 presents results of such simulations. These seem realistic, but in order to judge whether they sufficiently accurately describe reality, they should be validated. However, there is not sufficient reliable data available concerning particle concentrations inside tanks during operation. Section 6.2 discusses the available data and the validation which has been carried out. Due to the lack of data the validation on measurements was scarce. Therefore, to validate the model, on the one hand, the set up of the transport equations for the concentrations and their functioning have been tested thoroughly in several less complex flow situations, and on the other hand, sensitivity analyses have been carried out, to further test the model. Section 6.3 presents these sensitivity analyses of the model to uncertainties in the setup of the model. It discusses the effect of numerical diffusion, variations in the diffusion terms, variations in the bottom boundary conditions, and the use of a rigid lid.

6.1 Examples of flow and settling

The settling of particles in flowing water has been simulated for several situations. Firstly, the settling in the equilibrium situation for a free surface computation will be discussed. Next, the settling during filling will be explained.

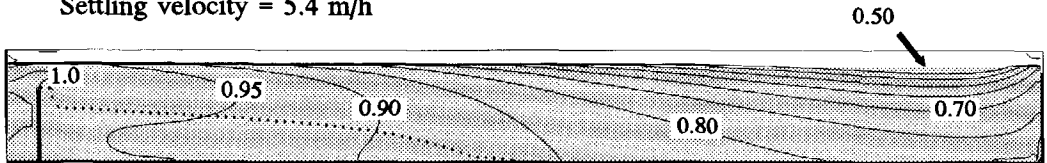
6.1.1 Stationary flow situation

For the equilibrium flow situation as presented in section 3.1, figure 6.1 gives the distribution of settling particles with a settling velocity of 5.4 m/h. The surface loading (the ratio of the flow rate and the surface area of the whole tank) is 10 m/h. The contour lines indicate relative concentrations between 0.5 and 1.0. Near the water surface at the right hand side of the tank, the relative concentration becomes smaller than 0.5, but, just before the external weir the concentration

increases again. Because of this, the outflow of particles with this settling velocity is 61% of the inflow and the removal ratio only 39%. The concentration in the re-circulation zone is about 1.0. The horizontal velocities parallel to the bottom are such that settling is hardly hindered. In the air, the relative concentration is negligible (see subsection 5.4.2).

Relative concentrations ranging from 0.5 to 1.0

Settling velocity = 5.4 m/h



$$L*B*H_e = 32.0*8.0*3.28, Q=0.8\text{m}^3/\text{s}$$

Figure 6.1: Relative concentrations of particles in tank with $B*L*H_e$ as indicated. $s_o = 10$ m/h.

6.1.2 Filling of a tank

This section presents simulation results of the settling during the filling of a tank. The inflow at the left hand side is taken uniformly over the lowest 0.57 m. The constant inflow rate per meter width is $q = 0.1 \text{ m}^3/(\text{sm})$, which corresponds to $0.8 \text{ m}^3/\text{s}$ in the 8 m wide tank. Consequently, the surface loading of the tank is $s_o = 12 \text{ m/h}$. The height of the internal weir $H_i = 1.5 \text{ m}$.

Figure 6.2 presents the distribution of particles with a settling velocity of 5.4 m/h during the filling of the tank, until the flow and particles distributions have reached an equilibrium distribution. The free surface method has been used to simulate both the flow of water and air. The air flow has not been presented in the figures. The figure gives the situations after 2, 6, 10, 14, 18 and 22 minutes. The water (containing the particles) enters the flow domain at the left, flows over the internal weir and fills the tank. The white lines indicate where the horizontal velocity is zero. At $t = 6$ minutes the water in most of the tank flows to the right, while just to the right of the internal weir, near the water surface, water flows to the left (negative velocity). At $t = 10$ minutes a re-circulation zone appears, as has been explained in Chapter 3. Meanwhile, further to the right are areas where water flows to the right as well as areas where water flows to the left. Later, when water is flowing out at the right, only in the re-circulation zone water flows to the left.

The inflow concentration has been set to 1.0. The colours indicate the relative concentrations of the settleable particles; blue means no particles (concentration=0.0) and red is the maximum amount of particles (concentration=1.05). Due to sedimentation and hindering of deposition on the bottom, the concentrations become a bit higher than the inflow concentration. Of note in the figure is the fact that the concentration near the external weir is much lower than the inflow concentration for the first 14 minutes. Apparently particles settle out there and before reaching that part of the tank.

Another remarkable point is that when the internal weir gets drowned (after about 8 minutes), and the final re-circulating flow is being created, a plume of high concentrations is pushed forwards along the bottom, while the water at the water surface hardly flows to the right, or even flows backwards (as has been indicated by the white zero velocity line in the middle of the tank in the

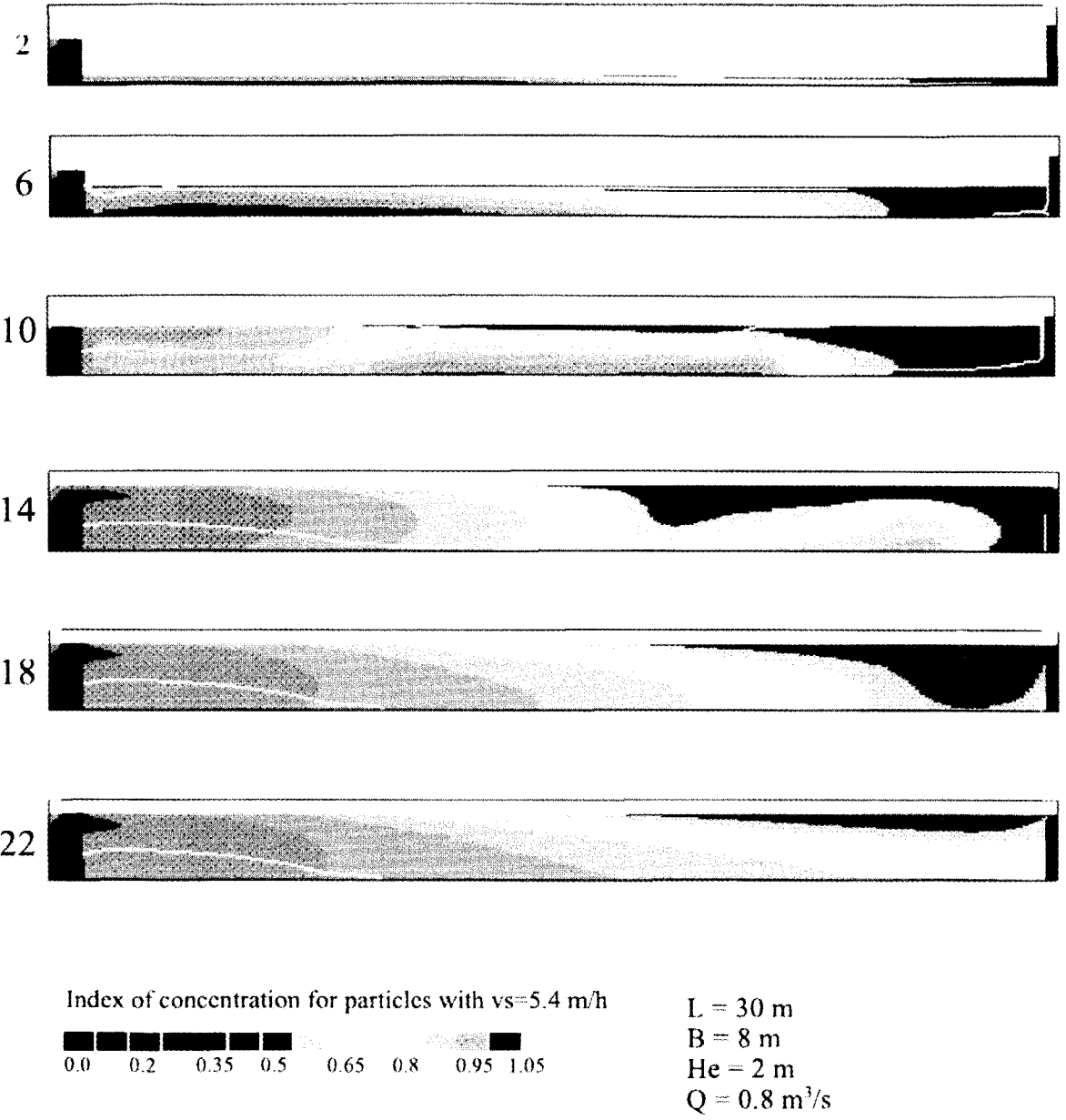


Figure 6.2: Distribution of settling particles during filling. The surface loading is 12 m/h. The settling velocity is 5.4 m/h.

TankB: L=30, B=8, H=2 m

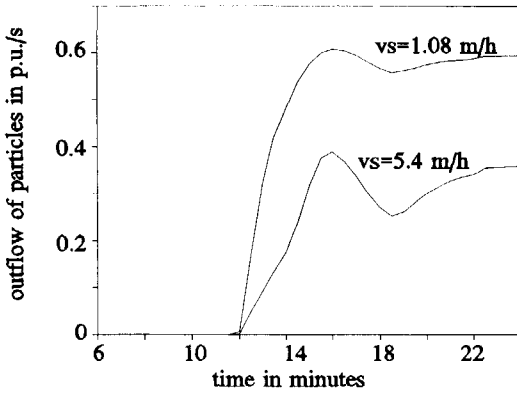


Figure 6.3: Outflow of particles with a settling velocity of 1.08 and 5.4 m/h.

figure for 6 minutes. After 12 minutes, the water reaches the top of the external weir and starts flowing out. The plume of high concentrations reaches the external weir after about 16 minutes. In figure 6.3 the effect of this plume is clear. The outflow of particles rapidly increases to a maximum at about 16 minutes, and then decreases to a minimum at 18 minutes. After 22 minutes, the particle concentration has almost reached less an equilibrium distribution, and the outflow concentration is almost constant.

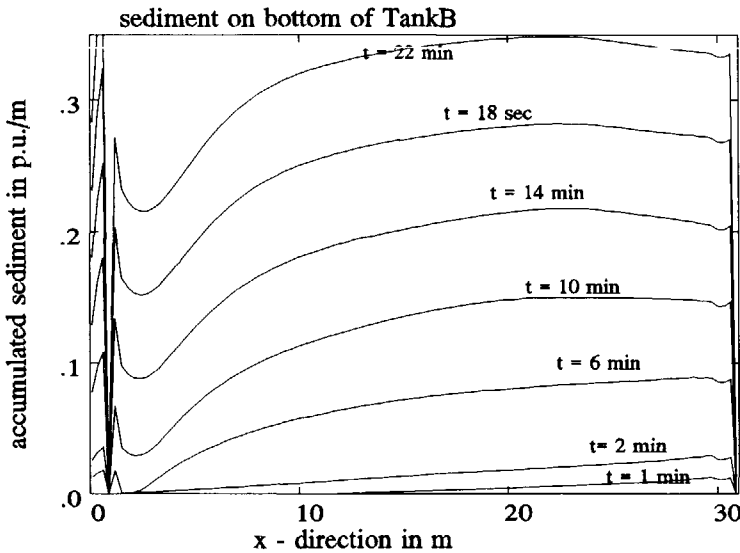


Figure 6.4: Accumulation of sludge on the bottom. x-axis is distance to inlet.

Figure 6.4 gives the accumulation of material on the bottom in pollution units per meter width of the tank (2-dimensional case). As the concentration at the inflow is set to 1.0, and the inflow rate equals $0.1 \text{ m}^3/(\text{sm})$, the inflow of particles is $c \cdot Q_{\text{in}} = 0.1 \text{ p.u./s}$. The deposition is computed as $c \cdot \Delta x \cdot v_s \cdot f(\tau_d) \text{ p.u./}(\text{sm})$ and the accumulated deposits in p.u./m .

The figure shows that close behind the internal weir much less particles deposit than further downstream. From 2 minutes upwards, the lines indicate the deposits at intervals of 4 minutes. Downstream of the re-circulation zone the deposits of particles with this settling velocity are almost equally divided. Towards the end it reduces somewhat, because the concentration diminishes.

Computation time

The computation time for the simulation of these 22 minutes was considerable. To restrict the computation time to an acceptable level, the grid applied in this simulation is coarser than the grid applied for the steady state simulations. For the time dependent simulations, the cell length is $\Delta X = 0.25 - 0.30 \text{ m}$ and the cell height $\Delta Y = 0.15 - 0.19 \text{ m}$. This resulted in $104 \cdot 15$ cells in the tank of $L \cdot H_c = 30 \cdot 2.0 \text{ m}^2$. Still, the computation time was considerable: 10 to 60 times longer than the real time in the prototype. Hence, for the simulation of an inflow of 60 minutes, 10 to 60 hours of computation time would be needed. This is due to the high velocities occurring during the filling. In order to prevent divergence of the computation (and consequently useless results), the Courant number must always and throughout the flow domain be smaller than 1 in computations with a free water surface. The water falls over the weir into the tank with a velocity of 2.7 m/s . With a cell height of 0.2 m the time step then has to be smaller than 0.074 s . The computations have been started with a time step of 0.025 s . After the filling the time step has been increased to 0.5 s .

6.2 Validation on measurements

The model for the simulation of flow and settling should be validated. The only data available of storm water settling tanks were some observations of the settling in an experimental setup and measurements of in- and outflow in real tanks. Sufficient reliable data concerning concentrations inside tanks during operation are lacking. To obtain a complete picture of the particle distribution in a tank, samples should be taken during operation at various points of time and at a range of representative locations. As it is impossible to know when a CSO will occur, the equipment must be ready permanently. Furthermore, the samples need to be analyzed. To realise this in covered storm water settling tanks is extremely troublesome and expensive. For these reasons extensive measurements of the water quality and of the flow situation inside tanks have never been carried out.

As an alternative to measurements in storm water settling tanks, measurements of other flow situations with settling could be used to validate the mathematical model. The flow in secondary clarifiers has been investigated, measured and simulated by several researchers (e.g. McCorquodale and Zhou, 1993; and Rodi and Krebs, 1995). The geometry of the flow with in- and outflow over weirs, and the presence of a baffle which creates a re-circulation zone, resembles the flow in a storm water settling tank. However, the settling conditions and some parts of the flow conditions are very different. In a secondary clarifier, the concentrations are so high and the flow velocities so small that density currents are present, settling is hindered, and sludge near the bottom creates a sludge blanket which consolidates. The flow in a storm water settling tank is far more turbulent, the concentrations are much lower, and the settling velocities can be much higher. Furthermore,

storm water settling tanks need to be filled before water flows out, and the flow rate changes. Therefore, measurements in secondary clarifiers have not been used to validate the model.

More data was studied, but not used. To provide data, measurements have been conducted in a scale model of a settling tank of the laboratory of Civil Engineering. The setup was different from the scale model presented in Chapter 3. Arévalo (1996) presents that the model seems to work properly, but that the measurements were not suitable to draw firm conclusions.

A final option for calibration data is measurements of water flowing over CSO's (with or without tank) and the inflow in a tank (both changing in time). Such measurements are available.

6.2.1 Storm water settling tank at Amersfoort

The measurements carried out for the storm water settling tank at Amersfoort ($32 \times 8 \times 2.6 \text{ m}^3$) concern the water depth and amongst other things, the concentrations of settleable COD in the inflowing and outflowing water. Only the data of rain events which resulted in external overflows have been registered. In 2.5 years, 17 events with external overflows have been recorded and sampled. One of these has been used to evaluate the functioning of the model.

The inflow and outflow is depicted in figure 6.5. The flow rate and the concentration of COD vary in time. For this event a first flush is apparent. Most of the pollution (in kg COD) is present in the first part of the inflow, as can be seen in the figure. The flow and settling resulting from this inflow has been simulated. The results showed a clear plug flow after the filling. Due to this plug flow, the high concentrations flowing in with the first water are pushed out by the clearer water entering later. Possibly, the total outflow of pollutants would have been less if the tank had been used only to catch the first flush⁽¹⁸⁾.

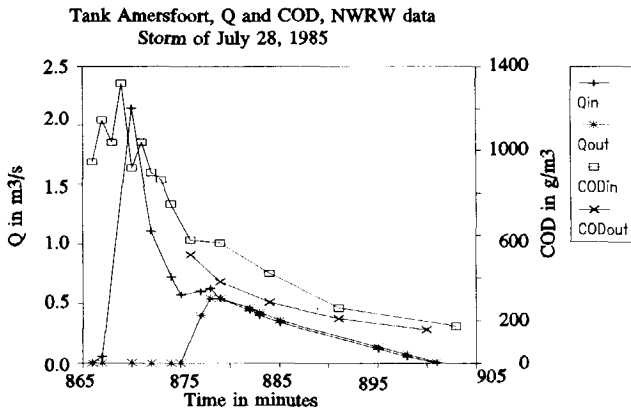


Figure 6.5: Measurements of in- and outflow in storm water settling tank.

⁽¹⁸⁾ The occurrence of a first flush and the advantages of creating a part of the tank as a detention tank, as to store the first flush, are not part of this research. This research focuses on the improvement of the settling conditions.

The settling velocity of particles to which the COD is connected is not known. The simulations predict the flow and settling for several settling velocities. Figure 6.6 gives the outflow of COD for a settling velocity of 1.08 and 8.9 m/h, as well as the measured in- and outflow in COD/s. The computed outflow of particles with a settling velocity of 8.9 m/s is about equal to the measured outflow (OUT). The computed outflow is later than the measured outflow. However, the measured outflow comes earlier than what would be expected, based on the inflow and the volume of the tank. It should start at 9 minutes. The shape of the outflow however, is sufficiently similar to gain confidence in the model.

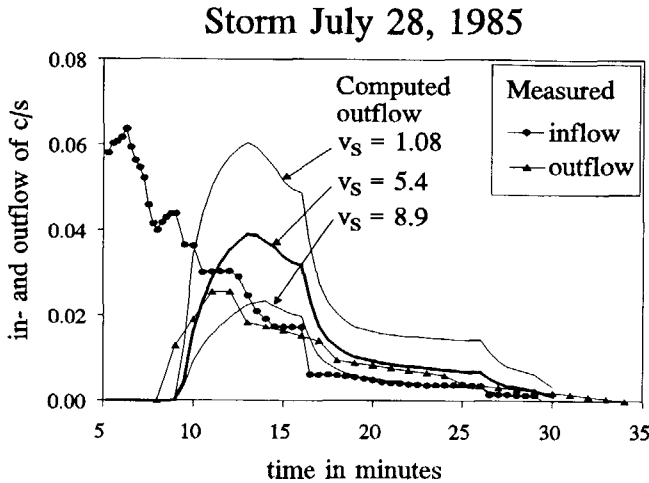


Figure 6.6: Measured in- and outflow and computed outflow for tank of Amersfoort.

6.2.2 Needed future measurements

Although the setup of the mathematical model is expected to be conceptually correct, measurements inside real tanks are needed to validate the simulations. Furthermore, more measurements of the in- and outflow are needed to evaluate the functioning of existing tanks. This can't be entirely based on flow simulations as the real settling velocities and flow rates are unknown.

The measurements should concern the quality and quantity of the inflow and outflow of the tank. This means flow rates, and concentrations of one or more chosen pollutants. The samples should be used to derive settling velocity distributions. With the measurements of the in and outflow, the tank can only be observed as a black box. To gain real insight in the processes in the tank, velocity and concentration profiles in the tank are needed. Because the flow is time-varying, such measurements require several measure gauges at a fixed location throughout the loading of the tank.

6.3 Sensitivity analysis

Due to lack of data the simulation of the settling could not be validated to full extent. However, the setup of the model is believed to assure a sufficient description of the most important processes in tanks, so that the simulation results are trustworthy. Away from the boundaries, the equations

are basically right and correctly model the settling of discrete particles with a given settling velocity, except for the following points:

- * The numerical diffusion might influence the particle distribution.
- * The effect of turbulence on the particle distribution has been modelled by means of a diffusion term (Reynolds analogy). The value of the Schmidt number, the constant in the diffusion terms, is uncertain.
- * The particles have been assumed not to influence each other or the water flow.

With regard to the boundary conditions are the following two points of importance.

- * Near the tank bottom particles might deposit or be eroded from the bottom. The way in which these processes have been modelled might influence the simulation results.
- * The modelling of the water surface as a rigid lid, or the assumptions in a free surface computation, might influence the particle distribution near the water surface.

In order to investigate the sensitivity of the simulation results to changes in the model, sensitivity analyses have been carried out. This section presents the results of sensitivity analyses of the model to numerical diffusion, variations in the Schmidt number, variations in the bottom boundary condition, and the use of a rigid lid.

6.3.1 Numerical diffusion

Chapter 3 has shown that numerical diffusion is important in comparison to turbulent diffusion in the equilibrium flow situation. However, for the computed velocities and eddy viscosity this appeared to be unimportant. Figure 6.7 shows that also for the distribution of settling particles, the use of the finer grid - and therefore the reduction of the numerical diffusion - does not influence the particle distribution significantly. Figure 6.7 presents the relative particle concentration at a distance of 7.5, 15, and 22.5 m from the inlet for rigid lid computations with a coarse and a fine grid (as presented in Chapter 3). The y-axis denotes the distance to the bottom. Next to these concentration profiles, the outflow and removal ratios have been evaluated. The removal ratio is the ratio of the outflow minus inflow to the inflow. They were almost identical for both grids, see table 6.1. The differences in the particle distribution and the removal ratios are so small that the coarse grid is considered to be good enough.

Table 6.1: Removal ratio for various settling velocities for coarse and fine grid.

v_s m/h	Coarse %	Fine %
1.08	9.1	9.1
1.80	14.8	14.9
2.52	20.3	20.4
3.60	28.2	28.2
5.40	40.0	40.0

6.3.2 Effect of the value for the Schmidt number in diffusion terms on the removal ratio

The Schmidt number influences the effect diffusion terms have in the transport equations. Its value is 1.0 by default. A threefold increase of the Schmidt number reduces the diffusion terms (both laminar and turbulent diffusion) to 1/3. The Schmidt number has been varied between 1/3 and

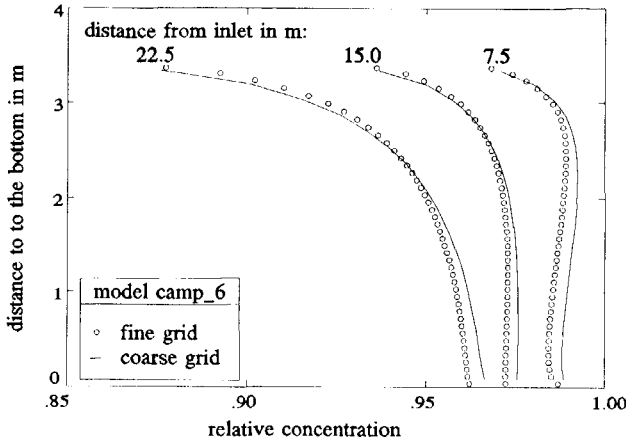


Figure 6.7: Distribution of settling particles for a coarse and a fine grid.

infinity (diffusion neglected). The effect appeared small and acceptable. Only when deposition was hindered, so that pollutant concentrations near the bottom rose, was there a significant effect.

Table 6.2: Removal ratio due to settling for standard and increased diffusion term (Schmidt number 1,0 or 1/3).

v_s m/h	Standard %	Increased diffusion terms %
1.08	9.1	8.9
1.80	14.8	14.5
2.52	20.3	19.8
3.60	28.2	27.2
5.40	40.0	38.2

See the column of the increased diffusion terms in table 6.2. Because of this, the value of the Schmidt number is not important. Apparently, like for the water flow, also for the transport of settling solids, the diffusive transport is only of minor importance.

The following remark should be made. Due to the use of the hybrid upwind scheme for the water flow variables, diffusion terms are not taken into account when they are small compared to the convective terms. However, for the distribution of the settling particles, always the fully upwind scheme has been used, so that the diffusion are always taken into account.

6.3.3 Sensitivity to changes in bottom boundary condition

The relation between velocity, turbulence, shear stress, concentration and the process of deposition or erosion is not sufficiently understood. This lack of insight, together with the lack of information on the characteristics of the particles and sediment, means that the chosen boundary condition might not give a sufficient description of reality. In order to test the functionality of the chosen boundary condition, this section shows the effect of variations in the parameters and the next section shows the effect of variations in the formulation of the bottom boundary condition.

Variations in τ_d affected the concentrations near the bottom. The value of τ_d , the critical value of the shear stress above which no particles deposit, has been changed in order to investigate the sensitivity of the removal ratios to the variations. The variations were such that the results ranged from increased deposition to no deposition at all. A lower value of τ_d resulted in more hindering of deposition, so higher concentrations near the bottom and further upwards. However, due to settling, the effect of this on the concentrations near the water surface was negligible. Furthermore, due to the fact that the deposition is a function of the concentration and higher concentrations result in more deposition, the effect of the variations in τ_d is limited. For flow situations in which the horizontal velocity is so high that settling is hindered, the effect is highest.

The effect of variations in the value of τ_c , the critical value of the shear stress above which particles erode, has not been investigated. The reason is that in the steady state simulations the effect of erosion is not present. It is not present, because if the shear stress would be so high that erosion would occur, then all sediment at that point would eventually be eroded, after which no sediment can be eroded any more.

Consideration has been given to the possibility that the computation of the shear stress τ_b as a function of u_{*1} (as presented in Chapter 2), might result in a wrong description of erosion and the hindering of deposition. This concern arose because u_{*1} tends to zero at the end of the re-circulation zone as the horizontal velocity goes to zero. This results in very small values for τ_b at the end of the re-circulation zone, indicating that particles can easily deposit there. In reality, relatively large eddies from the mixing layer are transported towards the bottom at the end of the re-circulation zone. These eddies might effectively hinder the deposition and even cause erosion of particles. If this were so, basing τ_b on u_{*1} would be incorrect. A more realistic approach is to base τ_b on u_{*2} , which is a function of the local value of the kinetic energy of turbulent motion (see also Chapter 2). Computed in this way, the values of τ_b do not tend to zero at the end of the re-circulation zone.

When the average horizontal velocities were so low that deposition was not hindered, the differences in removal ratio, computed with τ_b based on u_{*1} or u_{*2} , were small and acceptable. Only when deposition was hindered the effect becomes significant. The removal ratio was even lower as deposition was hindered to a greater extent.

Conclusion

The derivation of a more fundamentally based boundary condition requires further fundamental research into the behaviour of particles close to the bottom as a function of local factors such as velocity, kinetic energy of the turbulent motion, and eddy viscosity. Due to the lack of good calibration data it is not possible to precisely determine the bottom boundary conditions. Before more research with flow simulations using different boundary conditions is carried out, measurements are needed to validate the boundary condition and to gain more insight into the

processes. It is very well possible that the boundary condition in reality also depends on characteristics of the particles, so that these also need to be known.

The simulations have however showed that the removal ratio is not sensitive to this boundary condition if deposition is not hindered. For these cases the removal ratios are concluded to be reliable.

6.3.4 Rigid lid computation

In order to limit the computation time, the flow and settling in the steady state situation can be computed with a rigid lid model. The distribution of the settling particles appear to be just a little bit different from the computations with the free surface. See figure 6.8, which presents the relative concentrations for the lightest material at three cross sections in the tank (at x m from the internal weir, with $x = 7.5, 15,$ and 30 m). Table 6.3 gives the removal ratios for five particles with different settling velocities as computed with a free surface and with a rigid lid.

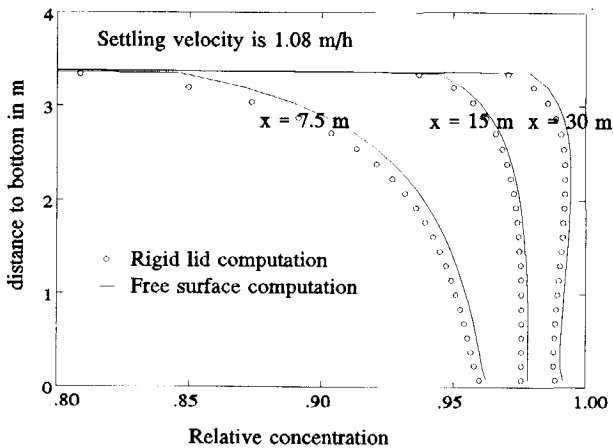


Figure 6.8: Effect of simplification to rigid lid on particle distribution for steady state.

Table 6.3: Removal ratios for free surface and rigid lid computation.

v_s m/h	Free surface	Rigid lid
1.08	8.7	9.1
1.80	14.2	14.8
2.52	19.5	20.3
3.60	27.1	28.2
5.40	38.6	40.0

For the steady state situation the rigid lid computation satisfies and is much faster than a free surface computation. The rigid lid simulation can compute towards the equilibrium situation in one

step, whereas the free surface method is a time dependent simulation which needs to simulate many small time steps until an equilibrium flow and particle distribution has been reached. This and the increased number of cells and variables present in the free surface computation, makes the rigid lid computation of the equilibrium situation 10 to 100 times faster.

The computation time is not important when only one or several flow situations need to be evaluated. But, for the investigation of the effect of changes in tank shape and in order to derive design rules it is important, since many flow situations will have to be evaluated. For that purpose, rigid lid simulations will be carried out.

6.4 Conclusion

In order to validate the model, measurements of the in- and outflow in a storm water settling tank have been used. The simulation results give confidence in the functioning of the model. However, a validation based on only this data is too scarce to draw firm conclusions. Therefore, the sensitivity of the model to variations in the setup has been checked. It showed that the model is not sensitive to variations, when the average horizontal velocity is so low that deposition is not hindered.

The model was concluded to sufficiently accurately model the processes. An important consideration is that the model will be used to compare different designs of tanks. In that point of view the exact prediction of the removal ratio is not needed. The model is useful if it sufficiently describes the processes and correctly predicts the effect of changes in the design.

Furthermore, as long as the characteristics of the pollutants are not sufficiently known, the exact outflow cannot be predicted anyway.

Chapter 7

DESIGN RULES FOR RECTANGULAR TANKS

7.1 Introduction

The mathematical model simulates the processes of flow and settling, and predicts the removal ratio. In theory, it can be used to obtain the optimum design in each case. However, it is not feasible to use the mathematical model for each design, because presently, the time needed to simulate and evaluate the functioning of different designs is far too long⁽¹⁹⁾. Furthermore, to obtain reliable results the designer has to have experience in using the CFD code. Therefore, the mathematical model has been used to derive a set of design rules which can be used in most common cases. Since most future tanks in the Netherlands will be rectangular tanks, design rules for rectangular tanks will be derived. To this end, the flow and settling have been simulated for a range of rectangular tanks and their functioning has been evaluated.

To derive such design rules, it is not possible to use only 3-dimensional time dependent flow simulations. The simulation of the full time-dependent processes in the tank (i.e. the process of filling and the flow through the tank, combined with settling) in a 3-dimensional flow domain is still far too time consuming. In order to obtain reliable results, the time steps and cell sizes must be so small that the simulation of a flow situation takes several weeks of continuous computational time on the work station used in this research. Therefore, the model has been simplified. The first simplification was to assume 2-dimensional flow situations in the vertical plane. This reduces the computational time considerably to between 10 and 60 times longer than the real time. This means

⁽¹⁹⁾ In the future, the computational time is expected to go down to an acceptable level due to the progress in computer hardware, and will eventually no longer be a problem. However, the setting up and use of a mathematical model and also the evaluation of the results will stay so time consuming that the use of such a model in design practice will remain limited to special cases.

that the simulation of the flow due to a discharge of 60 minutes would take 10 to 60 hours! This is too long for the evaluation of a large range of tanks.

A further simplification was required. The simplification chosen was to compare the functioning of various tanks under steady state conditions (i.e. with both the flow of water and the settling of particles in equilibrium). The computational time for the simulation of a steady state condition in a 2-dimensional model of a rectangular tank is small enough to allow the evaluation of many tanks with various flows. Section 7.2 describes the results of these simulations and the design rules which have been derived from them. These design rules help to estimate the removal ratio for rectangular tanks under 2-dimensional, steady state conditions.

To investigate whether the design rules, based on the 2-dimensional steady state simulations, result in reliable predictions for the removal ratio in time varying flow situations, a limited number of separate simulations of time varying flow situations have been carried out. Section 7.3 describes the effect of variations in the inflow and of the filling, on the functioning of a tank. Section 7.4 presents the effect of the simplification from 3-dimensional to 2-dimensional. Section 7.5 concerns the effect variations in the bottom boundary condition have on the results of this research. Section 7.6 discusses the probability of short-circuiting. The use of a baffle, or a diffusor, is generally expected to increase the removal ratio. The effect of these will be discussed in section 7.7. Finally, in section 7.8 the conclusions will be presented.

7.2 2-dimensional steady

Figure 7.1 depicts the general lay-out of the 2-dimensional flow domains for which the removal ratios for steady state conditions have been computed. As has been explained before, for steady state conditions the water surface can be replaced by a rigid lid. This reduces the computational time considerably. The simulation of an equilibrium situation (including the settling of particles) takes about 5 to 40 minutes on the work station. Therefore, the functioning of a large number of tanks can be evaluated under various flow conditions.

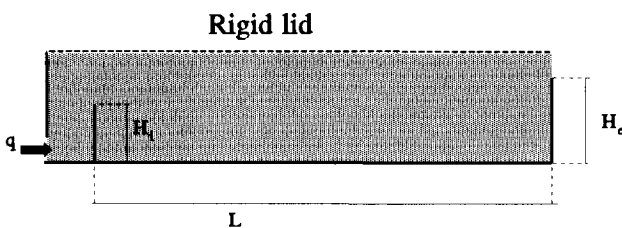


Figure 7.1: Lay-out of the 2-dimensional flow domain with rigid lid for the steady state.

In the steady state condition the removal ratio, RR, is entirely due to settling. It is a function of the inflow of the particles (IN) and the outflow of the particles (OUT):

$$RR = \frac{IN-OUT}{IN} * 100 \% \quad (7.1)$$

In the simulations, the settling velocities varied between the practical range of 0.25 and 25 m/h. The inflow boundary condition was a fixed inflow rate at the lower left hand side (see figure 7.1). The water flowed out over the external weir at the right hand side. Different tank volumes (or detention times) and different flow rates have been adopted. In addition, the effect of variations in L, B (width), and H_c has been investigated. The height of the internal weir H_i was in most cases 75 % of that of the external weir H_e .

Amongst the many situations considered were several sets of situations with a constant tank volume. The volume is one of the major determining factors of the total removal ratio. The greater the volume, the more water is stored and not spilled. The volume is also a major factor in the cost of a tank. For that reason, it is logical to investigate the effect of changes in design for tanks with the same volume. In the 2-dimensional model this was achieved by choosing combinations of the flow rate per m width (q), the length (L), and the height (H_c) in such a way that the average detention time $T = (L.H_c)/q$ was constant. These combinations can be regarded as those of 3-dimensional tanks with the same volume and flow rate.

7.2.1 Removal ratio in relation to the shape and the flow rate

This section describes the computed removal ratios for about 60 different flow situations with different values of the volume, the flow rate, the length, the width, or the height. For each flow situation, the removal ratios of five different settling velocities have been computed.

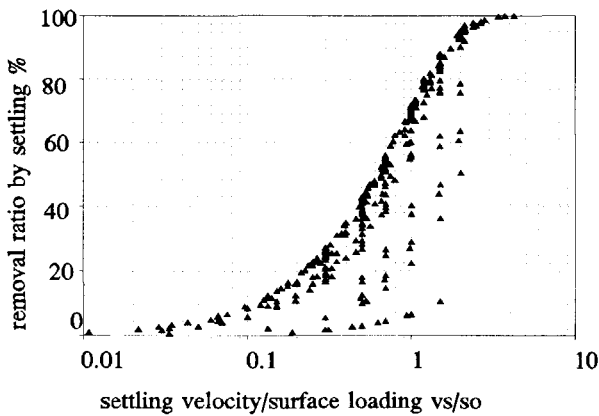


Figure 7.2: Computed removal ratios versus v_s/s_o for steady state conditions in rectangular tanks.

Figure 7.2 presents all the computed removal ratios. The x-axis represents the settling velocity, v_s , divided by the surface loading, s_o . All points are clearly below a curve. When only those removal

ratios are depicted, which are the result of simulations in which the average horizontal velocity, $u^{(20)}$, is less than 0.1 m/s, the remaining points appear to form the curve. See figure 7.3.

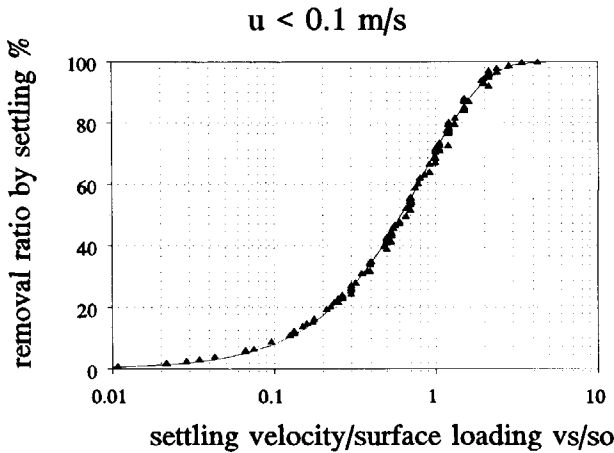


Figure 7.3: Computed removal ratios versus v_s/s_o for steady state conditions in rectangular tank and line representing the upper limit.

This curve is very well represented by the equation:

$$R_0 = 100 * \left(1 - e^{\left[-1.22 \left(\frac{v_s}{s_o} \right)^{1.16} \right]} \right) \% \quad (7.2)$$

where R_0 is the removal ratio due to settling for the steady state in rectangular tanks. As will be explained in the following, this equation is valid for situations in which the average horizontal velocity is less than 0.15 m/s. For increasing values of u the removal ratio rapidly decreases. This reduction is due to extra diffusion by turbulence, as well as due to hindering of deposition. In the first place, the higher turbulence levels coming with higher velocities cause more diffusion and thus have an adverse effect on the settling. In the second place, the deposition of particles on the tank bottom is increasingly hindered with increasing flow velocities near the bottom. When the shear stress along the bottom exceeds a critical value, no particles are deposited at all (see Chapter 5 and section 7.5).

In order to satisfactorily predict the removal ratio for values of u exceeding 0.1 m/s, a relationship between RR and several other variables has been sought. An obvious relation would be one between RR and v_s/s_o and v_s/u , as in the commonly used Camp graph (see Appendix B). Figure 7.4 presents

⁽²⁰⁾ The average horizontal velocity u equals $u = q/H$, in which H denotes the water depth, i.e. the height of the external weir plus the depth above the external weir.

some simulation results superimposed on the Camp graph. The horizontal axis gives the settling velocity divided by the average horizontal velocity: v_s/u , the vertical axis gives the removal ratio. The lines in the figure are the lines for equal values of v_s/s_o , as according to Camp.

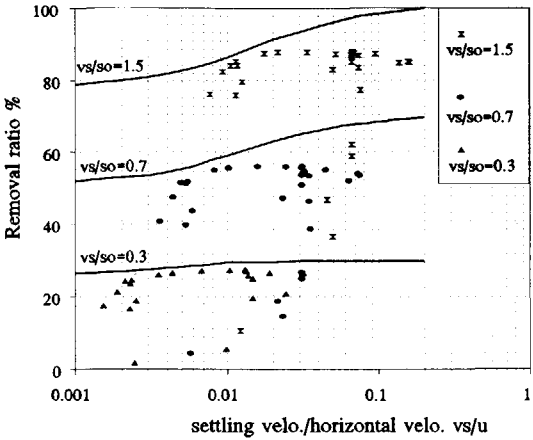


Figure 7.4: Removal ratio versus v_s/u graph according to Camp and this research.

Many of the points (i.e. the simulation results) for equal v_s/s_o values can be well represented by a single line. Only some points are remarkably lower. These lower points are the result of flow simulations with such high horizontal velocities that diffusion due to turbulence reduced the settling and deposition was hindered.

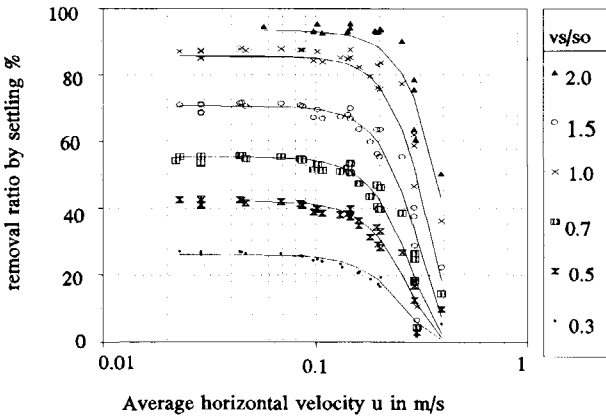


Figure 7.5: Removal ratio versus u for various values of v_s/s_o .

It appeared not to be possible to sufficiently accurately represent the removal ratio by an equation of v_s/s_o and v_s/u . An equation relating RR to v_s/s_o and u appeared to much better represent all simulation results. See figure 7.5, which presents the removal ratio for points with equal values of v_s/s_o , with the x-axis representing u . In this graph, the points with equal values of v_s/s_o can be represented much better by single lines, because the hindering of deposition in the model has been made independent of the particle size and thus of the settling velocity (see Chapter 5). Above a value of 0.10 m/s, the lines which can be drawn through points of equal values for v_s/s_o bend downwards. It can be seen that, above 0.20 m/s, the reduction of the removal ratio is of particular importance. Based on this graph a velocity of 0.15 m/s has been concluded to be a critical value. Below 0.15 m/s the reduction of the removal ratio due to hindering of deposition is assumed to be acceptable.

The lines in the figure can be described in the following empirical form:

$$RR = 100 * (1 - e^{\left[-1.22 \left(\frac{v_s}{s_o} \right)^{1.16} \right]}) * e^{A_1 u^{A_2}} \% \quad (7.3)$$

with	$A_1 = 100$	if $v_s/s_o < 0.8$
and	$A_1 = 146.7 - 58.3 * v_s/s_o$	if $0.8 \leq v_s/s_o < 2.5$
and	$A_1 = 0$	if $v_s/s_o \geq 2.5$
	$A_2 = 3.38 + 0.4 * v_s/s_o$	if $v_s/s_o < 1.3$
and	$A_2 = 3.9$	if $v_s/s_o \geq 1.3$

This equation predicts the removal ratio, RR, for steady state situations in rectangular tanks. For values of u smaller than 0.15 m/s, this equation results in almost the same values as the equation for R_0 (equation 7.2). The relation is presented in figure 7.6.

In the simulations the values for L/B ranged between 1 and 20. The fact that most points are close to the line in figure 7.3 for various L/B ratios, indicates that the length of the re-circulation zone does not significantly influence settling. For equal values of v_s/s_o , a short and wide tank retains about as much particles as a long and narrow tank. Only very long and narrow tanks result in a lower removal ratio. This is due to a greater effect of turbulence and hindering of deposition in the long and narrow tank, which is a result of the higher horizontal velocity.

The fact that one line represents the points for values of u less than 0.15 m/s so well, indicates that the removal ratio for those cases is a function of v_s/s_o only. This relation (equation 7.2) shows that the surface loading should be as small as possible to obtain the highest removal ratio. This requires a shallow tank with a large surface area. According to the simulation results, the only restriction is that the average horizontal velocity should not be too high. This can in theory always be met by making the tank wide enough⁽²¹⁾. However, in practice, it will be prohibitively expensive to construct a very shallow tank. Generally, the land requisition is expensive or the available land is

⁽²¹⁾ The results have been based on simulations of 2-dimensional situations. The wider a tank is, the sooner 3-dimensional flow situations will occur, unless these are prevented.

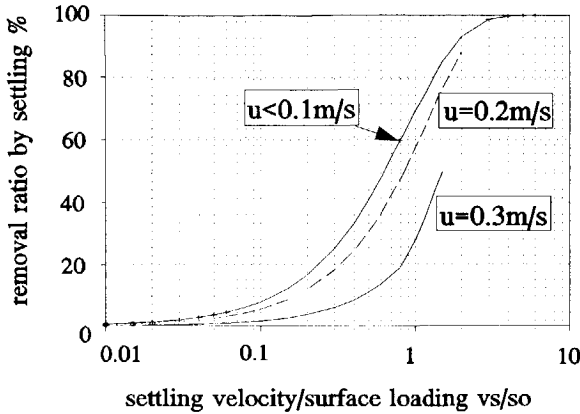


Figure 7.6: Removal ratio as a function of v_s/s_o and u for steady state conditions in rectangular tanks.

limited. Furthermore, the amount of construction material needed increases as the shape of a tank diverts more from the cubic one. Consequently, for the same costs, a larger volume can be constructed if the land requisition is kept minimal (a deeper tank). Because the storage of water reduces the pollution load, the overall efficiency can be higher for a tank with a larger volume, but a smaller surface area (and consequently a smaller removal ratio due to settling). A disadvantage of deep tanks are the costs for pumping the water back up to the sewer system. Furthermore, measures will have to be taken to prevent the tank from being pushed upwards due to the ground water pressure when the tank is empty.

7.2.2 Comparison of the Camp graph and the equation found.

The Camp graph is used in the present Dutch design method to bring into account the effect of turbulence on the removal ratio (see Appendix B). It is not possible to directly compare the removal ratios according to the Camp graph and those according to equation 7.3. To that purpose, firstly a value for the settling velocity must be chosen. Figure 7.7 presents the lines according to Camp and equation 7.3, for settling velocities of 2 and 10 m/h. The results are furthermore difficult to compare because the surface loading for the lines according to Camp are based on the surface loading of the settling zone of the tank only, whereas the surface loading for the lines according to the present research are based on the surface of the whole tank. Consequently, in order to compare these removal ratios, the removal ratios according to the simulations must be compared with those of Camp for lower values of v_s/s_o .

Unlike the lines of Camp, the lines of the present research do not predict a removal ratio equal to 100% or v_s/s_o for high values of v_s/u . For decreasing values of v_s/u , the lines of the present research predict a sharp decrease of the removal ratio. This is due to higher diffusion through turbulence and the resulting hindering of deposition arising from the higher horizontal velocities. This decrease in removal ratio is not present in the results of Camp, as he did not incorporate the hindering of deposition and applied a constant value for the coefficient for the diffusion due to

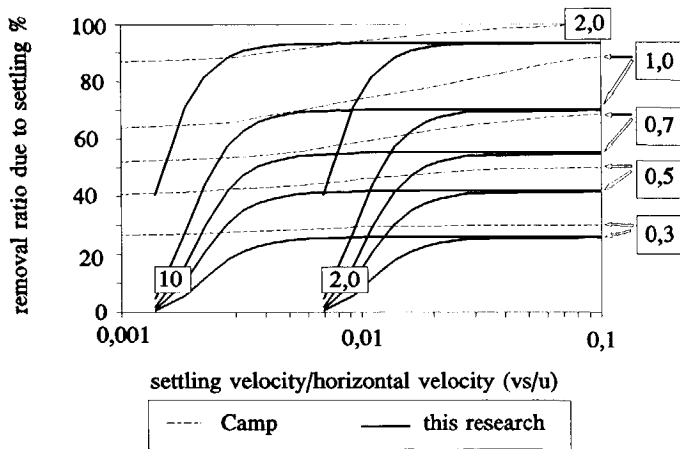


Figure 7.7: Presentation of the present results in the Camp graph. For the lines according to Camp, s_0 is based on the settling zone, whereas for the present research it is based on the whole tank.

turbulence.

For high values of v_s/u , the differences between the simulation results and the Camp graph are due to the fact that the simulations take into account the flow in the entire tank, including the re-circulation zone, whereas the Camp graph is based on the surface loading on the settling zone only. High values of v_s/u occur in wide, deep tanks (low values of u). In such tanks the re-circulation zone consumes a larger part of the tank. Indeed, because of this different method of computing s_0 , it is not possible to compare the removal ratios of the two methods in one graph for different designs.

Figure 7.8 depicts the differences between the removal ratios predicted with the Camp graph and those based on the equation developed in this research (equation 7.3). In order to determine the removal ratios according to Camp, the length of the settling zone has been assumed to be $L_s = L - 7 \cdot H_i$. From the left to the right the values of $1 - L_s/L$ increase, so the reduction of the length of the settling zone (and consequently the increase in surface loading in the settling zone for the Camp graph) is most important for the results at the right hand side of the figure. In each simulation, 5 settling velocities have been considered. The differences between the removal ratios according to the Camp graph and equation 7.3 can be large. The removal ration according to Camp was up to 34% greater than that according to equation 7.3 (for a situation with a very high horizontal velocity; 0.44 m/s), and up to (61%) lower (for a very deep tank, in which the re-circulation zone reduced the length of the settling zone to a few meters only).

In the cases in which the removal ratio according to Camp is higher than according to equation 7.3, the average horizontal velocity was high (hindering of deposition). The flow simulations in table 7.1 resulted in more than 10% higher removal ratios according to the Camp graph than found in this research.

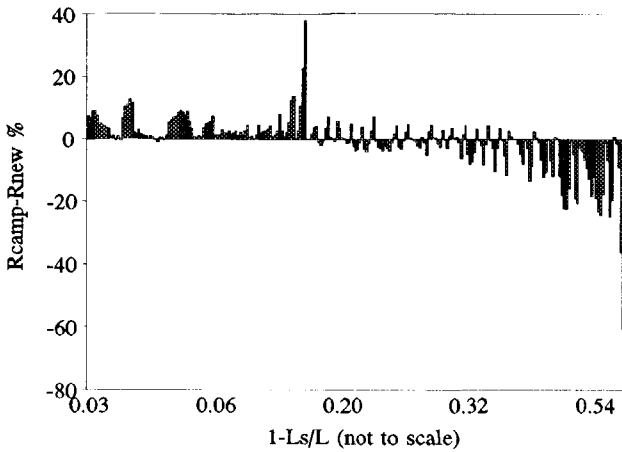


Figure 7.8: The removal ratios according to Camp minus the removal ratios according to the present research.

Table 7.1: Tanks for which the removal ratio according to the Camp graph is more than 10% higher than found in this research.

L m	B m	H _i m	H _e m	Q m ³ /s	u m/s	1-L _s /L
131	8	0.60	0.80	1.6	0.25	0.03
31	8	0.45	0.90	1.6	0.22	0.10
31	8	0.45	0.90	3.2	0.44	0.10

The removal ratios according to Camp were lower than those found during the present research for cases in which the re-circulation zone occupies an significant part of the total tank. In these cases the surface loading based on the settling zone, is considerably lower than the removal ratio based on the whole tank. The effect is most pronounced for particles with settling velocities almost equal to the surface loading. Table 7.2 presents the simulations which resulted in a more than 10% lower removal ratio according to Camp than found in this research. All average horizontal velocities are below 0.15 m/s.

Table 7.2: Tanks for which the removal ratio according to the Camp graph was more than 10% lower than found in this research.

L m	B m	H _i m	H _c m	Q m ³ /s	1-L _s /L	L/B
35	7.1	1.80	2.4	0.8	0.36	4.9
40	5.0	2.25	3.0	0.4	0.39	8.1
31	8.0	1.80	2.4	0.8	0.41	3.9
31	8.0	1.80	2.4	1.6	0.41	3.9
31	8.0	1.80	2.4	0.4	0.41	3.9
30	8.9	2.25	3.0	0.8	0.53	3.4
24	10.3	1.80	2.4	0.8	0.53	2.3
32	8.0	2.46	3.28	0.8	0.54	4.0
32	8.0	2.46	3.28	0.8	0.54	4.0
33	5.0	2.70	3.6	0.4	0.57	6.7
31	8.0	3.80	4.4	0.8	0.86	3.9

Except for the last tank, the tanks in the table are not exceptionally deep. The ratio of L/B in tables 7.1. and 7.2 varies between 2.3 and 8. Tanks are generally designed with an L/B ratio between 5 and 10.

Equation 7.3 gives a more realistic prediction of the removal ratio under steady state conditions than the results obtained by Camp. This is due to a more realistic description of the processes in this research:

- A) It bases the results on the simulated flow situation in the whole tank (i.e. including the re-circulation zone), and not on assumed uniform flow conditions in a part of the tank.
- B) The effect of turbulence on the distribution of the particles is accounted for based on the calculated local levels of turbulence. In the Camp graph, this effect is based on the turbulence in the equilibrium flow conditions in a channel.
- C) Hindering of deposition, and the effect of erosion, are accounted for based on the velocities near the bottom. In the Camp graph, these effects are absent.

Furthermore, the results of this research are easier to use than the Camp graph, since they predict the removal ratio in a single equation, while the removal ratio according to Camp has to be deduced from a graph. A second reason why it is easier to use is that the surface loading is based on the well defined total area of the tank, whereas for the Camp graph it is based on the area of the settling zone, the size of which must be estimated.

7.2.3 Conclusion

The flow simulations have resulted in an equation which predicts the removal ratio in the steady state situation for 2-dimensional flow in rectangular tanks. This removal ratio is a function of v_s/s_0 and u . For values of u below 0.15 m/s, the removal ratio only depends on the ratio v_s/s_0 . The highest removal ratio occurs in tanks with the highest values of v_s/s_0 . For higher values of u than 0.15 m/s, the removal ratio decreases. Tanks should be designed in such a way that an average horizontal velocity of 0.15 m/s is not exceeded too often.

The developed equation predicts removal ratios which differ from the ones following from the widely used Camp graph. It is based on more realistic assumptions than the assumptions which Camp made to predict the removal ratios, leading to more realistic rules. The refined and more realistic approach together with the ease of use, are the obvious benefits of the developed equation.

7.3 Time dependent 2-dimensional

The equation predicting the removal ratio is based on steady state situations. However, in reality, tanks will be empty at the beginning of a storm, so they must first be filled before water flows out. Furthermore, both flow rate and inflow pollution concentration will vary in time. This section describes simulations carried out to determine whether the design rules based on simulations of the steady state are reliable for real flow situations: i.e. under time-varying flow conditions and including tank filling. Variations in inflow concentration have not been considered. The model layout for the time dependent 2-dimensional simulations is about the same as that in figure 7.1. Each simulation was run for three to five different settling velocities.

7.3.1 Flow and settling in tanks loaded at a constant rate for a limited duration.

This section presents the results of simulations of flow and settling in tanks loaded at a constant rate for a limited duration. The total simulation time was extended after the inflow stopped, to permit the investigation of the trail off in the outflow. Table 7.3 shows the characteristics of the five tanks for which the process of filling and the consequent overflowing has been simulated. The volume is 480 m^3 , the flow rate is $2/3 \text{ m}^3/\text{s}$.

Table 7.3: Dimensions of tanks for which the process of filling and overflowing has been simulated.

	L	B	H _c	L/B	s _o
	m	m	m		m/h
TankA:	15	16	2	0.94	10
TankB:	30	8	2	3.75	10
TankC:	48	5	2	9.60	10
TankD:	30	16	1	1.88	5
TankE:	60	8	1	7.50	5

In the 2-dimensional model, the flow rate per running m width incorporates the differences in width. These simulations give insights into the effects which the L/B ratio and the surface loading have on the removal ratio in time dependent flow situations.

Particle concentrations in the computations are relative to the (constant) inflow concentration, which has been set to 1.0. To facilitate the following discussion, the inflow is given in pollution units (p.u.). The particle load flowing in, is given in pollution units per second and in this case equals $Q_m * 1.0 = 2/3 \text{ p.u./s}$.

The outflow of particles is also in p.u./s. Figure 7.9 shows the computed outflow of settling particles with a settling velocity of $1.08 \text{ m/h}^{(22)}$. Water fills the tank and starts to spill after about 12 minutes. When the inflow stops, the water level drops and the outflow diminishes. The figure presents the inflow and outflow for inflow durations of 14, and 24 minutes. The small perturbations in the inflow between 8 and 14 minutes are due to submergence of the internal weir.

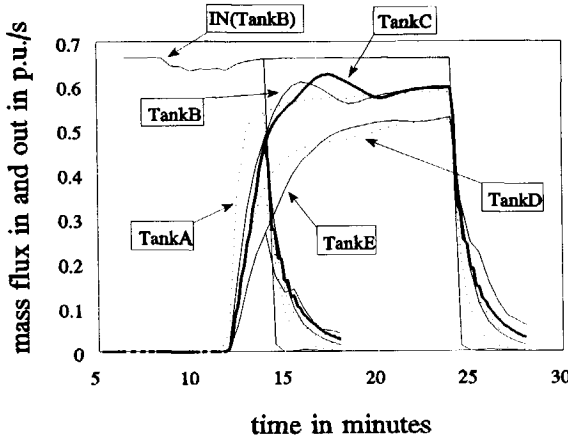


Figure 7.9: Particle outflow for 5 tanks of 480 m^3 , with $Q_{in} = 2/3 \text{ m}^3/\text{s}$ and durations of 14, and 24 minutes.

Besides durations of 14 and 24 minutes, also simulations with an inflow duration of 18 minutes have been carried out. Table 7.4 presents the outflow for durations of 14, 18, and 24 minutes. For 18 minutes of inflow, the total outflowing particle loads for TankA, TankB, and TankC (which have the same surface loading), are remarkably similar: 207, 205 and 203 pollution units, respectively. The inflow of $2/3$ pollution units per second during 18 minutes, adds up to a total of 720 pollution units. The outflow of TankA for a duration of 18 minutes thus equals 29% of the inflow. Figure 7.10 presents this percentage for the chosen durations. The outflow for the short and wide tank (TankA) is somewhat higher than that of TankB and TankC. The differences are most important for short durations of external overflow, but still only small. For an inflow duration of 14 minutes the TankA outflow is 120% of the TankC outflow. For a duration of 18 minutes it is only 101% of the TankC outflow.

⁽²²⁾ According to Stokes, sand grains ($\rho_s = 2650 \text{ kg/m}^3$) with a diameter of 0.0209 mm have such a settling velocity, for water of 13°C .

Table 7.4: Particle outflow as a ratio of inflow for different tanks and inflow durations (t_d in minutes) after filling of empty tanks.

	L m	B m	H_c m	s_o m/h	t_d :	$v_s=1.08$ m/h			$v_s=2.52$ m/h			$v_s=5.4$ m/h		
						14	18	24	14	18	24	14	18	24
TankA	15	16	2	10		0.13	0.29	0.44	0.10	0.23	0.36	0.06	0.14	0.24
TankB	30	8	2	10		0.11	0.28	0.43	0.08	0.23	0.35	0.04	0.14	0.23
TankC	48	5	2	10		0.11	0.28	0.43	0.07	0.23	0.36	0.03	0.15	0.23
TankD	30	16	1	5		0.09	0.23	0.36	0.05	0.13	0.23	0.01	0.04	0.08
TankE	60	8	1	5		0.09	0.23	0.37	0.05	0.14	0.24	0.01	0.05	0.09

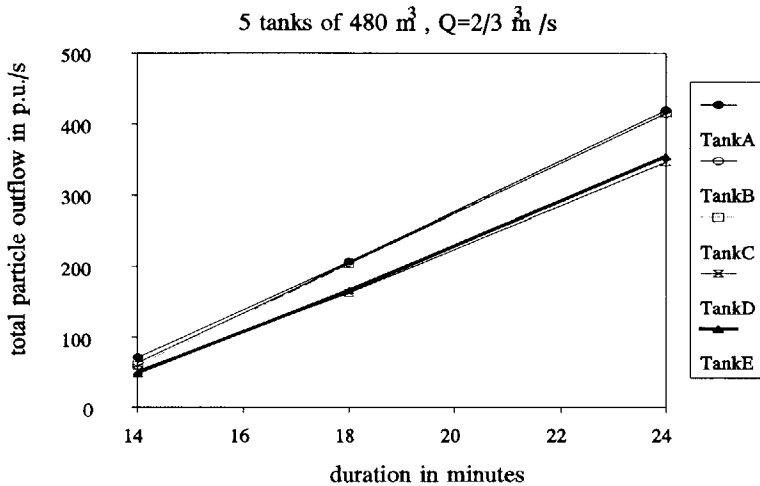


Figure 7.10: Particle outflow as a function of inflow duration for 5 tanks for a settling velocity of 1.08 m/h.

Because the inflow concentration is constant, the removal ratio due to settling R_s can be defined as:

$$R_s = 1 - \frac{OUT}{IN-VOL} \tag{7.4}$$

See table 7.5 and figure 7.11.

Table 7.5: Removal ratio (%) due to settling for different tanks and inflow durations (t_d in minutes).

	L	B	H_e	s_o	t_d	$v_s=1.08$ m/h			$v_s=2.52$ m/h			$v_s=5.4$ m/h		
						14	18	24	14	18	24	14	18	24
TankA	15	16	2	10	12	14	13	30	31	29	57	57	53	
TankB	30	8	2	10	21	15	14	43	32	29	72	58	54	
TankC	48	5	2	10	26	15	14	48	31	29	76	56	53	
TankD	30	16	1	5	35	32	28	65	61	54	90	88	83	
TankE	60	8	1	5	39	31	26	68	58	52	91	85	82	

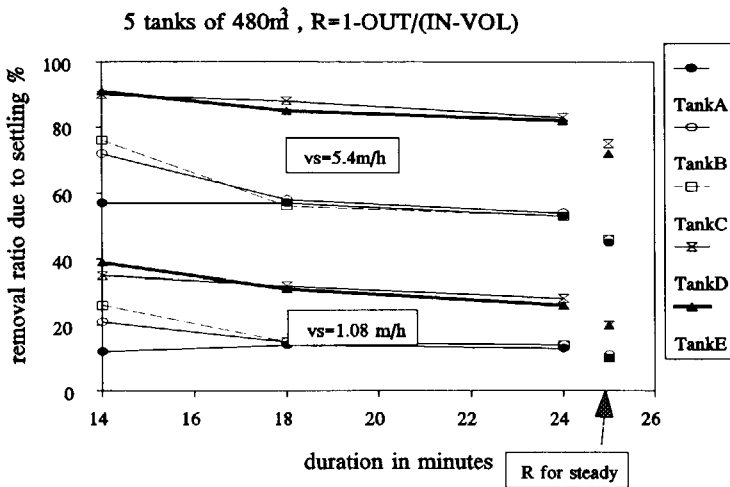


Figure 7.11: Removal ratio due to settling as function of inflow duration for 5 tanks.

The fact that TankA, TankB and TankC result in almost the same outflow of pollutants indicates that the L/B ratio is not important. This was also the result of the steady state simulations.

TankD and TankE are shallower. According to the 2-dimensional steady state simulations, the resulting lower surface loading should result in a higher removal ratio. Indeed, the outflow is much less than that of the deeper tanks. This indicates that, as already shown for steady state simulations, surface loading is also of major importance for the settling in time dependent flow simulations.

The removal ratio found for steady state simulations is smaller than that found for time dependent simulations. When the time dependent simulation was continued for a longer period, the difference diminished, but did not disappear completely. A part of this remaining difference is due to the fact that steady state simulations were rigid lid simulations, whereas in the time dependent simulations the varying location of the water surface was computed. This should be kept in mind when comparing results of rigid lid and free surface computations.

In the equilibrium situation for these simulations, the average horizontal velocities are smaller than 0.15 m/s. In fact, the highest value, which occurs in the tank with the smallest value of $L \cdot B$ (TankE), is 0.08 m/s. Hindering of deposition is therefore not expected in the equilibrium situation. Only during filling, locally higher horizontal velocities occur near the bottom and deposition is hindered. The highest horizontal velocities occur at the bottom near the inflow. Towards the outflow flow conditions are much more quiescent and settling is not hindered.

7.3.2 Step-loading

Various simulations of the flow in filled tanks show the effect of sudden fluctuations in the flow rate. In order to correctly bring into account the effects of changes in flow rate, the water-air interface was computed. Initially, the tanks are filled with quiescent clear water. At $t=0$, water starts flowing in at a rate of 0.8 m³/s. Next, the flow rate is doubled several times. Table 7.6 gives tank dimensions for which the effect of sudden changes in the flow rate have been investigated.

Table 7.6: Tank dimensions for which flow and settling in changing flow rate have been simulated.

	L	B	H _c
	m	m	m
TankF:	50	8	2.1
TankG:	25	16	2.1
TankH:	50	16	1.05

The flow rates taken are 0.8, 1.6, 3.2, and 6.4 m³/s, which for TankF and TankG result in surface loadings of 7.2, 14.4, 28.8, and 57.6 m/h. In TankH, the surface loading was 50% of these values.

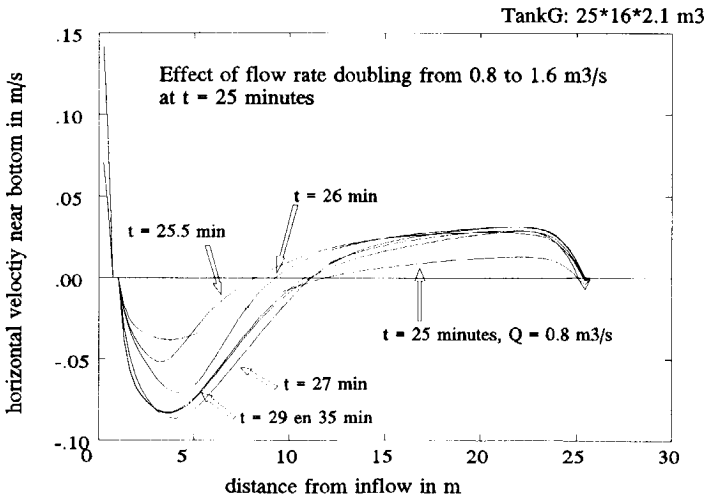


Figure 7.12: Horizontal velocity near bottom for a change in flow rate from 0.8 to 1.6 m³/s.

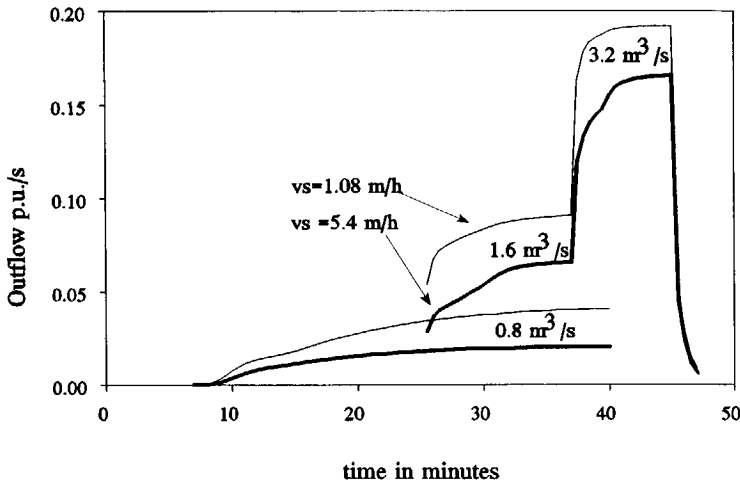


Figure 7.13: Outflow of particles due to step loadings for TankG with 0.8, 1.6, and 3.2 m³/s.

As can be seen in figure 7.12 the flow situation appears to reach a new equilibrium within a few minutes when the flow rate is doubled. It shows that when at $t=25$ minutes the flow rate is suddenly doubled, after half minute ($t=25.5$ minutes) the re-circulation zone is smaller, and grows again to approximately its former length after 2 minutes.

The distribution of settling particles, however, varies for a much longer period. See figure 7.13 which presents the outflow of particles with a settling velocity of 1.08 and 5.4 m/h. The figure shows that it takes about twice the average detention time before an equilibrium is reached when a tank is initially filled with quiescent clear water, and polluted water starts to flow in (for a flow rate of 0.8 m³/s the average detention time is 17.5 minutes). After 35 minutes the outflow seems to have reached an equilibrium. It takes so long because the clear water has to be pushed away by, or mixed with the inflowing water. When at $t=25$ minutes the flow rate is suddenly doubled, a new particle equilibrium is reached after approximately the average detention time (in this case, the detention times then is 8.74 minutes). In the steady state the outflow of particles becomes about equal to the $(1-R_0)$ times the inflow⁽²³⁾, with R_0 computed with equation 7.2.

7.3.3 Method to predict functioning of tanks in time-varying situations

Before computers became common tools for the design of sewer systems, it was impossible to determine the outflow out of a sewer system and the inflow into a tank as a result of a rainfall time series. The design of a tank could therefore not be based on such loadings, and was based on the evaluation of steady state situations. This way of designing has become common practice and at least gives some insight in the functioning of different tanks.

Nowadays it is possible to compute the outflow out of a sewer system as a result of a rainfall time series of several to many years. One of the Dutch water boards, Brabantse Waterkwali-teitsbeheerders (1995), requires that the design of tanks is based on their functioning for rainfall time series. It describes a method in which the functioning of a tank for such a loading can be assessed by separately taking into account the effect of storage and settling. The effect of filling

⁽²³⁾ The differences with the steady state simulations have been indicated in the previous section.

is taken into account by calculating the amount of water which is stored. The effect of settling is taken into account by assuming instantaneous steady state conditions for each flow rate, and in this way computing the removal ratio. However, the assumption that the removal ratio due to settling can be based on steady state flow conditions might result in an error in the calculation of the outflow. Simulations of step-loadings (like in section 7.3.2) showed that it takes roughly a duration equal the detention time before a new equilibrium has been reached. Furthermore, the effect of a previous the flow rate on the settling might be important, because it is logical that if the previous flow rate was low, more particles will be close to the bottom than when the previous flow rate was high. This is not taken into account. Finally also the effect of filling on the removal ratio is not taken into account.

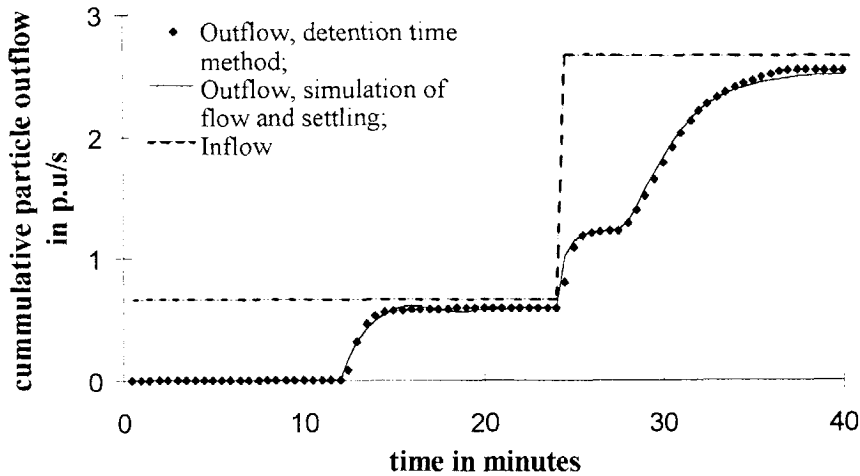


Figure 7.14: Cumulative outflow of settling particles according to model based on detention times and according to simulations of flow and settling (after De Cock et al. (1997)).

Based on the flow and settling simulations a method has been developed to assess the functioning of a tank under time-varying flow conditions, including the filling and changes in flow rate. The effect of changes in the flow rate is taken into account in a more realistic manner than assuming instantaneous steady state conditions. The method bases the outflow of a tank on equation 7.3 and on the time-varying detention time of water in the tank. This detention time (T) is computed by recording the time of entering and leaving of a package of water. Between these times the flow rate may have changed, and thus these changes are incorporated in the detention time. To this purpose equation 7.3 has been rewritten by replacing the surface loading, s_0 , by h/T (h is the water depth) and by replacing the average horizontal velocity, u , by L/T . De Cock et al. (1997) describe a model based on this method, and shows that the model can accurately predict the outflow predicted by the flow simulations of this research. As an example figure 7.14 presents the cumulative outflow computed with this model and the outflow of the flow simulations. De Cock et al. (1997) further shows that the model can fairly predict the measured outflow of the tank in Amersfoort (like in section 6.3). The model is still to be put in a user-friendly tool. De Cock and De Cock (in press) give a more elaborate description.

7.3.4 Conclusion

Filling of a tank and changes in the flow rate both influence the outflow of particles. The equation predicting the removal ratio based on v_r/s_o and u , is based on steady state conditions. Simulations of time dependent situations support the use of the steady state removal ratio for time varying conditions. The surface loading appeared to be equally important. The ratio of L/B appeared not to be important.

A method to assess the functioning of a tank under time-varying flow conditions, i.e. including the filling and changes in flow rate, has been set up.

7.4 Concerning 3-dimensional effects

The question that needs to be answered is whether the design rules, based on the 2-dimensional steady flow simulations also result in optimal removal ratios for 3-dimensional flow conditions.

2-dimensional simulation of the processes is a simplification, because in reality the flow situation is never completely 2-dimensional. In the first place, the side walls will affect the flow so that 3-dimensional effects will appear, even for a completely 2-dimensional inflow in a rectangular tank with a 2-dimensional lay-out of the outflow. In the second place, the inflow conditions will never be completely 2-dimensional, even when the construction has a 2-dimensional lay-out. Finally, in some cases, the inflow is not 2-dimensional at all.

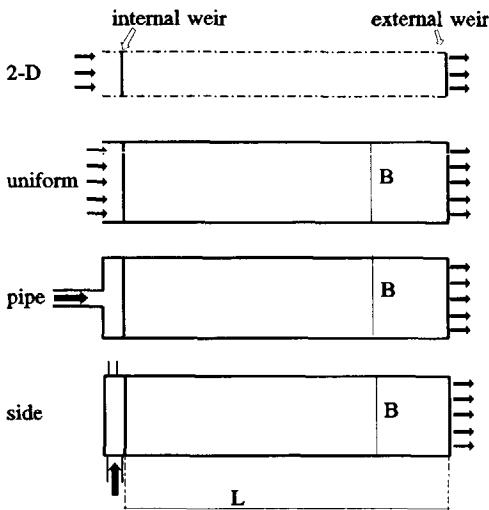


Figure 7.15: Top view of 2-dimensional and 3-dimensional flow situations.

To investigate the influence of 3-dimensional flow structures on the removal ratio for steady state flow situations, the flow situations in figure 7.15 have been simulated for a flow rate of $0.42 \text{ m}^3/\text{s}$ in a tank with $L*B*H_c = 28.75*5*2.4 \text{ m}^3$. In this arbitrarily chosen lay-out, the surface loading is 10.5 m/h . Table 7.7 presents the removal ratios. As a reference, a **2-dimensional** simulation has

been made. This is shown in the top situation in figure 7.15. A 3-dimensional simulation (with a **uniform** 2-dimensional inflow and friction along the side walls) resulted in removal ratios about equal to that of the 2-dimensional simulation. In practice, the water will not flow into the tank over the full width, but will flow in through a **pipe**. In the chosen example, the pipe enters the tank before the internal weir, as shown in figure 7.15. This pipe is located close to the bottom of the tank. It is remarkable that the simulations predict a higher removal ratio for the tank with the inflow via the pipe than for a tank with a uniform inflow. However, the differences can be considered small (less than 2%) and therefore negligible. With the inflow from the **side**, the flow field is as shown in figure 7.16. The removal ratio is then found to be considerably lower. See table 7.7.

Table 7.7: Removal ratios for 2-dimensional and 3-dimensional simulations for the same tank with different inflow configurations. The flow rate is $0.42 \text{ m}^3/\text{s}$ and $L*B*H_e = 28.75*5*2.4 \text{ m}^3$.

v_s m/h	model			
	2-d	3-d (uni.)	3d-pipe	3d-side
	RR %	RR %	RR %	RR %
0.25	2.2	2.3	2.2	2.2
1.54	13.5	13.6	13.6	12.5
6.19	47.1	47.4	48.2	38.9
13.9	80.5	80.8	82.4	64.3
24.7	96.6	96.6	97.3	83.3

Figure 7.16 shows five streamlines in the 3-dimensional flow simulation.

Based on these results, design rules based on 2-dimensional simulations are concluded to be reliable for flow situations in which the flow can be expected to be more or less 2 dimensional. For real 3-dimensional flow conditions, the removal ratio will be lower. For cases where particles have a settling velocity about equal to the surface loading (which was 10.5 m/h in this case), the reduction in removal ratio due to 3-dimensional effects becomes very significant. Consequently, large 3-dimensional flow structures should be prevented through effective design of the inflow construction and tank.

The performance of tanks with full 3-dimensional flow structures cannot be represented in one single graph or by simple design rules. For each particular case, new 3-dimensional flow simulations must be carried out.

The effect of filling and changes in flow rate for 3-dimensional flow situations has not been investigated.

7.5 Sensitivity of found equation to variations in bottom boundary

Chapter 6 presented the results of sensitivity analyses of the model to variations in the model. Variations in the bottom boundary conditions appeared to influence the removal ratio when

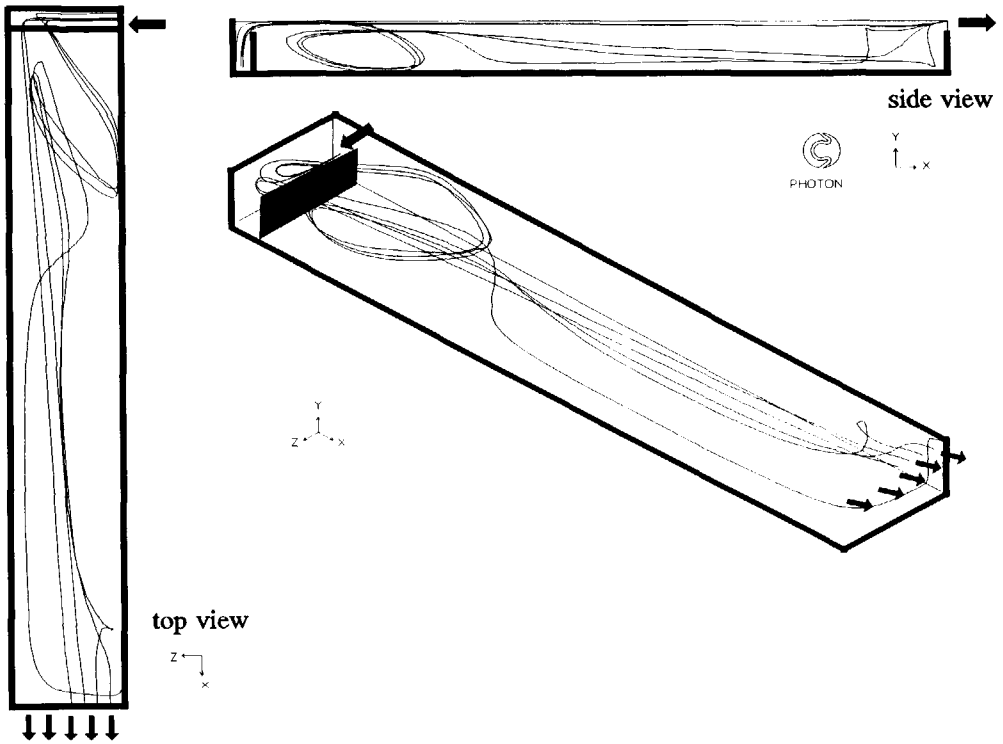


Figure 7.16: Streamlines for 3 dimensional flow situation with inflow from the side.

deposition was hindered. With regard to the found equation for the removal ratio (equation 7.3), the following should be added. According to the flow simulations (and therefore also according to equation 7.3), the removal ratio decreases when the average horizontal velocity exceeds 0.15 m/s, which therefore seems to be a critical value. However, this seemingly critical value has been influenced by the selected values of the critical stresses in the bottom boundary condition for deposition and erosion (see Chapter 5). As stated in Chapter 6, the removal ratios were hardly affected by changes in the value of τ_d , if deposition was not hindered. The simulations further showed that the horizontal velocity above which the removal ratio becomes smaller, varies slightly, but 0.15 m/s still seems a good estimate for a maximum allowable average horizontal velocity. For flow simulations in which u exceeds 0.20 m/s, the differences become significant. The removal ratio was even lower as deposition was hindered to a greater extent.

All previous simulations, including those used to derive equations for RR and R0 were simulations with τ_b based on u_{*1} . Simulations with τ_b based u_{*2} showed that the removal ratio was only marginally smaller for simulations in which the horizontal velocity was less than 0.15 m/s. The equation for R0 therefore still provides a good estimation of the removal ratio. For flow simulations in which u exceeds 0.20 m/s, the differences become significant. Like for the variations in τ_d , the removal ratio was even lower as deposition was hindered to a greater extent.

The simulations have showed that the removal ratio is not sensitive to this boundary condition if the horizontal velocity is below 0.15 m/s. Only when the horizontal velocity is higher, the removal ratio can be significantly influenced by changes in the bottom boundary conditions.

As shown above, to obtain high removal ratios, tanks should be designed in such a way that the horizontal velocity does not exceed 0.15 m/s too often. For these cases the removal ratios are concluded to be reliable.

7.6 Probability of short-circuiting

If water flows not uniformly divided over a cross section, but more along one side or in one part of the tank than the remaining part, water is short-circuiting. This results in a lower average detention time than the theoretical detention time ($T=V/Q$), and generally results in a smaller removal ratio. In fact, the re-circulation zone is a form of short-circuiting.

To restrict the probability of short-circuiting to an acceptable level (see Appendix B), the present Dutch design method requires the Froude number to be greater than $1 \cdot 10^{-5}$. The process of short-circuiting can only be partly accounted for by means of flow simulations. The CFD code only simulates continuous eddies, such as the re-circulation zone and, in the case of a 3-dimensional simulation, structures in the horizontal plane. The effect of these flow structures is taken into account. Short-circuiting is, however, not only due to steady state eddies. In turbulent flow situations, the flow varies irregularly in time and space. Large eddies cause the water to be unevenly divided over a cross section. When applying a turbulence model based on time-averaging of the turbulent fluctuations, these eddies cannot be represented directly. Furthermore, when the flow is simplified in a 2-dimensional model, all eddies in the horizontal plane are neglected.

Of course, in steady state simulations time-varying eddies cannot be modelled. Furthermore, for time-dependent flow simulations, there are reasons why time-varying eddies cannot be computed completely: firstly, numerical diffusion and the use of relaxation terms in the CFD code dampen irregularities; secondly, grid dependence of the flow direction force the flow in a mathematical model to be less irregular than in reality.

Since the effects of short-circuiting cannot be adequately modelled when using the turbulence model, the Froude number should still be used to assess the probability of short-circuiting.

Only through applying Direct Numerical Simulation, in which all eddies are simulated, is it possible to accurately compute the effect of short-circuiting. This is far beyond the capabilities of the current generation of computers.

7.7 Baffle or diffuser

A baffle or a diffuser (a wall with holes) deflects the water downwards, or spreads the water over the full cross section, and thus can destroy the re-circulation zone behind the internal weir. The destruction of this zone is generally expected to increase the removal ratio. This section presents flow simulations which have been carried out to investigate the effect of baffles and diffusers. These flow simulations have been limited to steady state conditions.

7.7.1 Baffle

Table 7.8 presents characteristics of flow situations which have been simulated with the intention of determining the effect that a baffle has on the removal ratio. The baffle to internal weir distances, and baffle submergence depths varied as indicated in the table.

Table 7.8: Characteristics of simulations with and without diffusor.

Length (m)	50	Flow rate (m ³ /s)	0.081
Width (m)	4.96	surface loading (m/h)	5.8
external weir depth (m)	2.4	internal weir depth (m)	1.8
baffle distance (m)	0.30, 0.90, 1.80		
baffle depth (m)	0.26, 0.41 0.71		

Table 7.9: Removal ratio, RR in %, for a tank with no baffle together with increase of RR due to baffle. The depth and distance of the baffle have been indicated.

v _s m/h	without %	Difference in RR (RRwith-RRwithout)				
		0.30 %	0.90 %	1.80 %	1.80 %	1.80 %
0.25	4.2	0.0	0.0	0.0	-0.2	-0.3
1.54	24.2	0.3	0.5	0.6	-0.1	-0.8
6.18	73.7	0.4	1.7	3.3	1.7	0.3
13.90	97.9	0.4	0.6	1.1	0.7	0.4

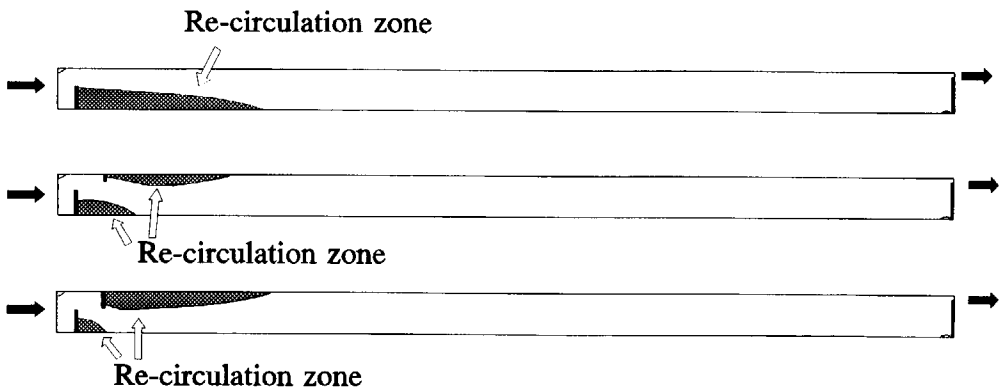


Figure 7.17: Effect of baffle depth on the re-circulation zone; baffle at 1.50 m from the internal weir and 0.25 and 0.70 m deep.

Table 7.9 presents the computed removal ratios for tanks with and without a baffle. For the observed flow condition, the re-circulation zone is reduced by the addition of the baffle. The table shows that a baffle of 0.257 m at 1.80 m from the internal weir is the optimal solution for this flow condition. The increase of the removal ratio due to the baffle was greatest for $v_s = 6.18$ m/h, for which the ratio of v_s/s_o is 1.1. This is still disappointing; only 3.3%. For deeper baffles, the re-circulation zone near the bottom is shorter, but the re-circulation zone near the water surface behind the baffle is longer. See figure 7.17. The volume involved in a re-circulating flow at the water surface is completely lost for settling, as particles which are entrained into this re-circulating flow settle out and subsequently, re-enter the main flow. A re-circulation zone at the bottom, on the contrary, might collect settling particles. Another reason that the effects of adding a baffle are so small is that the baffle bends the main flow downwards and so creates higher velocities and higher turbulence levels near the bottom, which hinders settling both below the baffle and further downstream.

Other flow rates and other tank dimensions will have a different optimal lay-out of the baffle. However, also for other flow rates and tank dimensions the effect of adding a baffle is expected to be minimal. The reason is that the size of the re-circulation zone does not seem to have much influence on the removal ratio, so that the destruction of the re-circulation zone by adding a baffle can not have that much effect.

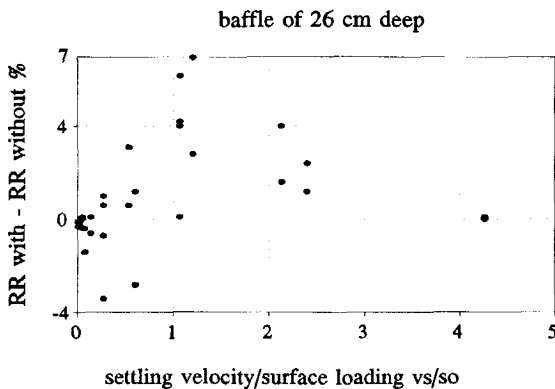


Figure 7.18: Removal ratio in tanks with and without a baffle.

In order to further investigate the effect of a baffle, additional simulations have been carried out with a baffle of 0.26 m deep located 1.80 m from the internal weir. For two tanks with the same volume, the removal ratios have been computed for several flow rates.

$$L = 25 \text{ m}, \quad B = 9.92 \text{ m}, \quad H_c = 2.4 \text{ m}, \quad H_i = 1.8 \text{ m}.$$

$$L = 50 \text{ m}, \quad B = 4.96 \text{ m}, \quad H_c = 2.4 \text{ m}, \quad H_i = 1.8 \text{ m}.$$

$$Q = 0.4, 0.8, \text{ and } 1.6 \text{ m}^3/\text{s}.$$

$$s_o = 5.8, 11.6, \text{ and } 23.2 \text{ m/h}.$$

$$v_s = 0.25, 1.54, 6.19, 13.9, \text{ and } 24.7 \text{ m/h}$$

Figure 7.18 presents the results. The vertical axis gives the removal ratio for the situation with baffle minus the removal ratio for the situation without a baffle. Consequently, positive values

indicate a positive effect of the baffle. Remarkably, the effect is not always positive. The effect is largest for v_s/s_o values near 1.0 in combination with low flow rates. For high flow rates and v_s/s_o values below 1.0, the baffle can have a negative effect on the removal ratio. This is due to the increased hindering of deposition caused by the higher bottom velocity. For low flow rates, the horizontal velocity is so small that even with a baffle, the bottom velocity does not really hinder the deposition. In these cases, the baffle has a positive effect.

For high flow rates, the positive effect of the destruction of the re-circulation zone can be lost due to a reduction of deposition. Figures 7.19 and 7.20 illustrate this for a tank with a high and a low loading.

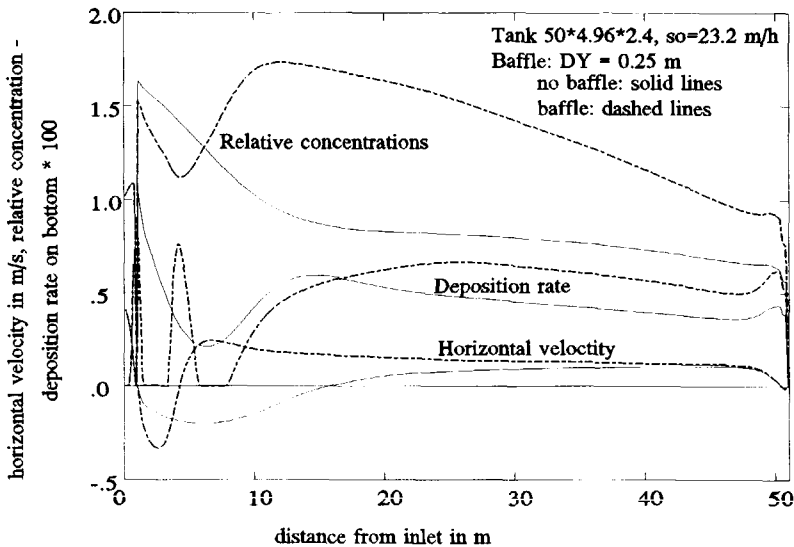


Figure 7.19: Near bottom values of variables concerning deposition of particles with $v_s = 6.2$ m/h and $s_o = 23.2$ m/h in a tank with and without a baffle.

Figure 7.19 presents the values of several variables near the bottom for a long tank with and without a baffle, loaded with a high flow rate ($Q = 1.6$ m³/s and $s_o = 23.2$ m/h). The bottom horizontal velocity shows a long recirculation zone if the tank has no baffle, and a short one with a baffle. With a baffle, the bottom horizontal velocity just downstream of the baffle becomes so high that no particles deposit at all (see the dashed line representing the deposition of particles), whereas with a baffle deposition occurs everywhere along the bottom (but is smallest in the recirculation zone, where the horizontal velocity is highest). Due to hindering of deposition for the flow with a baffle, the removal ratio (in the equilibrium situation) for particles with a settling velocity of 6.2 m/h is less than in a tank with a baffle; 17.2% versus 20.6%. This can also be seen in figure 7.19: the area below the deposition line for the tank without a baffle is larger than the area below the line for the tank with a baffle. Therefore, (in the equilibrium situation) more material flows out of the tank with a baffle.

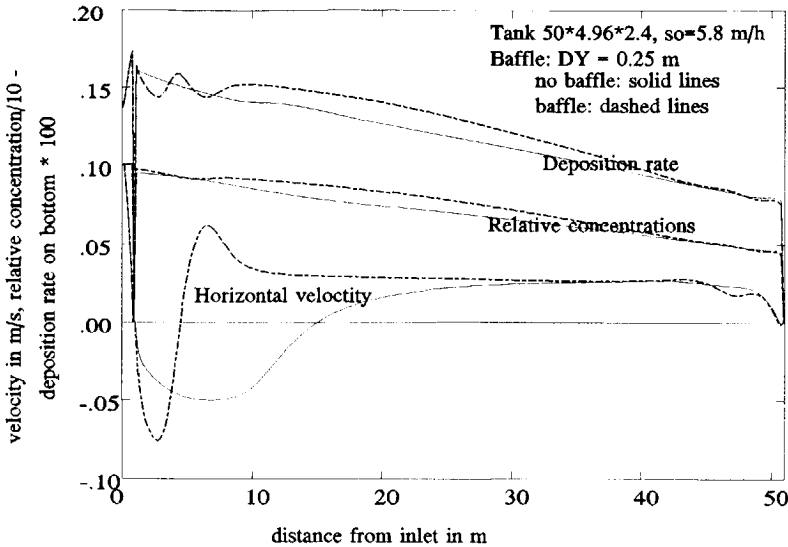


Figure 7.20: Near bottom values of variables concerning deposition of particles with $v_s = 6.2$ m/h and $s_o = 5.8$ m/h in a tank with and without a baffle.

Figure 7.20 presents the horizontal velocity along the bottom, the deposition rate and the concentration near the bottom of particles with a settling velocity of 6.2 m/h for a flow rate of 0.4 m³/s ($s_o = 5.8$ m/h). For this smaller flow rate, the critical shear stress is not exceeded and deposition occurs along the entire bottom (see deposition line). Although the horizontal velocities along the bottom are for most of the tank greater in the tank with a baffle than in the tank with no baffle, the deposition is still higher. This is due to the higher relative concentrations near the bottom (see concentration lines), because the deposition is a function of shear stress, settling velocity, and local relative concentration. The baffle seems to affect the flow conditions in such a way that more particles settle bottomwards. However, for this case, the baffle only increases the removal ratio by only about 1 percent; 75.0% versus 73.8%.

7.7.2 Diffusor

A diffusor reduces the turbulence levels and disperses the water. The effect of a diffusor has been investigated for the following configurations.

- L = 40 m,
- H_c = 2.4 m,
- H_i = 1.8 m,
- s_o = 5, 6, 7, 10 and 20 m/h.

The diffusor was implemented in the mathematical model by blocking cells in the flow domain. The grid was coarse compared to the structure. More elaborate flow simulations should be carried out, using locally a finer grid. Other points of interest had higher priorities. Even though the grid was

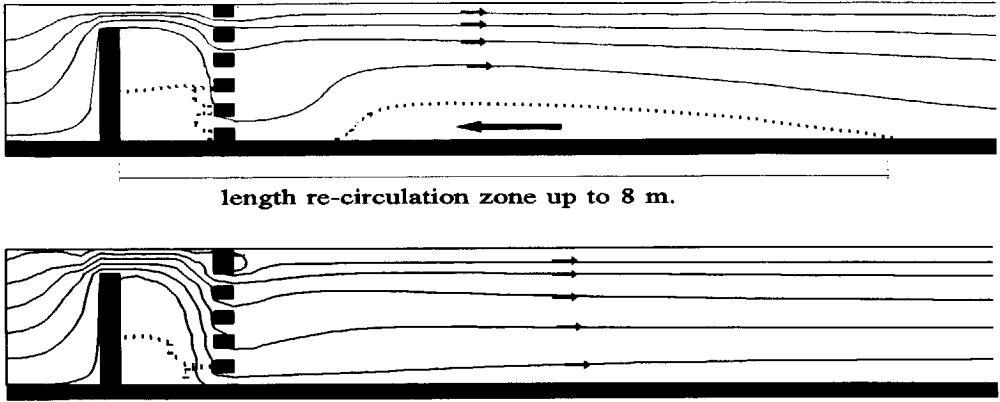


Figure 7.21: Effect of diffuser on stream lines.

coarse, the following results are assumed to give a right indication of the effect of a diffuser. Figure 7.21 presents the effect of the diffuser on the streamlines.

The shape of the diffuser appeared to be important for the destruction of the re-circulation zone. A diffuser with more holes near the bottom than near the top appeared to destruct the re-circulation zone almost completely, whereas uniformly distributed holes still resulted in a re-circulation zone at the bottom behind the diffuser.

Indeed, the turbulence level became significantly smaller with the optimal diffuser. At five meters downstream of the internal weir, the values of the kinetic energy of turbulent motion were two to three times smaller for the tank with a diffuser than for the tank with no diffuser. Simulations with a diffuser at 1.5 and at 4.5 m downstream of the internal weir both resulted in a similar destruction of the re-circulation zone. Because the diffuser at 1.5 m left a larger part of the tank with approximately uniform flow conditions, this option was selected for further investigation.

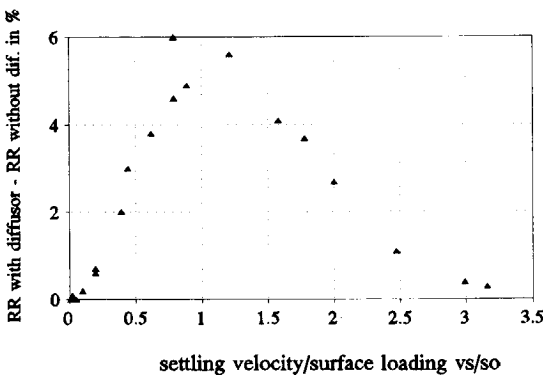


Figure 7.22: Effect of diffuser on removal ratio based on PHOENICS simulations.

However, yet again, no significant increase in the removal ratio occurred. Figure 7.22 presents the difference in removal ratio between tanks with and without diffusor. The effect is largest for particles with a settling velocity about equal to the surface loading. For heavier particles, the removal ratio is already almost 100%, so the possible gain is very limited. For lighter particles the removal ratio tends to zero.

Only some of the particles have a settling velocity equal to the surface loading. Hence, the increase in the removal ratio will be even less than 6%.

7.7.3 Effect diffusor in 3-dimensional flow situations

A diffusor can help to make a clear 3-dimensional flow situation approximately 2-dimensional. Section 7.4 has shown that the removal ratio in a tank with a clear 3-dimensional flow situation is considerably less than in a tank with an approximately 2-dimensional flow situation. If a diffusor can help to make a clear 3-dimensional flow situation approximately 2-dimensional, it can increase the removal ratio.

Indeed, a flow simulation of the last situation of figure 7.15, but with a diffusor behind the internal weir resulted in almost the same removal ratios as the 2-dimensional case.

7.7.4 Conclusion

Simulations for tanks both with and without baffles and diffusors have shown that such attributes generate only a small increase in the removal ratio if the flow situation is already approximately 2-dimensional. A diffusor seems more effective than a baffle. The highest computed increase in the removal ratio was only 6%. It is doubtful if the increase of the removal ratio will compensate for the extra costs, the increased risks of clogging and extra maintenance.

However, a diffusor can help to make 3-dimensional flow situations more 2-dimensional, and consequently, increase the removal ratio.

7.8 Conclusions

For the design of rectangular tanks an equation has been derived which can be used to predict the removal ratio of a tank under steady state conditions. The removal ratio has been shown to mainly depend on surface loading. Shallow tanks are therefore more efficient. Within the investigated range, the ratio of L/B has been shown not to be important. The only restriction is that the average horizontal velocity should be less than 0.15 m/s. The effect of a re-circulation zone on the removal ratio has been shown to be small.

The equation found indicates that the surface loading should be kept as small as possible. This should obviously be taken in context with the total project costs and the overall efficiency of the tank (i.e. reduction of pollution load through storage and settling). The use of the Camp graph resulted in important differences with the new relation⁽²⁴⁾. The developed equation is based on

⁽²⁴⁾ However, the differences mostly concern the exact value of the predicted removal ratio. Designs of tanks based on the Camp graph will not be much different from those with the predictions of the present result. The Camp graph also tends to the smallest possible surface loading. Furthermore, the design methods generally contain a restriction on the average horizontal velocity, so that the design is not made in the left hand side of figure 7.7, where the differences are largest. Consequently, these designs result in more or less the same tanks.

more realistic assumptions than the assumptions which Camp made to predict the removal ratios, leading to more realistic rules. The refined and more realistic approach, together with the ease of use, are the obvious benefits of the developed equation.

Based on the found equation, a method has been set up, that takes into account the filling process and variations in the inflow rate. This method can be used to investigate the efficiency of different tanks for a rainfall times series.

These conclusions have been derived from 2-dimensional flow simulations.

The use of baffles or diffusors to destruct the recirculation zone was shown to have a limited effect when the flow situation was already almost 2-dimensional. A diffusor can help to make a 3-dimensional flow situations more 2-dimensional.

Chapter 8

CONCLUSIONS

To reduce the pollution of surface water by CSOs, Dutch water authorities have formulated more stringent regulations, which result in the construction of a large number of storm water settling tanks. However, no satisfactory design methods - ones that take into account the time-varying flow situations - exist for these tanks. It has also not been proven that the current design practices result in tanks that function in an optimal way.

The aim of this PhD research was to develop design methods for optimally functioning storm water settling tanks that store and clarify overflowing water. To this end, a mathematical model was used to simulate the processes (flow and settling) in tanks of various shapes. The functioning of the mathematical model has been validated by measurements in experimental setups. These measurements comprised both measurements of flow and settling, but the latter were really insufficient to draw firm conclusions. However, because of the conceptual setup of the model, the simulation results are useful for the evaluation of different designs. The mathematical model can be used as a design tool, since it can help to evaluate the functioning of tanks. The model is capable of modelling both steady state and time dependent situations, e.g. including the filling of a tank and changes in the flow rate. Furthermore, the mathematical model can be applied to evaluate the design of other structures in which particles have to settle or float (clarifiers, etc.).

The setting up and use of a mathematical model for each individual situation is far too complicated and time-consuming (although, as computers become faster, computation time will eventually no longer be a problem. However, the setting up and use of a mathematical model and also the evaluation of the results will stay so time consuming that the use of such a model in design practice will remain limited to special cases). Therefore, the mathematical model has been used to derive design rules which can be used for the most common case (i.e. 2-d flow in rectangular tanks). For that purpose, many steady state flow situations have been simulated for different combinations of

the flow rate per meter width, length, height, and settling velocity. Each simulation resulted in the removal ratios for five particles, characterized by their settling velocity. A remarkable result of these flow simulations is that, if the horizontal velocity is less than about 0.15 m/s, the removal ratio of a tank only depends on the ratio of the settling velocity to the surface loading. This means that for these situations, the ratio of length to width is not important. Another remarkable result is that the surface loading in the computations is based on the total surface of the tank. This implies that the volume occupied by the re-circulation zone is not important for the removal ratio.

The developed design rule predicts the removal ratio as a function of the ratio of the settling velocity to the surface loading and the average horizontal velocity: $RR = f(v_s/s_o, u)$. For flow situations with an average horizontal velocity exceeding about 0.15 m/s, the removal ratio will be significantly less than for flow situations with lower horizontal velocities. This is due to the hindering of deposition on the bottom and the higher turbulence levels. Tanks should therefore be designed in such a way that the critical horizontal velocity of about 0.15 m/s is not exceeded too frequently.

The developed design rule predicts removal ratios which differ from the ones following from the widely used Camp graph. The developed design rule is based on more realistic assumptions than the assumptions which Camp made to predict the removal ratios, leading to more realistic predictions of the removal ratio. Furthermore, they it is also easier to use, because the removal ratio is predicted by a single equation, while the removal ratio according to Camp has to be deduced from a graph. A second reason why they are easier to use is that the surface loading is based on the well defined total area of the tank, whereas for the Camp graph it is based on the area of the settling zone, the size of which must be estimated.

There are 4 major differences between the removal ratios predicted by Camp and those according to the design rules developed in this research:

- A) The Camp graph predicts that the removal ratio is dependent on the horizontal velocity, whereas the results of this research predict no influence for $u < 0.15$ m/s.
- B) The Camp graph does not predict a sharp decrease in the removal ratio for $u > 0.15$ m/s, which this research does.
- C) The Camp graph predicts a removal ratio equal to v_s/s_o (or 100% if $v_s/s_o > 1.0$) for large values of v_s/u , i.e. for low horizontal velocities. This research resulted in smaller removal ratios for low horizontal velocities.
- D) The surface loading in the Camp graph is based on the area of the settling zone only. Ergo, according to Camp, increasing this area by destructing the re-circulation zone would result in an increase of the removal ratio. This research predicts a much smaller effect.

Nevertheless, a design based on the new design rules does not differ much from one based on the Camp graph. It is evident that both methods predict a high removal ratio for a low surface loading. Furthermore, the fact that the Camp graph is used in combination with a restriction on the value of the shear stress, ensures that designs are, in general, not made in the area of the graph where (according to this research) the removal ratio sharply decreases.

The probability of the occurrence of short-circuiting could not be predicted with the mathematical model. The currently used restriction on the value of the Froude number should therefore still be used for the design of tanks.

As, the volume occupied by the re-circulation zone does not appear to be important for the removal ratio, it is logical that the destruction of that zone by a diffusor or a baffle after the inlet, does not significantly increase the removal ratio. This has been shown in simulations where baffles and diffusor were present.

The simulations on which the design rules were based and those conducted to examine the effect of baffles and diffusors were 2-dimensional. Analysis of 3-dimensional simulations showed that the removal ratio is manifestly reduced if the flow regime is strongly 3-dimensional, i.e. if the length scale of the eddies in the horizontal plane are of the same order of magnitude as the dimensions of the tank. However, if the flow is approximately 2-dimensional (i.e. not strongly 3-dimensional), the removal ratio is almost equal to that in the 2-dimensional simulation. Simulations showed that a diffusor can help to make a strong 3-dimensional flow situation more 2-dimensional. In that case, a baffle or diffusor can enlarge the removal ratio.

Simulations of the time dependent flow through a tank showed that, except for the re-circulation zone, the flow can be represented well by a plug flow. Based on this, a model has been set up which predicts the removal ratio of a tank during a time-varying flow. Such a model is useful to evaluate the long term functioning of a tank (as a result of a rainfall time series).

Further research

Next to more insight into the processes present in storm water settling tanks, this study has resulted in insight into what information is missing. In order to fill in the gaps, the following topics should be the subject of further research.

Further research will be needed to define the exact bottom boundary conditions for deposition and erosion. In order to gain more insight in the real processes near the bottom, such research would have to be based on experiments.

The characteristics of the pollutants in CSOs are not sufficiently known. Measurements are needed to overcome this lack of data. As the settling velocity is of paramount importance for the removal ratio, a relation between different pollutants and settling velocity distributions should be obtained. With such a relation the pollution can be characterized by its settling velocity distribution and will it be possible to optimise the design of tanks. To that purpose the outflow of sewer systems, i.e. the potential inflow into the storm water settling tank, should be sampled and analyzed.

Another point of interest for further research is the effect of density differences on the flow. For storm water settling tanks the effects are expected to be minor. However, the mathematical model should be adapted to incorporate density differences, so that it can also be used for situations in which density currents are important.

Although the setup of the mathematical model is expected to be conceptually right, measurements in real tanks are needed to validate the model results.

The mathematical model has mainly been used to evaluate the design of rectangular tanks. The settling in differently shaped tanks remains to be investigated. To that purpose flow simulations would have to be conducted. The following should be investigated.

- * The effect of a sloping bottom.

- * Settling in circular tanks
- * Settling in sewers.

The fact that the bottom of a tank is generally sloping upwards from the internal weir towards the external weir might influence its functioning. Due to this the average horizontal velocity is higher near the outflow. Furthermore the fact that the bottom is sloping might result in a more quiescent flow situation during filling.

The simulation of the flow through a diffusor has been modelled in a rather coarse manner. More research should be carried out.

LIST OF SYMBOLS

A_1	constant	f	factor for shape of particles
A_2	constant	f	friction coefficient
A_b	bottom area of cell	g	gravity acceleration
A_s	coefficient to impose source term	H	water depth
A_t	time coefficient	H	height of backward facing step
$A_{x(i)}$	coefficient of inflow and diffusion in x-direction at the i cell face	H_e	height of external weir
$A_{y(j)}$	coefficient of inflow and diffusion in y-direction at the j cell face	H_i	height of internal weir
a	constant (ϵ boundary)	h	water depth
a	variable	h_c	water depth above weir crest
B	width	h_d	difference between the upstream water level and the weir crest
C	constant	IN	inflow of particles
C	Chezy factor	k	kinetic energy of turbulent motion
C_D	drag coefficient	k_N	equivalent sand-grain roughness
C_{de}	constant of turbulence model	L	length
C_e	constant for erosion	L	length scale of eddies
CF	inflowing flux of concentration c	L_r	length of re-circulation zone
C_{pe}	constant of turbulence model	L_s	length settling zone
$C_{\mu D}$	constant of turbulence model	N_C	Courant number
C_v	constant of turbulence model	OUT	outflow of particles
c	concentration	Pk	production of k
c_1	constant	p	hydraulic pressure
c_2	constant	p_0	fraction
c_v	volumetric concentration	Q	flow rate
D	deposition flux	Q_{in}	Inflow rate
D	diffusion coefficient	q	flow rate per running meter width
Dif_i	diffusion flux in x-direction at the i cell face	R	hydraulic radius
Dif_j	diffusion flux in y-direction at the j cell face	R_0	removal ratio
D_N	numerical viscosity coefficient	Re	Reynolds number
D_{ND}	coefficient for numerical diffusion	Re r	wall Reynolds number
DSC	dry solids content	Re $_s$	Reynolds number for settling
D_y	coefficient for diffusion	RR	removal ratio
d	diameter	R_s	removal ratio due to settling
E	erosion flux	S_σ	source term
E	roughness parameter	S_ϵ	source of ϵ
F	outflowing volume flux	s_0	surface loading
Fr	Froude number	T	detention time
f	factor to estimate the flow rate over a weir	TSS	total suspended solids
		t	time
		t_A	probable flowing through time
		t_d	duration of inflow
		t_d'	time

t_f'	time	ρ	density
t_i	minimum flowing through time	σ	Prandtl number
u	velocity component in x-direction	σ	variable
u	average horizontal velocity	σ_k	constant of turbulence model
u_*	shear velocity	σ_c	constant of turbulence model
u_{*1}	shear velocity based on a logarithmic velocity distribution	σ_e	constant of turbulence model
u_{*2}	shear velocity computed as a function of k	τ_b	bottom or wall shear stress
u bar	time averaged velocity	τ_d	critical shear stress for deposition
u'	turbulent fluctuating part of velocity component in x-direction	τ_c	critical shear stress for erosion
V	volume	τ_{kollm}	time scale
VFOL	volume fraction of liquid	φ	variable
VOL	volume	φ_s	variable value to impose source term
VSS	volatile suspended solids		
v	velocity component in y-direction	superscript	
v_s	settling velocity	n	time step indicator
v'	turbulent fluctuating part of velocity component in y-direction	subscripts	
w	velocity component in z-direction	g	gas
w	width of the crest of the weir	i	spatial step indicator for x-direction
w'	turbulent fluctuating part of velocity component in z-direction	j	spatial step indicator for y-direction
x	variable	l	liquid
y	distance to the wall	m	mixture
y	distance to water surface	s	solids
y_0	distance	t	first derivative to time
y^+	dimensionless wall distance	tt	second derivative to time
		w	water
		x	first derivative to x
		xx	second derivative to x
Greek			
ΔL	spatial step		
ΔL	distance between two cell centres		
Δt	time step		
Δu	difference of u velocity over two cells		
Δv	difference of v velocity over two cells		
Δx	spatial increment in x-direction		
Δy	spatial increment in y-direction		
Γ_φ	exchange coefficient of variable φ		
ϵ	dissipation of kinetic energy of turbulent motion		
κ	von Kármán constant		
λ_{kollm}	length scale		
ν_t	eddy viscosity		
ν	kinematic viscosity		

REFERENCES

- Aalderink R.H. (1995). *Cursus "Vuiluitworp uit rioolstelsels", Mogelijkheden en beperkingen van vuiluitworpmodellen; resultaten van een vergelijkend onderzoek*, PATO, Delft, The Netherlands.
- Arévalo F.H. (1996). *Metingen in een schaalmodel van een bezinktank voor de toetsing van stromingssimulaties*, DUT, Delft, The Netherlands.
- Ashley R.M., Wotherspoon D.J.J., Goodison M.J., McGregor I. and Coghlan B.P. (1992). *The deposition and erosion of sediments in sewers*. *Wat. Sci. Techn.* **26**, 1283-1293.
- Ashley R.M. (1995). *International conference on sewer solids-characteristics, movement, effects and control*, University of Abertay Dundee, UK.
- ATV A128 (1983). *Richtlinien für die Bemessung und Gestaltung von Regenentlastungen in Mischwasserkanälen*, ATV, Germany.
- Balmforth D.J. and Henderson R.J. (1988). *A guide to the design of storm overflows structures*, WRc Engineering, UK.
- Battjes J.A. (1990). *Vloeistofmechanica*, lecture notes b70, DUT, Delft, The Netherlands.
- Blom, P. (1994). *Turbulent free-surface flow over a sill*, Ph.D-thesis, DUT, Delft, The Netherlands.
- Booij R. (1992). *Turbulentie in de waterloopkunde*, lecture notes b82, DUT, Delft, The Netherlands.
- Booij R. (1995). *Communication on Introductory measurements of sediment transport in vertical direction*. XXVIth IAHR congress, London, paper 3b12.
- Booij R. (1996). *Turbulence modelling of curved flows*. PHOENICS User day, Leuven, Belgium.
- C2100 (1995) *Leidraad Riolering, Module C2100-1, 1995: Rioleringsberekeningen, hydraulisch functioneren*, Samson en Willink, Alphen aan den Rijn. The Netherlands.
- Camp T.R. (1946). *Sedimentation and the design of settling tanks*, *Trans ASCE*, **111**, pp 895-936.
- CHAM (1987). *PHOENICS beginners guide*, CHAM Ltd., TR100, London, UK.
- CHAM (1991). *The PHOENICS reference manual part a + b*, CHAM Ltd., TR200a+b, London, UK.
- CHAM (1992). *The height of liquid method for free surface flows, lecture notes*, Phoenix advanced seminar, CHAM Ltd., London, UK.
- CHAM (-). *PHOENICS Equations*, CHAM Ltd., TR99, London, UK.
- Chebbou G., Musquerre P. and Bachoc A. (1990). *Solids transferred into sewers*, in Proc. First Conf. Storm Drainage, Osaka, pp 885-890.
- Chen Y.S. and Kim S.W. (1987). *Computation of turbulent flows using an extended k- ϵ turbulence closure model*, NASA, CR-179204.
- CIRIA (1987). *Sediment movement in combined sewerage and storm-water drainage systems*, Project report 1, London, UK.
- Crabtree (1988). *A classification of combined sewer sediment types and characteristics*. Water Research Centre.
- CUWVO VI (1992). *Aanbevelingen voor het beleid en de vergunningverlening met betrekking tot overstorting uit rioolstelsels en regenwaterlozingen*, CUWVO VI: subwerkgroep Eisen rioolwateroverstorten.
- Franke P.G. (1980). *Abfluss über Wehre and Überfalle*, *Abriss der Hydraulik*, T.U. Munchen, Germany.

- Hanjalic K., Launder B.E. and Schiestel R. (1980). Multiple-time-scale concepts in turbulent transport modelling, in *Turbulent Shear Flows* (edited by Bradbury L.J.S. et al.), vol 2, pp 36-49, Springer-Verlag, New York.
- Hoffmans G.J.C.M. and Booij, R. (1993). *Two dimensional mathematical modelling of local scour holes*, Journal of Hydraulic Research, Vol. 31, No. 5.
- Huisman L. (1989). *Sedimentation and flotation and mechanical filtration*, lecture notes N4, DUT, Delft, The Netherlands.
- Jandard S. (1994). *Optimal design of stormwater sedimentation tanks - Calibration measurements for a mathematical model*, Ecole Nationale des Ponts en Chaussees, Paris, France.
- Jayatellike C.L.V. (1969). *The influence of the Prandtle number and surface roughness on the resistance of the sublayer to momentum and heat transfer*. Prog in Heat & Mass Transfer, Vol 1, Pergamon press.
- Kleywegt R.A. (1992). *On sediment transport in circular sewers with non-cohesive deposits*, Ph.D.-thesis, DUT, Delft, The Netherlands.
- Kluck J. (1993). *Het modelleren van een vrij wateroppervlak in bergbezinktanks*, DUT, Delft, The Netherlands.
- Kluck J. (1994). *Modeling of flow and settling in storm water sedimentation tanks*. DUT, Delft, The Netherlands.
- Kluck J. (1995). *Calibration of flow model an method to compute particle transport*. DUT, Delft, The Netherlands.
- Launder, B.E. and Spalding, D.B. (1972). *Lectures in mathematical models of turbulence*. Academic Press, London.
- McCorquodale and Zhou (1993). Effects of hydraulic and solids loading on clarifier performance, Journal of Hydraulic Research, Vol 31, no 4, pp 461-477.
- Michelbach S. and Wörle C. (1992). Settleable solids in a combined sewer system - measurements, quantity, characteristics, *Wat. Sci. Tech.* Vol 25, no. 8.
- Michelbach S. and Wörle C. (1992). Settleable solids from combined sewers: settling, stormwater treatment, and sedimentation rates in rivers. *Wat. Sci. Tech.* Vol 29, no. 1-2, pp 95-102.
- Moffa, P. E. (1990). *Control and treatment of combined-sewer overflows*, Van Nostrand Reinhold, New York, USA.
- Noord-Brabantse waterkwaliteitsbeheerders (1995). *Handleiding Ontwerp Randvoorzieningen II 1995*, Noord-Brabantse waterkwaliteitsbeheerders, The Netherlands.
- NWRW (1987). *Rendement randvoorziening bergbezinkbassin Amersfoort*, nr. 8.1, The Netherlands.
- NWRW (1989). *Eindrapportage en evaluatie van het onderzoek 1982-1989*, final report.
- Pargneux L. le (1995). *Optimal design of storm water sedimentation tanks, Testing of the settling tube to determine settling distribution of sludge*, Ecole Nationale des Ponts et Chaussees, Paris, France.
- Patankar, S.V. (1980). *Numerical heat transfer and fluid flow*, Hemisphere, Washington, USA.
- POLIS, (1994). PHOENICS on line information system, part of PHOENICS version 2.0 software, CHAM ltd, London, UK.
- Rijn L.C van. (1989). *Handbook, Sediment transport by currents and waves*, Delft Hydraulics, report H461. The Netherlands.
- Rodi W. and Krebs P. (1995). *Berechnung der Stromungs- und Abscheidvorgange in Abzets- und Flotationsbecken*. Abschlussbericht zum DFG Ro 558/13-1, Universitat Karlsruhe, Germany.

- Rodi W. (1980). *Turbulence models and their application in hydraulics - a state of the art review*, International Association for Hydraulic Research, Delft, The Netherlands.
- Rompaey D. van (1991). *Bergbezinkbassins in gemengde rioolstelsels*, KUL and DUT, Leuven, Belgium.
- Ruan M. (1995). Preliminary research of sediment behaviour in sewer systems, DUT, Delft, The Netherlands.
- Sharon J.D. et al. (1989). *Combined sewer overflow pollution abatement*, Water Pollution Control Federation, USA.
- Stahre P. and Urbonas B. (1990). *Storm water detention, for drainage, water quality, and CSO management*, Prentice Hall, ISBN 0-13-849837-7.
- Toornman E.A. (1993). *Simulation of free surface flow of mud*, VII Int. Conf. on Finite Elements in Fluids, Barcelona, Spain.
- Tropea C. (1982). *Die turbulente stufenströmung in flachkanalen und offenen gerinnen*, Germany.
- Veldkamp R.G. (1992). Een nieuwe visie op het rendement van bergbezinktanks, *H2O*, pp 623-628, The Netherlands.
- Veldkamp R.G. and Wiggers J.B.M. (1996). *Pollutant emission from combined sewer systems - A statistical approach*, 7th international conference on urban storm drainage, Hannover, Germany.
- Verbanck M.A. et al. (1990). *Sewer sediments and its relation with the quality characteristics of combined sewer overflows*, Water science technology, vol 22, no 10/11,
- Verbanck M.A. Ashley R.M. and Bachoc A. (1994). *International workshop on origin, occurrence, and behaviour of sediments in sewer systems: summary of conclusions*, Water Resource. Vol 28, no 1, p 187-194, UK.
- Vermeer E.A. (1990). *Optimaliseren nabezinktanks*, STORA, rapport 1.1.6, The Netherlands.
- Wotherspoon D.J.J. and Ashley R.M. (1992). Reological measurements of the yield strength of combined sewer sediment deposits. in Proc. First IAWQ workshop on sewer sediment, Brussels. Wat. Sci. Techn. 25, pp 165-169.
- Weiß and Michelbach (1995). Vortex separator: dimensionless properties and calculation of annual separation efficiencies. *International conference on sewer solids - Characteristics, movement, effects, and control*. University of Abertay Dundee, Dundee. UK.
- Wiggers J.B.M. (1991). Overleefde de overstortingsfrequentie, *H2O*, nr. 6, pp152-156, The Netherlands.
- Winterwerp J.C. et al. (1993). *Erosion of natural sediments from the Netherlands, Model simulations and sensitivity analysis*, Delft Hydraulics, Delft, The Netherlands.

APPENDIX A: POINT RAINFALL METHOD

In the Netherlands the point rainfall method has been used for many years to assess the functioning of a sewer system. This method is based on the simplification of a storm to a rainfall depth in mm and the rainfall duration in minutes. Figure A.1 presents a storm as a point in a graph with the duration on the horizontal axis and the depth on the vertical axis. The rainfall depth is assumed to have fallen at a constant rainfall intensity (dotted line in the figure). However, in reality, the intensity will have varied. For example, the dashed line in the figure represents a storm with a high rainfall intensity at the beginning of the storm, and a lower intensity at the end of the storm.

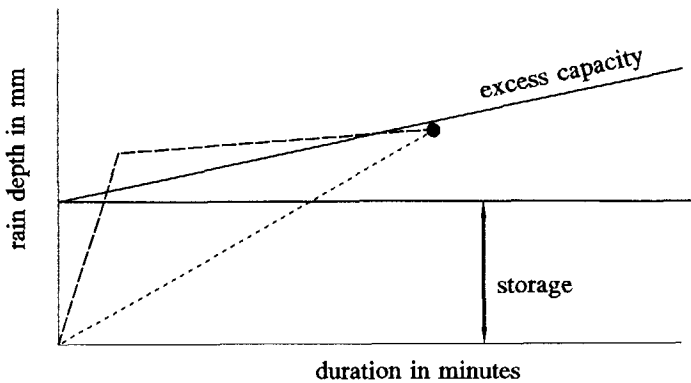


Figure A.1: Presentation of storm and sewer system in duration-depth graph.

The sewer system can be depicted in this graph in a simplified manner. The horizontal line represents the static storage capacity of the sewer system. This storage capacity is expressed in mm related to the impervious of the sewer system: 1 mm is equal to 10 m³ per hectare impervious area. The sloping line, starting from the point at which the storage line touches the y-axis, represents the excess capacity of the pumps (in mm/min). The excess capacity equals the total installed capacity minus the dry weather flow. If the point representing the storm is below the sloping line (as is the case in the figure), it is assumed that the water can be stored and consequently, can be pumped to the treatment plant. If the point is above the sloping line, it is assumed that an overflow occurs. By presenting all the storms of a year in this graph, and counting the number of points above the lines representing the sewer system, the number of overflows in that year can be estimated.

Up until recently, the point rainfall chart (figure A.2) was widely used in the Netherlands. This graph contains the measured rainfall depths of 37 years. The frequency of overflowing of a sewer system is estimated as the number of points above the lines representing the sewer system divided by the number of years.

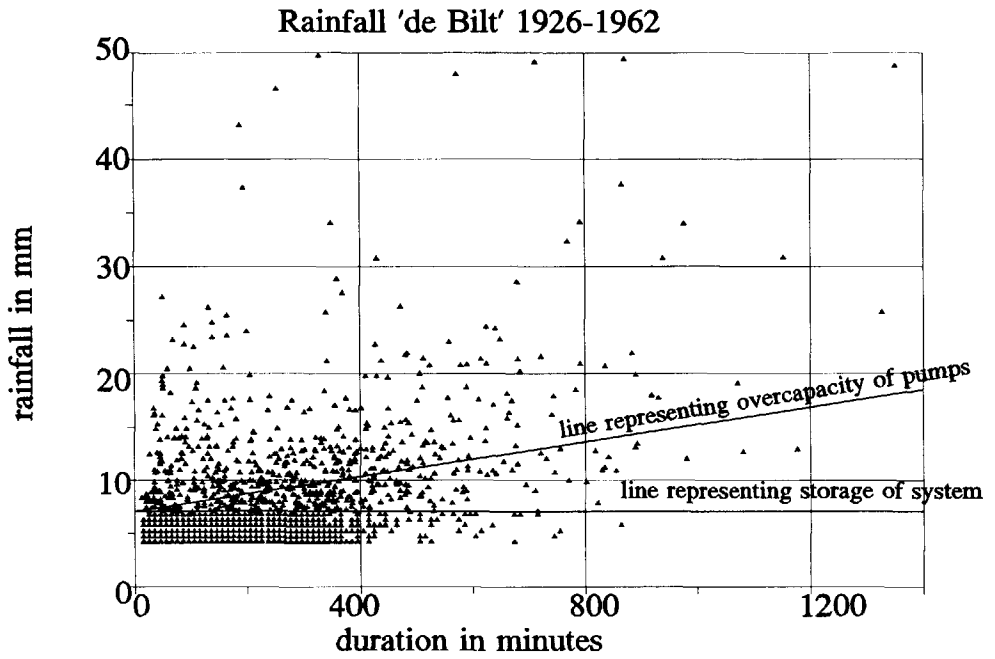


Figure A.2: Dot graph: duration-depth graph with rainfall for 37 years.

The use of the point rainfall chart does not necessarily result in the actual frequency of overflowing, because of various simplifications built into this method, such as:

- 1) The method assumes a constant rainfall intensity during the storm. A storm like presented in figure A.1 explains the possible effect of this assumption. A constant rainfall intensity (dotted line) results in no overflow. If the rainfall intensity in the beginning would have been as high as given by the dashed line, then the line rises above the line representing the system. This would mean that water flows over.

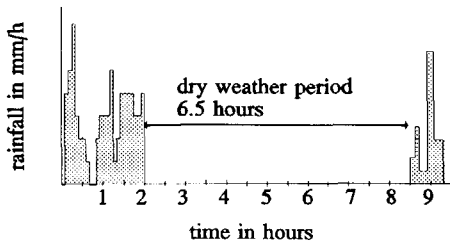


Figure A.3: Rainfall built up out of steps of 5 minutes.

- 2) The long rainfall time series from which the distinct storms (i.e. points in the graph) have been derived, consists of data on the rainfall depth per 5 minutes. A distinct storm consists of the duration and cumulative depth of the 5 minutes steps belonging together. Which steps belong together (i.e. the definition of the duration of a storm) is based on an arbitrarily selected minimum length of dry weather before the storm. When the definition of a storm is based on a shorter period of dry weather, some first distinct storms will be combined. E.g; if the dry weather period is defined as 6 hours, then the rainfall in figure A.3 does not belong to one storm, whereas if the dry weather period is defined as 7 hours, they belong to one storm. This will influence the computed frequency of overflowing.
- 3) The system is assumed to be empty at the start of each storm.
- 4) The pumps are assumed to start immediately at full capacity at the beginning of the rainfall, which cannot be the case.

Except for determining the frequency of overflowing, the point rainfall chart can be used to estimate the amount of overflowing water. The height in mm of the point above the line representing the system represents the amount of overflowing water. For sewer systems with more than one CSO, this method applies to the CSO with the lowest weir crest. This CSO generally has the highest frequency of overflowing. To gain more insight into the functioning of such systems, more accurate flow simulations are needed to evaluate the importance of the different CSO's. However, the point rainfall method can still be used to gain insight into the functioning of the system.

APPENDIX B: PRESENT DUTCH DESIGN METHOD

Generally, in the Netherlands, the method applied for the design of storm water settling tanks first determines a required volume and then shapes this volume in such a way that settling is expected. Only the flow in the steady state for one or several flow rates is considered. In order to explain the method, this appendix first explains some background theory first.

The design method is based on equilibrium flow conditions (steady state) like in figure 1.5 (Chapter 1). Behind the internal weir the water is re-circulating. Downstream of this re-circulation zone, the flow is divided approximately evenly over the full depth. The tank is divided into three zones; the inflow zone, the settling zone and the outflow zone, like indicated in figure 1.5. It is assumed that particles only settle in the settling zone. The flow in the settling zone is assumed to satisfy certain flow conditions which ensure ideal settling conditions:

- * stationary flow;
- * flow divided uniformly over the depth and the width;
- * no turbulence (but the effect of turbulence is accounted for, as will be explained further on);
- * a homogeneous distribution of the concentration of settling solids over the vertical at the beginning of the settling zone;
- * no coagulation;
- * no erosion of sediments from the bottom;
- * no hindering of deposition at the bottom.

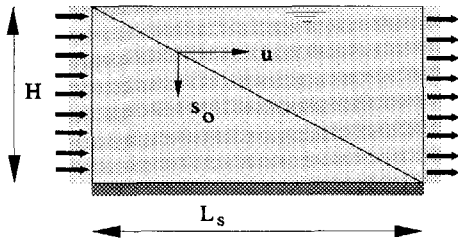


Figure B.1: $s_o/u = H/L_s$

Under these ideal settling conditions, a particle which enters the settling zone at the top, settles just before the end of the settling zone if the depth, H , divided by the settling velocity, equals the length of the settling zone, L_s , divided by the horizontal velocity, u , i.e. the time needed to reach the bottom equals the time needed to reach the other side of the settling zone. See figure B.1. It is convenient to define the surface loading s_o :

$$s_o = \frac{uH}{L_s} = \frac{uHB}{L_s B} = \frac{Q}{L_s B} \quad (\text{B.1})$$

B denotes the width of the flow situation, and Q the flow rate.

The size of the settling zone depends on the in- and outflow conditions. In unfavourable flow situations the settling zone can be restricted to a small part of the tank. The surface loading then is higher and thus the removal ratio smaller.

However, flow in storm water settling tanks is generally turbulent. The Reynolds number gives an indication of the turbulence.

Reynolds number

The Reynolds number gives the quotient of mass forces and the viscous forces.

$$\text{Re} = \frac{uR}{\nu_1} = \frac{Q}{(B+2H)\nu_1} \quad (\text{B.2})$$

R = hydraulic radius = $B \cdot H / (B + 2H)$

ν_1 = viscosity $\approx 1.31 \cdot 10^{-6} \text{ m}^2/\text{s}$ for water of 10°C .

For low velocities and high viscosities, the values of the Reynolds number are below 2000 and the flow is not turbulent but laminar. Turbulence hinders the settling as it reduces concentration differences. In practice the flow situations are always turbulent. To obtain as less turbulence as possible, the hydraulic radius has to be short and the horizontal velocity small. This requires a wide and deep tank.

The negative effect of turbulence on the sedimentation can be taken into account by using the so called Camp graph. Camp (1946) derived a graph to estimate the removal ratio due to settling from the transport equation of particles for the steady state in a 1-dimensional flow:

$$u \frac{\partial c}{\partial x} = D_y \frac{\partial^2 c}{\partial y^2} + v_s \frac{\partial c}{\partial y} \quad (\text{B.3})$$

In this equation, c denotes the particle concentration, and x and y denote the horizontal and vertical directions respectively. Particles reaching the bottom are assumed to remain on the bottom and not to influence the flow. The effect of turbulence is accounted for as a diffusion term, via a coefficient for this diffusion, D_y . The transport equation was evaluated analytically to estimate the removal ratio due to settling. This resulted in a graph with lines for equal values of v_s/s_o . The horizontal and vertical axes represent $v_s H / 2D_y$ and the removal ratio, respectively. In order to make this graph independent of D_y , Camp assumed D_y to be constant and the horizontal velocity to be a parabolic function of the distance to the bottom⁽²⁵⁾ (parabolic velocity distribution) (Camp, 1945). D_y can then be estimated as

⁽²⁵⁾ As lined out in (Camp, 1945), this is contradictory to the assumption of a uniform velocity distribution.

$$D_y = 0.075 H u \sqrt{\frac{f}{8}} \quad (\text{B.4})$$

Assuming that the coefficient for bottom friction, f , equals 0.024, the term $v_s H / 2D_y$ on the horizontal axis can be replaced by $122v_s/u$. This results in the generally used so called Camp graph. See figure B.2.

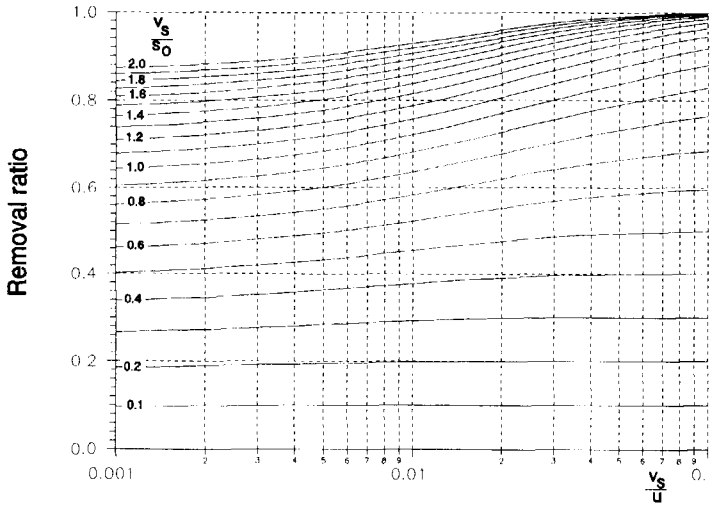


Figure B.2: Camp graph: v_s/s_0 versus v_s/u graph to determine the removal ratio under turbulent flow conditions.

With the horizontal velocity, based on the flow rate and a chosen design of the tank, the reduction of the removal ratio by turbulence can be read in the Camp graph.

The flow rate in the design used to be based on a stationary flow through the sewer system (e.g. 40 l/s/ha). In the future, time-dependent hydraulic calculations of the performance of the sewer system for rainfall time series are expected to be used more and more.

The volume of the tank generally follows from preset requirements, for instance 20 m³ per hectare impervious area (usually expressed as 2 mm) as promoted in (CUWVO, 1992). For sewer systems with only one CSOS, the size of the impervious area is equal to the total impervious area. For sewer systems with more than one overflow structure, this requirement is not unambiguous, since the impervious area which belongs to each CSO is depending on the storm analyzed. Therefore, the required volume is not well defined. However, the aim is to create a system with a pollution load smaller than or equal to that of the reference system⁽²⁶⁾, so engineers advising the municipi-

⁽²⁶⁾ Combined sewer systems should not pollute the surface water more than the following system, which has been defined as the reference: A static storage (below the lowest weir crest) of 7 mm, extra storage of 2 mm in storm water settling tanks behind each CSO, and an excess capacity of the pumps (i.e. the total pump capacity minus the dry

palties and the water boards can and have to be creative and can deviate from the reference system.

Next, this volume is shaped in such a way that settling is expected.

Based on these ideal settling conditions, the size and shape of the settling zone is determined by rules of thumb, calculations on the expected removal efficiency (taking into account the effect of turbulence), and restrictions on probability of short-circuiting.

The design is generally made for several chosen settling velocities (e.g. 5 to 10 m/h). Surface loadings applied are between 5 or 10 m/h. These values were based on the perception that storm water settling tanks are allowed to perform less well than primary clarifiers of waste water treatment plants of which the surface loading is about 2 m/h at the maximum. In combination with the design flow rate the maximum surface loading results in the minimum area of the settling zone: $L_s B > Q/s_0$. Instead of a certain value of the surface loading, also a certain value of the removal ratio due to settling can be required (based on the Camp graph). Often settling velocities of 5 or 10 m/h are chosen.

The depth and width of the tanks follow from rules of thumb (like $L/B = 6$ to 10) or from wishes to reach a low as possible Reynolds number or on restriction on the Froude number. The Froude gives an indication of the probability of short-circuiting. By making changes in the design, finally the desired removal ratio can be met.

Froude number

The Froude number gives the quotient of the inertial forces and the gravity force.

$$Fr = \frac{u^2}{gR} \quad (B.5)$$

g = gravity acceleration (m/s^2)

The Froude number gives an indication of the probability of short-circuiting, which reduces the removal ratio of the tank. Flow conditions are assumed to be stable if the Froude number is not smaller than 10^{-5} . A higher value of the Froude number further reduces the probability of short-circuiting, but then also the turbulence will be higher. A high value of the Froude number requires a narrow, deep tank. Because this is contradictory to the demand for a low Reynolds number, some designers create an 'optimal design' by choosing the dimensions in such a way that the Froude number is exactly 10^{-5} . That this is not the right approach becomes clear if the graph from which this value stems is observed.

The graph is the result of experiments measuring the flowing-trough time of dye (Camp, 1946). The minimal flowing trough time (t_i) is the time of initial appearance of dye in the effluent. Small values of t_i and t_A , the average flowing through time, indicate serious short-circuiting. To obtain dimensionless variables the flowing through times have been divided by the detention time T , which is equal to the volume V divided by the flow rate Q . The experimental results are represented as two bands in figure B.3. The dimensionless variables t_i/T and t_A/T increase with higher Froude numbers. There is however not a remarkable change in flowing trough times at a Froude number

weather flow) of 0.7 mm/h (7 m³/h per hectare of impervious area).

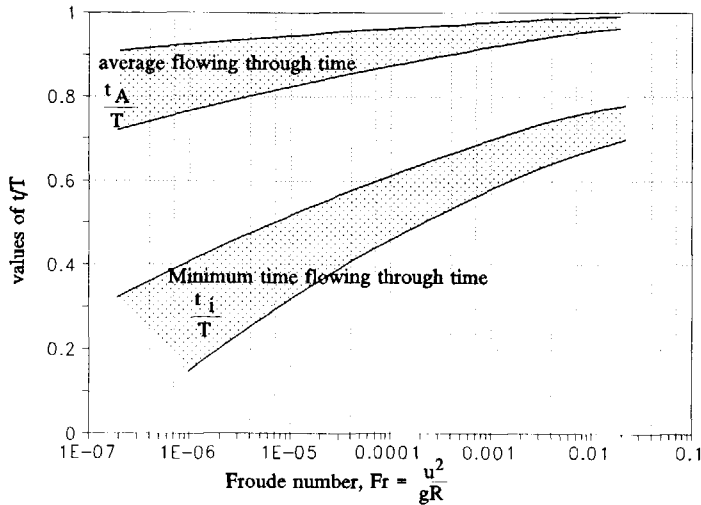


Figure B.3: Average and initial flowing trough times versus Froude number.

of $1 \cdot 10^{-5}$ and consequently no reason to chose exactly $Fr = 1 \cdot 10^{-5}$. The value of $1 \cdot 10^{-5}$ appears not to be a strict boundary between a small or large probability on short-circuiting, but merely gives an indication for the probability of short-circuiting.

The tank is designed in such a way that the demand for the Froude number is met as close as possible and the turbulence is as small as possible. The restriction for the Froude number is usually met for large flow rates.

Remarks

It is stressed that this method is set up for stationary flow conditions which prevail in clarifiers (settling tanks) of drinking water and waste water treatment with approximately constant inflow conditions. Storm water settling tanks will first have to be filled and then the inflow will vary in time. Consequently, the use of this method in order to design storm water settling tanks is doubtful. The design method is not valid in the in- and outflow zones of the tank. The size of these three zones will depend on the lay-out and the (time-varying) flow conditions. In unfavourable flow conditions the in- and outflow zones can take up a considerable part of the tank. Therefore, the removal ratio can not be estimated accurately with the above methods. Furthermore, even in the settling zone the flow conditions will vary in time, the horizontal flow will not be uniform over the full depth and width, and the particles will not be divided evenly over the full depth. Therefore, the best removal ratio is not guaranteed with these methods. For odd shapes or in tanks with walls and flow diverters the functioning can not be estimated well.

Expected effects of variations in dimensions

This section discusses the expected effects of variations in the dimensions. According to the currently used Dutch design rules the removal ratio is mainly influenced by the surface loading; the lower the surface loading, the higher is the removal ratio. The surface loading in these design

rules is based on the settling zone only. The larger the horizontal area of the settling zone, the smaller is the surface loading, so the higher is the removal ratio. This results in a shallow tank.

The re-circulation zone consumes a smaller part of the total volume in a long and narrow tank, than in a short and wide tank, because its length L_r is roughly a constant function of the height of the internal weir (L_r is between 7 and 9 times H_i). Hence, the removal ratio in a long and narrow tank is expected to be higher than in a short and wide tank with the same depth and volume.

The tank should, however, not be too shallow and narrow, because then the horizontal velocity will be higher, which means increased turbulence levels and higher shear stresses along the bottom. Higher turbulence levels mean more diffusion due to turbulence, and thus less settling. Furthermore, above a certain critical value of the shear stress the deposition of particles will be hindered or particles will be eroded from the bottom.

The current Dutch design method assumes that no particles settle in the inflow zone (re-circulation zone), because the high turbulence level hinders the settling. In fact, it can be argued that without turbulence and without the re-entrainment of particles out of the re-circulation zone into the main flow, the presence of the re-circulating flow would have no effect at all on the settling of particles, because the smaller flow depth or fall depth (i.e. the depth of the flow above the re-circulation zone) compensates for the higher velocity. This becomes clear if the length of the flow is divided into sections of equal length Δx . See figure B.4. In each section, of the particles, the part that settles equals v_s/s_0 . This ratio is the same for each section, because the surface loading s_0 equals $q/\Delta x$ (with q is the flow rate per meter width of the tank) and is independent of the height of the section. Consequently, under these assumptions, the presence of the re-circulation zone does not reduce the settling.

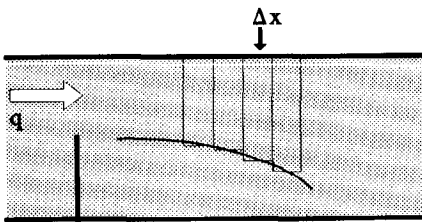


Figure B.4: The flow domain above the re-circulation zone split up in sections of length Δx .

However, due to the turbulence, the settling of particles is hindered in and after the re-circulation zone and some particles which settled in the re-circulation zone flow back into the main flow. Ergo, it is expected to be profitable to destruct the re-circulation zone, or the keep it as small as possible.

Consequently, based on the assumptions of the present Dutch design method tanks which are shallow (with a low surface loading) and long (with a small part lost to the re-circulation zone), or tanks with baffles or diffusers to destruct the re-circulation zone are expected to have the highest removal ratio due to settling.

APPENDIX C: FLOW MODEL

C.1 Introduction

This appendix explains the equations describing the flow of the water.

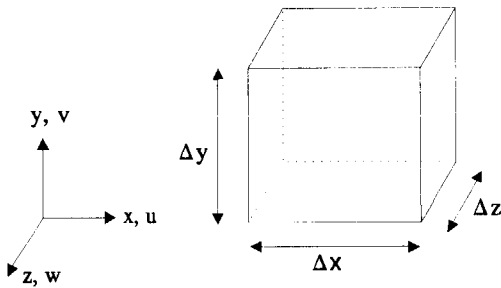


Figure C.1: Basis element.

The flow domain has been divided into many cells. For each cell, transport equations for mass, momentum, and variables describing the turbulence have to be solved. The transport equations have been set up for elements in Cartesian coordinates. See figure C.1. The shape of the elements is fixed (Eulerian approach).

Sections C.2 and C.3 give the differential equations describing the water flow. The k - ϵ turbulence model has been adopted to simulate the turbulent flow. See section C.4.

C.2 Continuity equation

The continuity equation is derived from the mass equation which reads:

$$\frac{\partial \rho}{\partial t} + \frac{\partial \rho u}{\partial x} + \frac{\partial \rho v}{\partial y} + \frac{\partial \rho w}{\partial z} = 0 \quad (\text{C.1})$$

in which t denotes the time, ρ the density and u , v and w the velocities in x -, y - and z -direction respectively. In the flow situations considered, the water flow can be assumed to be incompressible ($D\rho/Dt = 0$)⁽²⁷⁾. The continuity equation therefore becomes:

⁽²⁷⁾ This, however, does not mean that the density is constant and uniform!

$$\frac{\partial u}{\partial x} + \frac{\partial v}{\partial y} + \frac{\partial w}{\partial z} = 0 \quad (\text{C.2})$$

C.3 Momentum equations

The equilibrium of momentum is given by the familiar Navier-Stokes equations for the x-, y- and z-direction. After substitution of the continuity equation this becomes for incompressible fluids:

$$\frac{\partial u}{\partial t} + u \frac{\partial u}{\partial x} + v \frac{\partial u}{\partial y} + w \frac{\partial u}{\partial z} = - \frac{1}{\rho} \frac{\partial p_x}{\partial x} + \nu_1 \left(\frac{\partial^2 u}{\partial x^2} + \frac{\partial^2 u}{\partial y^2} + \frac{\partial^2 u}{\partial z^2} \right) \quad (\text{C.3})$$

$$\frac{\partial v}{\partial t} + u \frac{\partial v}{\partial x} + v \frac{\partial v}{\partial y} + w \frac{\partial v}{\partial z} = - \frac{1}{\rho} \frac{\partial p_y}{\partial y} + \nu_1 \left(\frac{\partial^2 v}{\partial x^2} + \frac{\partial^2 v}{\partial y^2} + \frac{\partial^2 v}{\partial z^2} \right) - g \quad (\text{C.4})$$

$$\frac{\partial w}{\partial t} + u \frac{\partial w}{\partial x} + v \frac{\partial w}{\partial y} + w \frac{\partial w}{\partial z} = - \frac{1}{\rho} \frac{\partial p_z}{\partial z} + \nu_1 \left(\frac{\partial^2 w}{\partial x^2} + \frac{\partial^2 w}{\partial y^2} + \frac{\partial^2 w}{\partial z^2} \right) \quad (\text{C.5})$$

ν_1 is the kinematic viscosity of the liquid. p_x , p_y and p_z are the hydraulic pressures in the given directions. g denotes the acceleration due to gravity. For the simulation of the storm water settling tanks the axes have been chosen in such a way that the y-direction is the upward direction. Consequently, the gravity force only works in the y-direction and is absent in the momentum equations for the x- and z-direction.

The change of the velocity in time is in equilibrium with the convective transport of momentum ($u\partial u/\partial x$ etc.), a pressure force, and diffusion of momentum due to molecular exchange with the surrounding fluids.

C.4 Turbulence modelling

In turbulent flow conditions, the variables (e.g. velocities) vary irregularly in time and space. Eddies of different sizes cause an extra exchange of impulse, heat, solved and suspended matter, etc. In this section, the effect of the turbulence on the velocities is discussed.

The Navier-Stokes equations describe both laminar and turbulent flow conditions. Solving the Navier Stokes equations directly with very small time steps and cell sizes and with the correct boundary conditions should result in a correct computation of the turbulent flow. In this method, called Direct Numerical Simulation (DNS), the time steps and cells are so small that even the smallest eddies are computed⁽²⁸⁾. However, for the time being, this is only possible in certain

⁽²⁸⁾ The smallest eddies are so small that viscous forces become important and the energy of turbulent motion is dissipated into heat by molecular diffusion. The length and time scale of these eddies are called the Kolmogorov micro scales, which can be estimated as (Booij, 1992):

$$\lambda_{\text{kolm}} = \left(\frac{\nu_1^3}{\epsilon} \right)^{\frac{1}{4}}$$

flow conditions, i.e. for low Reynolds numbers. This is due to the enormous amount of computer memory needed to store and carry out the computations. The computers are not yet powerful enough to simulate a for this research interesting flow situation by solving the Navier-Stokes equations directly⁽²⁹⁾. Therefore, the effect of the turbulence is described by a simplifying model. With the turbulence model it is possible to apply cells much larger than the sizes of the eddies, even though throughout each cell the values of the variables are assumed to be constant. This means that the smallest eddies cannot be represented. The turbulence model brings the effect of the small eddies into account. Thus, in using the turbulence model, the time step can be taken so large that the turbulent fluctuations are averaged out. This will be discussed in the next section.

C.4.1 Time averaging

Because the time scales at which the turbulent fluctuations take place are much smaller than the times scale at which the boundary conditions vary, the exact simulation of the turbulent flow is not necessary. Velocities (and the other turbulent fluctuating variables) can be averaged over a period which is relatively small compared to the changes in the flow conditions, but which is large compared to the largest time scale of the turbulence. The instantaneous velocity in the x-direction can be subdivided into an average, \bar{u} , and a fluctuating or turbulent component, u' :

$$u = \bar{u} + u' \quad (\text{C.6})$$

For the velocity terms in the y- and z-direction similar components exist:

$$v = \bar{v} + v' \quad (\text{C.7})$$

$$w = \bar{w} + w' \quad (\text{C.8})$$

The Navier-Stokes equations, averaged over a small period, are the Reynolds equations. For the x-direction, the Reynolds equation for an incompressible fluid becomes:

In this equation, and in the coming equations, the following notation has been used:

$$\tau_{\text{kolm}} = \sqrt{\frac{\rho_i}{\epsilon}}$$

The dissipation of energy of turbulent motion in a free surface flow is roughly equal to

$$\epsilon = \frac{u_{\text{avg}}^3}{C^2 h}$$

With $C=60 \text{ m}^{1/2}/\text{s}$, $u=0.1 \text{ m/s}$ and $h=0.3 \text{ m}$ (just behind the inflow in a storm water settling tank) this results in $\epsilon=9 \cdot 10^{-6} \text{ m}^2/\text{s}^3$. Thus, the Kolmogorov length and time scale are 0.5 mm and 0.3 seconds.

⁽²⁹⁾ At present, Direct Numerical Simulation of the flow of, for instance, a storm water settling of $30 \cdot 8 \cdot 2.5 \text{ m}^3$, would require $5 \cdot 10^{12}$ cells and very small time steps to prevent divergence. This would require 40,000 years of computation time on the workstation used in this research.

$$\begin{aligned} \frac{D\bar{u}}{Dt} = & -\frac{1}{\rho} \frac{\partial \bar{p}_x}{\partial x} + \frac{\partial}{\partial x} \left(\nu_1 \frac{\partial \bar{u}}{\partial x} - \overline{u'u'} \right) + \\ & + \frac{\partial}{\partial y} \left(\nu_1 \frac{\partial \bar{u}}{\partial y} - \overline{u'v'} \right) + \\ & + \frac{\partial}{\partial z} \left(\nu_1 \frac{\partial \bar{u}}{\partial z} - \overline{u'w'} \right) \end{aligned} \quad (C.9)$$

$$\frac{Du}{Dt} = \frac{\partial u}{\partial t} + u \frac{\partial u}{\partial x} + v \frac{\partial u}{\partial y} + w \frac{\partial u}{\partial z} \quad (C.10)$$

To simplify the notation of these equations, the overbars are omitted from now on. Hereafter, the characters u , v and w represent the averaged velocities (in x -, y - and z -direction respectively), and the terms $u'u'$, $u'v'$, $u'w'$, etc. represent the time-averaged multiplications of the variations in the velocities.

The turbulence creates extra internal stresses, the turbulent or Reynolds stresses, e.g:

$\rho u'v'$ = transport of x -momentum in y -direction.

In most turbulent flow situations the Reynolds, or turbulent shear stresses, are much larger than the laminar stresses $\rho \nu_1 \partial u / \partial x$ etc. For the turbulent flow situation in a storm water settling tank the laminar part is negligible⁽³⁰⁾.

The modelling of the turbulence is in fact a matter of estimating these turbulent stresses. One of the existing methods uses the eddy-viscosity-concept. The Reynolds stresses are dealt with in a similar manner as the viscous forces, by the introduction of an extra viscosity: the eddy viscosity ν_t . The model assumes that the turbulent stresses are a function of the gradients of the average velocities:

$$-u'u' = 2\nu_t \frac{\partial u}{\partial x} - \frac{2}{3}k \quad (C.11)$$

$$-u'v' = \nu_t \left(\frac{\partial u}{\partial y} + \frac{\partial v}{\partial x} \right) \quad (C.12)$$

$$-u'w' = \nu_t \left(\frac{\partial u}{\partial z} + \frac{\partial w}{\partial x} \right) \quad (C.13)$$

(30)

However, in the flow simulations, the laminar part is taken into account, because it is incorporated in the CFD package. Furthermore, it helps to prevent problems with convergence.

The k term in the equations of the normal stresses ($u'u'$, $v'v'$ and $w'w'$) ensures that the sum of the normal stresses equals $2k$ (Rodi, 1980). The variable k represents the kinetic energy in turbulent motion (turbulent kinetic energy) per unity of mass.

$$k = \frac{1}{2}(u'^2 + v'^2 + w'^2) \quad (\text{C.14})$$

Thus, modelling the turbulence means the determination of k and ν_t . However, the eddy viscosity ν_t is not a real property of the fluid like the molecular viscosity, since it depends on the turbulence. Many proposals to determine k and ν_t have resulted in a range of turbulence models. See (Rodi, 1980). Most models assume a relation between ν_t and a scale for the sizes of the large eddies, L , and the turbulent kinetic energy. E.g.:

$$\nu_t = C_\nu L \sqrt{k} \quad (\text{C.15})$$

in which C_ν is a model constant.

Simple turbulence models with a fixed length scale for the eddies, or a length scale derived from simple algebraic equations, are not appropriate for modelling the flow in constructions like storm water settling tanks. The reason is that, during filling and in case of time varying flow rates, the length scale varies in time and place. A model computing this length scale has to be used. The variable k is solved by means of the transport equation, which is given in the next section.

C.4.2 k - ϵ turbulence model

The k - ϵ turbulence model is commonly used for flow situations in which the length scales of the eddies are not easy to estimate. The length scale is determined by assuming a relation between ϵ , the dissipation of turbulent kinetic energy (from the largest eddies to the small eddies where energy is lost in molecular heat production), the turbulent kinetic energy and the length scale. Consequently, the length scale can be omitted from the equations:

$$\nu_t = C_{\mu D} \frac{k^2}{\epsilon} \quad (\text{C.16})$$

with $C_{\mu D}$ is a constant of the model.

In this way, the problem is shifted to solving the values of k and ϵ . Both k and ϵ are obtained from transport equations (Booij, 1992):

$$\frac{Dk}{Dt} = \nabla_i \left(\frac{\nu_t}{\sigma_k} \nabla_i k \right) + \nu_t \left((\nabla_i v_j)^2 + (\nabla_i v_j)(\nabla_j v_i) \right) + \frac{g}{\rho_w} \frac{\nu_t}{\sigma_c} \frac{\partial \rho}{\partial y} - \epsilon \quad (\text{C.17})$$

$$\frac{D\epsilon}{Dt} = \nabla_i \left(\frac{\nu_t}{\sigma_\epsilon} \nabla_i \epsilon \right) + C_{p\epsilon} k \left((\nabla_i v_j)^2 + (\nabla_i v_j)(\nabla_j v_i) \right) - C_{d\epsilon} \frac{\epsilon^2}{k} \quad (\text{C.18})$$

In these equations, the subscripts mean that summations have to be made with both the subscripts i and j varying from 1 to 3, representing the x -, y - and z -direction. As much as 5 constants are

used in the k - ϵ model ($C_{\mu D}$, C_{pe} , C_{de} , σ_k en σ_ϵ) to ensure that the model is valid for a range of flow conditions. These constants have been declared as follows (Rodi, 1980; and POLIS):

$$\begin{aligned} C_{\mu D} &= 0.09 \\ C_{pe} &= 1.44 \\ C_{de} &= 1.92 \\ \sigma_k &= 1.0 \\ \sigma_\epsilon &= 1.314 \\ \sigma_c &= 0.7 \end{aligned}$$

The change of kinetic energy in turbulent motion (turbulent kinetic energy) is in equilibrium with the diffusion terms, the production by friction, the dissipation and a damping term due to density differences. This damping term is positive (and thus increases the turbulent kinetic energy) when $\delta\rho/\delta y$ is positive (heavier fluid on top of lighter fluid. When the heavier fluid is below the lighter fluid, this term will be negative and dampen the turbulent kinetic energy. The value of the σ_c is reported to depend on the flow situation (POLIS).

The equations for k and ϵ are solved together with the continuity equation and the Reynolds equations for turbulent flow:

$$\begin{aligned} \frac{Du}{Dt} &= -\frac{1}{\rho} \frac{\partial p_x}{\partial x} + \frac{\partial}{\partial x} \left[(\nu_l + \nu_t) \frac{\partial u}{\partial x} - \frac{2}{3}k \right] + \\ &+ \frac{\partial}{\partial y} \left[(\nu_l + \nu_t) \frac{\partial u}{\partial y} \right] + \\ &+ \frac{\partial}{\partial z} \left[(\nu_l + \nu_t) \frac{\partial u}{\partial z} \right] \end{aligned} \quad (C.19)$$

$$\begin{aligned} \frac{Dv}{Dt} &= -\frac{1}{\rho} \frac{\partial p_y}{\partial y} + \frac{\partial}{\partial y} \left[(\nu_l + \nu_t) \frac{\partial v}{\partial y} - \frac{2}{3}k \right] + \\ &+ \frac{\partial}{\partial x} \left[(\nu_l + \nu_t) \frac{\partial v}{\partial x} \right] + \\ &+ \frac{\partial}{\partial z} \left[(\nu_l + \nu_t) \frac{\partial v}{\partial z} \right] + g \end{aligned} \quad (C.20)$$

$$\begin{aligned} \frac{Dw}{Dt} &= -\frac{1}{\rho} \frac{\partial p_z}{\partial z} + \frac{\partial}{\partial z} \left[(\nu_l + \nu_t) \frac{\partial w}{\partial z} - \frac{2}{3}k \right] + \\ &+ \frac{\partial}{\partial x} \left[(\nu_l + \nu_t) \frac{\partial w}{\partial x} \right] + \\ &+ \frac{\partial}{\partial y} \left[(\nu_l + \nu_t) \frac{\partial w}{\partial y} \right] \end{aligned} \quad (C.21)$$

C.4.3 Remarks on the k- ϵ turbulence model

The reasonably simple way of modelling the turbulence in the k- ϵ turbulence model, contains some deficiencies. The standard k- ϵ turbulence model employs a single time scale (k/ϵ) to characterize the various dynamic processes occurring in turbulent flows. This single time scale cannot describe all the fluctuating motions with different time scales that are present in turbulence flows (Hanjalic et al. 1980).

Furthermore, the k- ϵ model assumes isotropic turbulent values. It is, however, likely that the eddies are hindered by the presence of walls and the water surface. Consequently, near the water surface, the eddies in the horizontal plane are larger than those in the vertical plane. Thus the turbulence will not be isotropic

These deficiencies cause the k- ϵ model does to predict a turbulent flow situation imperfectly. Booij (1992) reports that the standard k- ϵ model underestimates the length of the re-circulation zone. Probably, the value of the eddy viscosity in the mixing layer (on top of the re-circulation zone) becomes too high. This results in an overestimation of the width of the mixing layer and of the entrainment of ambient fluid in the mixing layer (Booij, 1996). Consequently, the computed re-circulation zone becomes too short. The eddy viscosity will be smaller if the value of k is smaller or the value of ϵ larger. Some modified forms of the k- ϵ model take into account this aspect.

C.4.4 Modified forms of the k- ϵ turbulence model

Except for the standard form of the k- ϵ turbulence model, some modified forms are available within PHOENICS. To improve the outcome of the simulations, investigations were performed to determine whether the modified forms of the turbulence model result in better predictions.

Chen and Kim modifications of k- ϵ model

In order to ameliorate the working of the standard model, Chen and Kim (1987) proposed a modification which increases the value of ϵ when du/dy or dv/dx are large by introducing an additional time scale (k/Pk), where Pk is the volumetric production rate of k . In addition, several of the standard model coefficients have been adjusted so that the model maintains good agreement with experimental data on classical turbulent shear layers:

$$\sigma_k = 0.75; \sigma_\epsilon = 1.15; C_{pe} = 1.15; C_{de} = 1.9.$$

The extra time scale k/Pk is included in the transport equation for ϵ via the following additional source term per unit volume:

$$S_\epsilon = 0.25 \frac{(Pk)^2}{k} \quad (C.22)$$

RNG modified k- ϵ model

Another form of the k- ϵ model provided within PHOENICS is the Renormalization Group (RNG) k- ϵ model. In this turbulence model an additional source term decreases the value of ϵ for large

strains (du/dy or dv/dx large). The PHOENICS manual (POLIS) gives a description of this form of the $k-\epsilon$ model.

Two scale $k-\epsilon$ turbulence model

In order to obtain better computational results, the two scale split $k-\epsilon$ model splits the turbulent kinetic energy into two parts: a production part and a transfer part. For each part a differential equation is solved. Moreover, an extra variable for the dissipation of turbulent kinetic energy from the production to the transfer range (where the energy is dissipated) is solved. More information is given in the PHOENICS manual (in Chapter 4, the results of simulations with the standard and some adapted forms of the $k-\epsilon$ model have been compared to measurements).

C.4.5 Other turbulence models

The $k-\epsilon$ turbulence model is probably the best working, generally applicable, turbulence model. It is widely used, and its validity is proven in many different flow situations. The $k-\epsilon$ model is therefore preferred above other means of modelling the turbulence. As earlier explained, Direct Numerical Simulation (DNS) is not applicable. Large Eddy Simulation (LES), in which only the large turbulent eddies are computed directly and finer eddies are simulated by some kind of model, cannot yet be used with the chosen CFD package. A simpler model (than these and the $k-\epsilon$ turbulence model) assumes a constant relation between k and the representative length scales of the eddies. $k/L = \text{constant}$. Such a model is inappropriate for flow situations with varying representative length scales of the eddies such as in storm water settling tanks. Finally, the Reynolds stress model models the turbulence in a more accurate (and more complex) way than the $k-\epsilon$ model. However, the latter is preferred, because the Reynolds stress model has only recently been added to the PHOENICS package. This means that the reliability - in terms of program bugs for different kind of flow situations and in combination with other features of PHOENICS - is less than for the older $k-\epsilon$ model.

APPENDIX D: PHOENICS EQUATIONS

This appendix explains the way in which PHOENICS solves the equations for any variable φ in the 2-dimensional case. (CHAM, -) and (POLIS) provide more information.

$$\frac{\partial \rho \varphi}{\partial t} + \frac{\partial u \rho \varphi}{\partial x} + \frac{\partial v \rho \varphi}{\partial y} = \frac{\partial}{\partial x} \left[D \frac{\partial \rho \varphi}{\partial x} \right] + \frac{\partial}{\partial y} \left[D \frac{\partial \rho \varphi}{\partial y} \right] + S_\varphi \tag{D.1}$$

For the explanation, initially the sources, S_φ , and the diffusion terms, will be assumed to be zero. These terms do not influence the following derivations, and disregarding them facilitates the explanation.

$$\frac{\partial \rho \varphi}{\partial t} + \frac{\partial u \rho \varphi}{\partial x} + \frac{\partial v \rho \varphi}{\partial y} = 0 \tag{D.2}$$

Fully upwind discretisation gives the following equation for the situations in which the horizontal velocity, u , is positive from cells $i-1$ to cells i , and the vertical velocity, v , is positive from cells $j-1$ to cells j :

$$\frac{(\rho \varphi)_{i,j}^{n+1} - (\rho \varphi)_{i,j}^n}{\Delta t} + \frac{(u \rho \varphi)_{i,j}^{n+1} - (u \rho \varphi)_{i-1,j}^{n+1}}{\Delta x} + \frac{(v \rho \varphi)_{i,j}^{n+1} - (v \rho \varphi)_{i,j-1}^{n+1}}{\Delta y} = 0 \tag{D.3}$$

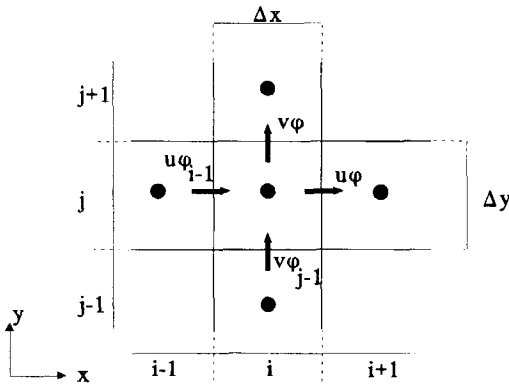


Figure D.1: In- and outflow of φ for 2-dimensional basic element.

The superscript n denotes the time step, the subscripts i and j denote the spacial steps in x - and y -direction respectively. Figure D.1 gives the convective fluxes for a 2-dimensional situation. The velocities are given at the cell boundaries, but all the other variables are located at the cell centres.

With the x-direction from the left to the right in the figure, the horizontal velocity, indicated as u_i , is the velocity at the right hand side of the cell and u_{i-1} is the velocity between the cell considered and the cell at the left.

When the horizontal and the vertical velocities are positive, the $i-1$ cell and the $j-1$ cell are the upwind cells for the horizontal and the vertical direction respectively. To simplify the notation in the coming equations, the superscripts have been omitted when the new time step $(n+1)$ is meant. The spacial indices, the subscripts, have been omitted when the index of the current cell is meant (i.e. i or j). The transport equation is:

$$\begin{aligned} \Delta x \Delta y \rho \varphi - (\Delta x \Delta y \rho \varphi)^n &= \Delta t (\Delta y u \rho \varphi)_{i-1} - \Delta t \Delta y u \rho \varphi + \\ &\Delta t (\Delta x v \rho \varphi)_{j-1} - \Delta t \Delta x v \rho \varphi \end{aligned} \quad (D.4)$$

The equilibrium of mass gives:

$$\begin{aligned} \Delta x \Delta y \rho - (\Delta x \Delta y \rho)^n &= \Delta t (\Delta y u \rho)_{i-1} - \Delta t \Delta y u \rho + \\ &\Delta t (\Delta x v \rho)_{j-1} - \Delta t \Delta x v \rho \end{aligned} \quad (D.5)$$

Multiplying the mass transport equation D.5 by φ (at $n+1$, i and j) and subtracting it from the particle transport equation D.4 results in the following equation:

$$(\Delta x \Delta y \rho)^n (\varphi - \varphi^n) = \Delta t (\Delta y u \rho)_{i-1} (\varphi_{i-1} - \varphi) + \Delta t (\Delta x v \rho)_{j-1} (\varphi_{j-1} - \varphi) \quad (D.6)$$

Rewriting and replacing some terms by coefficients results in:

$$A_t (\varphi - \varphi^n) = A_x (\varphi_{i-1} - \varphi) + A_y (\varphi_{j-1} - \varphi) \quad (D.7)$$

or

$$\varphi = \frac{\varphi^n A_t + \varphi_{i-1} A_x + \varphi_{j-1} A_y}{A_t + A_x + A_y} \quad (D.8)$$

$$\begin{aligned} A_t &= (\Delta x \Delta y \rho)^n / \Delta t = \text{time coefficient;} \\ A_x &= (\rho \Delta y u)_{i-1}; \\ &= \text{coefficient of inflow from the upwind cell in x-direction;} \\ A_y &= (\rho \Delta x v)_{j-1}; \\ &= \text{coefficient of inflow from the upwind cell in y-direction;} \end{aligned}$$

All inflowing fluxes are taken into account. It is possible that the fluxes are directed inwards from both sides. In general, thus also for the upwind direction from the other sides, the equation is:

$$\varphi = \frac{\varphi^n A_t + \varphi_{i-1} A_{x(i-1)} + \varphi_{i+1} A_{x(i)} + \varphi_{j-1} A_{y(i-1)} + \varphi_{j+1} A_{y(i)}}{A_t + A_{x(i-1)} + A_{x(i)} + A_{y(i-1)} + A_{y(i)}} \quad (D.9)$$

With

$$\begin{aligned} A_{x(i-1)} &= \max(0, (\rho \Delta y u)_{i-1}); \\ A_{x(i)} &= \max(0, -(\rho \Delta y u)_i); \\ A_{y(i-1)} &= \max(0, (\rho \Delta x v)_{j-1}); \\ A_{y(i)} &= \max(0, -(\rho \Delta x v)_j); \end{aligned}$$

Boundary conditions

Boundary conditions are given as sources.

$$A_t(\varphi - \varphi^n) = A_x(\varphi_{i-1} - \varphi) + A_y(\varphi_{j-1} - \varphi) + S_\varphi \quad (D.10)$$

The source S_φ is defined as $A_s(\varphi_s - \varphi)$, so the transport equation becomes:

$$\varphi = \frac{\varphi^n A_t + \varphi_{i-1} A_{x(i-1)} + \varphi_{i+1} A_{x(i)} + \varphi_{j-1} A_{y(i-1)} + \varphi_{j+1} A_{y(i)} + \varphi_s A_s}{A_t + A_{x(i-1)} + A_{x(i)} + A_{y(i-1)} + A_{y(i)} + A_s} \quad (D.11)$$

Diffusion terms

The diffusion terms of equation D.1 have been neglected thus far, but are present in the equations solved by PHOENICS. The diffusion in x-direction is discretised as follows:

$$\frac{\partial}{\partial x} \left(D \frac{\partial c}{\partial x} \right) = \frac{D + D_{i-1}}{2} \frac{c_{i-1} - c}{\Delta L_{i-1}} - \frac{D + D_{i+1}}{2} \frac{c - c_{i+1}}{\Delta L} \quad (D.12)$$

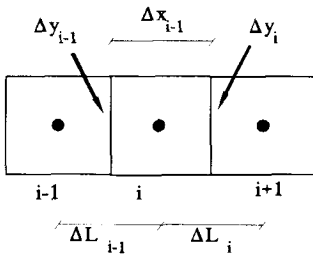


Figure D.2: 3 cells in x-direction

D is the diffusion term, e.g. $(\nu_1 + \nu_2)/\sigma$. The terms for the diffusion in the other directions are similar. Consider cell i , with neighbouring cells $i-1$ and $i+1$. See figure D.2. The distance between cell centres $i-1$ and i is ΔL_{i-1} , the distance between cell i and $i+1$ is ΔL_i . The cell face between cell $i-1$ and i is A_{i-1} , the cell face between cell i and $i+1$ is A_i . Δx is the width of cell i .

The diffusion terms have been written as coefficients in combinations with the upstream, downstream, or in-cell value of the variable concerned. These coefficients have been added to the coefficients for the convection. The coefficients A_x , and A_y of equation D.11 therefore are:

$$A_{x(i-1)} = \max(0, (\rho \Delta y u))_{i-1} + \frac{D + D_{i-1}}{2 \Delta L_{i-1}} \Delta y_{i-1} \quad (\text{D.13})$$

$$A_{x(i)} = \max(0, -(\rho \Delta y u))_i + \frac{D + D_{i+1}}{2 \Delta L_i} \Delta y_i \quad (\text{D.14})$$

$$A_{y(j-1)} = \max(0, (\rho \Delta x v))_{j-1} + \frac{D + D_{j-1}}{2 \Delta L_{j-1}} \Delta x_{j-1} \quad (\text{D.15})$$

$$A_{y(j)} = \max(0, -(\rho \Delta x v))_j + \frac{D + D_{j+1}}{2 \Delta L_j} \Delta x_j \quad (\text{D.16})$$

APPENDIX E: FLOW OF WATER OVER A WEIR

The HOL method is based on the fluid balance per column. All water is assumed to be in the lower part of the column. This means that water which enters a column somewhere above the water level is transported instantly to the water level. This makes the free surface computation relatively simple, because the location of the water-air interface is well defined. The draw-back of this method that it is not suited for flow situations with a steep water level gradient. Because water is instantly transported to the water level, and because no further tricks are part of the method, the potential energy of the water above the water level is simply lost.

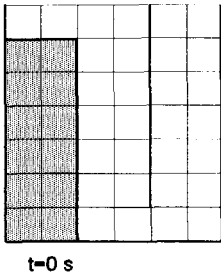


Figure E.1: Flow situation in test case at $t = 0$ sec.

To test this, the following case was set up with a very coarse grid: the flow over a weir with initially no water at the downstream side and upstream of the weir the water air interface at two cells above the weir crest, see figure E.1. No inflow or outflow is provided. The top of the model is open. A vertical baffle goes down from the top to the second cell near the bottom, so that below that baffle the opening is only one cell.

For several seconds the flow in this situation was simulated. The mass balance is of course right. The energy balance was expected not to be correct.

Simulations of this flow situation (a weir of 4 cells high (0.4 m)) appeared to be almost equal to the flow over a of 6 cells high. This proves that the potential energy is not accounted for.

It is expected that if the cells are less wide a higher water column can build up the column just downstream of the weir. This will be more realistic, since water in this high column will flow downward and a pressure difference will build up.

Smaller cells however request smaller time steps in the computations to prevent divergence, since for the water surface the Courant number should be strictly below one, i.e. the velocity at the water surface should be smaller than cell width divided by the time step.

After 0.6 sec the flow situations for a coarse grid (time step = 0.05 sec) and a fine grid (time step = 0.05 sec) are as in figures E.2 and E.3. The differences are clear. In the model with a fine grid the water is for a longer period in the first column downstream of the weir. The water level there will be higher, and because the water will indeed flow down and create a hydraulic pressure so that water leaves that column at a higher speed.

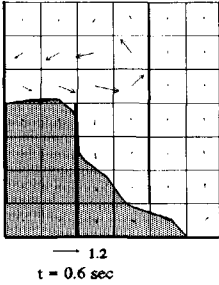


Figure E.2: Flow situation in test case at $t = 0.6$ sec.

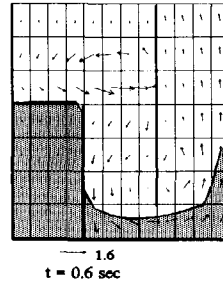


Figure E.3: Flow over a weir with a finer grid at $t = 0.6$ s.

This means that the simulation of the water flow over a weir with a lower downstream water level is only reliable if the width of the cells just downstream of the weir is small enough, like in figure E.4. The impulse and kinetic energy of the water entering a column is preserved, if the grid is fine enough. This is however not applicable for full scale tanks.

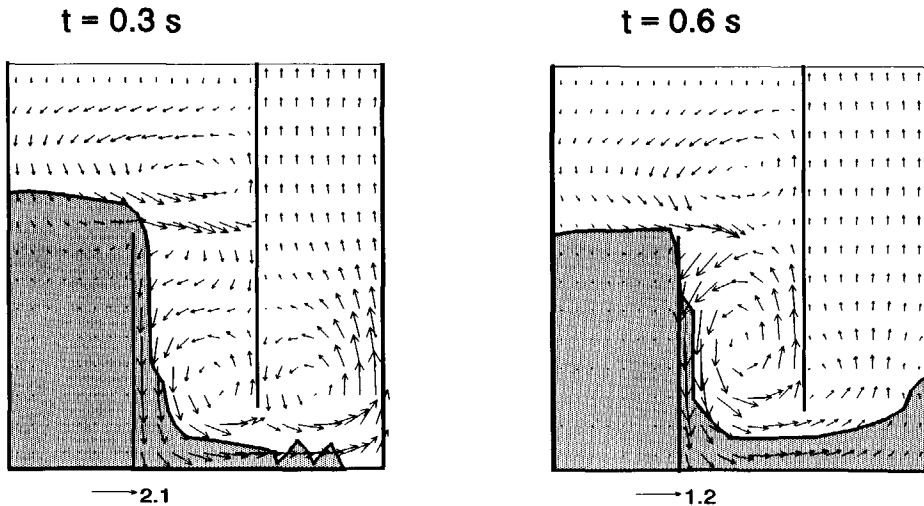


Figure E.4: Flow over a weir with a fine grid.

APENDIX F: ROUGHNESS PARAMETER E

PHOENICS applies a roughness parameter E in the wall boundary conditions. The roughness parameter E equals 9.0 for smooth walls. A wall is considered to be smooth if the wall Reynolds number, Rer, is below 3.7.

$$Rer = u_* \frac{k_N}{\nu_1} \tag{F.1}$$

k_N is the equivalent sand-grain roughness of Nikuradse. If Rer is greater than 100 the wall is considered to be rough. E then equals 29.7/Rer. For Rer values between 3.7 and 100, the wall roughness is in the transitory range. The value of E is determined with the empirical equation of Jayatellike (1969) giving a smooth transition between both ranges:

$$E = \frac{1}{\sqrt{a * (\frac{Rer}{29.7})^2 + \frac{1-a}{9.0^2}}} \tag{F.2}$$

$$a = 1+2x^3-3x^2 \tag{F.3}$$

$$x = 0.02248 \frac{100-Rer}{Rer^{0.564}} \tag{F.4}$$

Battjes (1990) applies a simpler equation for the transitory between smooth and rough.

$$u_* = \frac{u\kappa}{\ln \left[\frac{y}{y_0} \right]}, \text{ with } y_0 = 0.11 \frac{\nu_1}{u_*} + \frac{k_N}{30} \tag{F.5}$$

y denotes the distance to the bottom. The use of either the equation of Jayatellike, or Battjes, has only a small effect on the flow in the tank.

Figure F.1 presents the shear velocity u_* and the horizontal velocity at 0.025 m from the bottom as a function of the equivalent roughness, k_N , according to both sets of equations. The solid lines are the shear velocities, the dashed lines are the horizontal velocities. The heavy lines (solid and dashed) are according to Jayatellike, the normal lines (solid and dashed) are according to the Battjes. The values of the shear stress have been divided by the maximum shear stress in the graph region (Battjes). The values of the horizontal velocity have been divided by the maximum horizontal velocity in the graph region (Jayatellike).

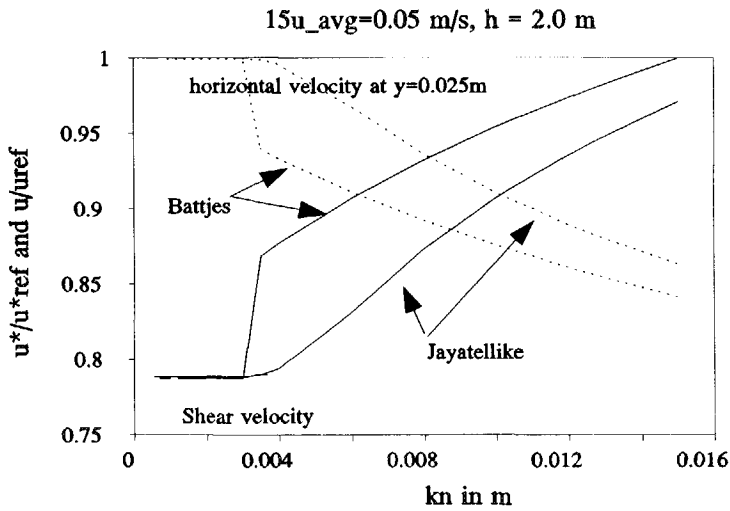


Figure F.1: The shear velocity u_* and the horizontal velocity near the bottom as two functions of the k_N .

The equations of Jayatellike, which are provided within PHOENICS, give a smoother transition between smooth and rough walls. The differences in the example in the figure are smaller than 10%. For the flow in storm water settling tanks, the flow is either smooth or in the transitory range. Jayatellikes equations have been used within PHOENICS.

APPENDIX G: PHOENICS INPUT FILE Q1.

The model is defined in an ASCII file called Q1, which contains the lines to set up a flow model. This file is read by PHOENICS in order to run the simulation. The Q1-file can be constructed directly by the user, or by means of a menu system. In order to simulate the settling of particles the lines given below must be present in the Q1-file. These lines are not in the PHOENICS manual or provided via the menu system and must be added to the Q1-file. The flow model set up should meet the following requirements:

- * It should provide: P1, U1, V1, KE, EP, ENUT, DEN1.
- * The flow can be transient or steady.
- * positive y-direction as upward
- * 2-dimensional or 3-dimensional

Lines needed in Q1 in for the computation of settling particles

- LSG1=T Switch on computation of STn (STn is settling partilce of type n, e.g. ST1, ST2, etc.).
- ISG10=5 Number of types of particles (settling velocities).
- LSG2=T Switch on the diffusision terms for the particles. When LSG2=F (by default) and RSG24=0.0 (by default), then diffusion of STn is neglected.
- RSG24=.... Constant by which the diffusion terms are multiplied if LSG2=T. Is reciproke of Schmidt number.
- LSG3=F When LSG3=F (by default), then τ_d , τ_e , and c_{ero} in the bottom boundary condition are 0.15, 0.3 and $1 \cdot 10^{-6}$ resp. When LSG3=T they are given by RSG21, RSG22, and RSG23, resp.
- RSG21=.... τ_d if LSG3=T
- RSG22=.... τ_e if LSG3=T
- RSG23=.... c_{ero} if LSG3=T
- LSG5=F $\tau_d=f(u_{,1})$, else $\tau_d=f(u_{,2})$
- RSG6=... RSG6 needs to be equal to the inflow velocity, for the inflow of particles.
- RSG7=... REFCIN is reference value for the concentration at the inflow.
- LSG7=F If LSG7=T, then REFCIN=RSG7, else REFCIN = 1.0.
- ISG21=7 Indicate in which x-collumn is the internal weir.
- ISG5=10 Interval of number of sweeps for output to file.

NAME(Cn)=STn;SOLVE(STn)

Create name for particles of number n, with n is an integer between 1 and 10, e.g. C1 and ST1, or C2 and ST2, etc..

TERMS(STn,Y,N,N,N,P,P)

This orders PHOENICS only to create space in the PHOENICS-array, but not to compute the time-dependent, convective, and the diffusion terms.

NAME(C10+n)=STnO;STORE(STnO)	Create name for old time step values of particles with number n, e.g. C11 and ST1O, or C12 and ST2O, etc..
NAME(C20+n)=SEDn;STORE(SEDn)	Create name for sediment of particles with number n, e.g., C21 and SED1, or C22 and SED2, etc..
FIINIT(STn)=.0	Optionally, initially no particles
RSG10+n=0.0000148	Diameter of particles STn, e.g., RSG11 for ST1, etc. The settling velocity is computed with the Stokes equations from this diameter, using $\rho_s=2650 \text{ kg/m}^3$ and $\nu_1=1.31\text{e-}6 \text{ m}^2/\text{s}$. In fact, instead of a diameter a settling velocity should be given in the future. The coding has not be changed yet, because then all the old q1-files should be changed too.
SOLVE(BRON)	Create name for inflow source.
TERMS(BRON,Y,N,N,N,P,P)	Create storage location.
STORE(VFOL)	The variable VFOL should always be available. For rigid lid simulations its value will be 1.0. In free surface simulations it is used.
PATCH(IN,WEST,1,1,1,3,1,NZ,1,LSTEP)	
....	
COVAL(IN,BRON,FIXVAL,GRND2)	The inflow patch points to subroutine GRND2 (see APXZ) for the inflow of particles.
ISG1=.... (ixf)	Location of outflow patch, in first and last locations in x- and y direction.
ISG2=.... (ixl)	
ISG3=.... (iyf)	
ISG4=.... (iyl)	

APPENDIX H: FORTRAN SUBROUTINES FOR SETTLING PARTICLES

The FORTRAN subroutines in this paragraph have been used to compute the transport of settling particles. They have been written in the file GROUND.F, which is provided by PHOENICS to enable the user to add coding to the program. See (CHAM, 1991) and (POLIS). PHOENICS takes care that the subroutines are carried out at defined moments in the simulations. For the settling particles the subroutines have been put in that places that they are carried out at the start of each time step and at the end of each SWEEP (iteration).

No other than these equations are solved for the settling particles. At the beginning of each time-step the old values (i.e. of the former time step) for the particles and the sediment are stored. Then at the end of each SWEEP the transport equation for each particle is solved in each cell. When required, removal ratios are printed to a file called 'RENDEM.ENT'.

Explanation of variables, terms and functions used:

C1=	integer indicator of variable ST1. Its value is 16. The variables ST2 up to STn have indicator numbers equal to 17 up to 15+n.
LOF(...)	Determines location of variable in PHOENICS array.
STn	Settling particles of type n.
STOLD	Old time value of settling particle. The indicator number of STOLDn equals that of STn + 10.
SEDI	Sediment of settling particle. The indicator number of SEDI equals that of STn + 20. The present time step value is in the bottom row (iy=1), while the old time step value is stored in the row for iy=3.
DT	Time step
U1	Horizontal velocity
V1	Vertical velocity
BRON	Source term to bring into account the inflow of settling particles.
DEN1	Density of fluid: i.e. water, air, or mixture, depending on VFOL
VFOL	Volume fraction of liquid for free surface (HOL) computations. Its value equals 1.0 for rigid lid computations.
VISL	Viscosity of fluid (see also DEN1).
ENUT	Eddy viscosity
KE	Kinetic energy of turbulent motion

C FILE NAME GROUND.F-----20-11-1995

...

C--- GROUP 1. Run title and other preliminaries

C

```

1 GO TO (1001,1002),ISC
1001 CONTINUE
COKA=0.435
OPEN(5,FILE='RENDEM.ENT')
```

```

CALL MAKE(YG2D)
CALL MAKE(DXU2D)
CALL MAKE(DYV2D)
CALL MAKE(DXG2D)
CALL MAKE(DYG2D)
RETURN
...
C
C--- GROUP 13. Boundary conditions and special sources
C          Index for Coefficient - CO
C          Index for Value      - VAL
13 CONTINUE
  GO TO (130,131,132,133,134,135,136,137,138,139,1310,
        11311,1312,1313,1314,1315,1316,1317,1318,1319,1320,1321),ISC
130 CONTINUE
...
C----- SECTION 14 ----- value = GRND2
c Inflow of settling particles via variable BRON
c The inflow equals RSG6*dy*STin.
c RSG6 should be given in Q1 equal to the inflow velocity.
  IF (NPATCH.NE.'IN') RETURN
  IF (INDVAR.EQ.LBNAME('BRON')) THEN
    REFCIN=1.
    IF(LSG7) REFCIN=RSG7
    LOVAL=L0F(VAL)
    LODY=L0F(DYG2D)
    DO IY = IYF,IYL
    DO IX = IXF,IXL
      IADD = IY +(IX-1)*NY
      F(LOVAL+IADD)=F(LODY+IADD)*RSG6*REFCIN
    END DO
  ENDDO
  END IF
  RETURN
...
C
C--- GROUP 19. Special calls to GROUND from EARTH
C
19 GO TO (191,192,193,194,195,196,197,198,199,1910,1911),ISC
191 CONTINUE
C * ----- SECTION 1 ---- Start of time step.
c Store 'old-time' values for SEDn (sediment) and STn: STOLDn
c lsg1 must be true for STn computation.
  IF (.NOT.LSG1) RETURN
C lsg10 is number of STn (maximum = 5, can easily be expanded to 10)
  IF (ISG10.EQ.0) ISG10=1
  DO ITEL=1,ISG10
    LOST=L0F(C1+ITEL-1)
    LOSTOLD=L0F(C1+ITEL+9)
    LOSEDI=L0F(C1+ITEL+19)
    DO IX = 1,NX
      F(LOSEDI+NY*(IX-1)+3)=F(LOSEDI+NY*(IX-1)+1)
    IF (STEADY) F(LOSEDI+NY*(IX-1)+3)=0.
    DO IY = 1,NY
      IITEL=IY+NY*(IX-1)

```



```

      F(LOSTOLD + IITEL) = F(LOST + IITEL)
    ENDDO
  ENDDO
ENDDO
RETURN
...
197 CONTINUE
C * ----- SECTION 7 ---- FINISH OF SWEEP.
C Distribution of particles STn
  IF (.NOT.LSG1) RETURN
C In each SWEEP, iimax iterations of STn
  IIMAX = 3
  DT2 = DT
  IF (STEADY) THEN
    DT = 1.E + 10
    DT2 = 1.
  ENDF
C Taud, taue, and cero are constants for bottom boundary condition.
  TAUD = 0.15
  TAUE = 0.3
  CERO = 1E-6
C If lsg3 = t (default = f) then taud, taue and cero get the values rsg21, rsg22 and rsg23 resp.
  IF (LSG3) THEN
    IF (RSG21.GT.0.) TAUD = RSG21
    IF (RSG22.GT.0.) TAUE = RSG22
    IF (RSG23.GT.0.) CERO = RSG23
  ENDF
C All diffusion terms are multiplied by con1. (E.G. 1/Prandtl).
  CON1 = 1.
C If lsg2 = f then con1 = rsg24. By default lsg2 = f and rsg24 = 0.0 => no diffusion.
  IF (.NOT.LSG2) CON1 = RSG24
  LOU1 = LOF(U1)
  LOV1 = LOF(V1)
  LOBRON = LOF(LBNAME('BRON'))
  LODEN1 = LOF(DEN1)
  LODX = LOF(DXU2D)
  LODY = LOF(DYV2D)
C DXU2D = cell length      DXG2D = distance between 2 cell centres
C XG2D = distance from zero plane to cell centre
C ANORTH = free north face area after reduction of blockages
  LODXX = LOF(DXG2D)
  LODYY = LOF(DYG2D)
  LOY = LOF(YG2D)
  LOVFOL = LOF(LBNAME('VFOL'))
  LOVISL = LOF(VISL)
  LOENUT = LOF(LBNAME('ENUT'))
  LOKE = LOF(KE)
  LOAN = LOF(ANORTH)
  LOAE = LOF(AEAST)
C Location of outflow boundary:
  IUITXF = ISG1
  IUITXL = ISG2
  IUIYF = ISG3
  IUIYL = ISG4
C For the outflow of particles the average horizontal velocity at the outflow

```



```

+       DIFE=((F(LOVISL+II)+F(LOENUT+II))+(F(LOVISL+II+NY)
+         +F(LOENUT+II+NY)))/2*F(LOAE+II)/F(LODXX+II+NY)
SDIFE=DIFE*F(LOST+II+NY)*F(LOVFOL+II)
DIFE=DIFE*F(LOVFOL+II+NY)
ELSE
SFLHOR1=MAX(0.,F(LOU1+II-NY))*F(LOST+II-NY)*F(LOAE+II-NY)
FLHOR3=MIN(0.,F(LOU1+II-NY))*F(LOAE+II-NY)
DIFW=((F(LOVISL+II)+F(LOENUT+II))+(F(LOVISL+II-NY)
+       +F(LOENUT+II-NY)))/2*F(LOAE+II-NY)/F(LODXX+II)
SDIFW=DIFW*F(LOST+II-NY)*F(LOVFOL+II)
DIFW=DIFW*F(LOVFOL+II-NY)
IF (IX.LT.NX) THEN
SFLHOR4=MIN(0.,F(LOU1+II))*F(LOST+II+NY)*F(LOAE+II)
FLHOR2=MAX(0.,F(LOU1+II))*F(LOAE+II)
DIFE=((F(LOVISL+II)+F(LOENUT+II))+(F(LOVISL+II+NY)
+       +F(LOENUT+II+NY)))/2*F(LOAE+II)/F(LODXX+II+NY)
SDIFE=DIFE*F(LOST+II+NY)*F(LOVFOL+II)
DIFE=DIFE*F(LOVFOL+II+NY)
ELSE
SFLHOR4=0.
FLHOR2=0.
SDIFE=0.
DIFE=0.
ENDIF
ENDIF

```

C Terms for vertical direction

```

VSLIP=VSWATER
IF (F(LOVFOL+II).LE.0) VSLIP=VSAIR
IF (IY.EQ.1) THEN

```

C If lsg5=f (by default) the taub=f(uster1)

```

IF (.NOT.LSG5) THEN
EMAX=F(LOSEDI+II+2)/DT2*F(LOAN+II)
EW=9.
USTER=ABS(F(LOU1+II))/10.+TINY
YBOT=F(LOY+1+(IX-1)*NY)-.5*F(LODY+1+(IX-1)*NY)
YLENG=F(LOY+IX*NY)+.5*F(LODY+IX*NY)-YBOT
DO III=1,4
CKSPLUS=USTER*WALLA/F(LOVISL+II)
IF(CKSPLUS.GT.3.7) THEN
EW=29.7/CKSPLUS
IF (CKSPLUS.LT.100) THEN
CONX=0.02248*(100-CKSPLUS)*(CKSPLUS**(-0.564))
ALF=1.0+CONX*CONX*(2.0*CONX-3.0)
EW=EW/SQRT(ALF+(1.0-ALF)*(EW/9.0)**2)
ENDIF
ENDIF
USTER=COKA*ABS(F(LOU1+II))/
+       (LOG(1.001+(F(LOY+II)-YBOT)*USTER/F(LOVISL+II)*EW))
ENDDO

```

C If lsg5=t then taub=f(uster2)=f(ke)

```

ELSE
USTER=(F(LOKE+II)*.3)**.5
ENDIF
TAUB=USTER*USTER*F(LODEN1+II)
FLVER3=0

```

```

IF (TAUB.GT.TAUE) THEN
  EROSIE=CERO*(TAUB/TAUE-1.)*F(LODX+II)
ELSE
  EROSIE=0
  IF (TAUB.LT.TAUD) THEN
    FLVER3=-VSLIP*F(LOAN+II)*(1.-TAUB/TAUD)
  ENDIF
ENDIF
C SFLVER1=erosion voor iy=1
C No more erosion than sediment + deposition in time step
SFLVER1=MIN(EMAX,EROSIE)
F(LOSEDI+II)=F(LOSEDI+II+2)-(F(LOST+II)*FLVER3+
+ SFLVER1)*DT2/F(LODX+II)
VSLIP=VSWATER
IF (F(LOVFOL+II+1).LE.0) VSLIP=VSAIR
SFLVER4=MIN(0.,F(LOV1+II)-VSLIP)
+ *F(LOST+II+1)*F(LOAN+II)/(MAX(.1,F(LOVFOL+II+1)))
FLVER2=MAX(0.,F(LOV1+II)-VSLIP)*F(LOAN+II)
SDIFS=0.
DIFS=0.
DIFN=((F(LOVISL+II)+F(LOENUT+II))+
+ (F(LOVISL+II+1)+F(LOENUT+II+1)))/2*F(LOAN+II)/F(LODY+II+1)
SDIFN=DIFN*F(LOST+II+1)*F(LOVFOL+II)
DIFN=DIFN*F(LOVFOL+II+1)
ELSE
SFLVER1=MAX(0.,F(LOV1+II-1)-VSLIP)*F(LOST+II-1)*F(LOAN+II-1)
FLVER3=MIN(0.,F(LOV1+II-1)-VSLIP)*F(LOAN+II-1)
+ /(MAX(.1,F(LOVFOL+II)))
DIFS=((F(LOVISL+II)+F(LOENUT+II))+
+ (F(LOVISL+II-1)+F(LOENUT+II-1)))/2*F(LOAN+II-1)/F(LODY+II)
SDIFS=DIFS*F(LOST+II-1)*F(LOVFOL+II)
DIFS=DIFS*F(LOVFOL+II-1)
IF (IY.LT.NY) THEN
  VSLIP=VSWATER
  IF (F(LOVFOL+II+1).LE.0) VSLIP=VSAIR
  SFLVER4=MIN(0.,F(LOV1+II)-VSLIP)
  + *F(LOST+II+1)*F(LOAN+II)/(MAX(.1,F(LOVFOL+II+1)))
  FLVER2=MAX(0.,F(LOV1+II)-VSLIP)*F(LOAN+II)
  DIFN=((F(LOVISL+II)+F(LOENUT+II))+
  + (F(LOVISL+II+1)+F(LOENUT+II+1)))/2*
  + F(LOAN+II)/F(LODY+II+1)
  SDIFN=DIFN*F(LOST+II+1)*F(LOVFOL+II)
  DIFN=DIFN*F(LOVFOL+II+1)
ELSE
  SFLVER4=0.
  FLVER2=0.
  SDIFN=0.
  DIFN=0.
ENDIF
ENDIF
C Time-dependent and inflow terms
STOLD=(F(LOSTOLD+II)*F(LODX+II)*F(LODY+II)/DT
+ F(LOBRON+II))
C Outflow term
UITSTROOM=0

```

```

        IF ((IX.GE.IUITXF).AND.(IX.LE.IUITXL)) THEN
            IF ((IY.GE.IUITYF).AND.(IY.LE.IUITYL)) THEN
C With nohol computations the uit-patch can be more than one
C Cell high too. The outflowing flux will be given with P1,FXP,0
C The outflowing velocity will be equal to (u_in*dy+(v_in-vout)*dx)/dy
C This will be called u_gem for the cell
            IF (.NOT.HOL) THEN
                DX=F(L0DX+II)
                DY=F(L0DY+II)
                VBOT=F(L0V1+II-1)
                VTOP=F(L0V1+II)
                IF(II.EQ.1) VBOT=0
                IF(II.EQ.NY) VTOP=0
                U_GEM=(F(L0U1+II-NY)*DY+
+                 (-VTOP+VBOT)*DX)/DY
            ENDIF
            UITSTROOM=U_GEM*F(L0AE+II)
        ENDIF
        ENDDO
C Transport equation of stn
        F(L0ST+II)=((SFLVER1-SFLVER4+SFLHOR1-SFLHOR4+STOLD
+                 +CON1*(SDIFE+SDIFW+SDIFN+SDIFS))/
+                 (FLVER2-FLVER3+FLHOR2-FLHOR3+TINY+UITSTROOM
+                 +F(L0DX+II)*F(L0DY+II)/DT
+                 +CON1*(DIFE+DIFW+DIFN+DIFS)))
        SOM=SOM+F(L0ST+II)
    ENDDO
    ENDDO
C Back to next iteration of IIMAX
    ENDDO
cccccccccccccccccccccccccccccccccccccccccccccccccccccccccccc
c print output naar file
cccccccccccccccccccccccccccccccccccccccccccccccccccccccccccc
        IF (ISWEEP.EQ.LSWEEP.OR.ENUFSW) THEN
            IF (ISTEP.EQ.LSTEP.OR.
+             ((MOD(ISTEP,NTPRIN).EQ.0))) THEN
C Determine inflow of STn: u*st*dy at ix=isg21
C Isg21 indicates the x-location of the internal weir and should be given in Q1.
            STIN=0.
            DO IY=1,NY
                IADD=(ISG21-1)*NY+IY
                STIN=STIN+F(L0ST+IADD)*F(L0DY+IADD)*F(L0U1+IADD)
            ENDDO
            STUIT=0.
            DO IY=IUITYF,IUITYL
                IADD=(IUITXF-1)*NY+IY
                IF (.NOT.HOL)
                    VBOT=F(L0V1+IADD-1)
                    VTOP=F(L0V1+IADD)
                    IF(IY.EQ.1) VBOT=0
                    IF(IY.EQ.NY) VTOP=0
                    U_GEM=(F(L0U1+IADD-NY)*F(L0DY+IADD)+
+                     (-VTOP+VBOT)*F(L0DX+IADD))/F(L0DY+IADD)
                ENDIF
                STUIT=STUIT+U_GEM*F(L0DY+IADD)*F(L0ST+IADD)
            ENDIF
        ENDIF
    ENDDO

```


APPENDIX I: DISCRETISATION

In order to solve the differential equations in a computer program, the equations have been approximated by replacing the time and spatial derivatives with finite difference approximations. PHOENICS applies by default an implicit hybrid upwind scheme. This scheme is based on the fully upwind scheme, which will be discussed first in this Appendix.

The fully upwind scheme is very robust and always results in positive concentrations, but, it implies an important numerical diffusion (or numerical viscosity) if the grid chosen is too coarse.

The numerical diffusion is worked out for the 1-dimensional transport equation of a concentration c . The differential equation is given by:

$$\frac{\partial c}{\partial t} + u \frac{\partial c}{\partial x} - \frac{\partial}{\partial x} D \frac{\partial c}{\partial x} = 0 \quad (\text{G.1})$$

In which D is diffusion coefficient.

The time period to be simulated is divided into time steps. All variables have a value at the first time step. The next time step is the new time step. In the implicit discretisation, the new time step values of the variables are used. Fully upwind implies that for the convective terms, only inflowing fluxes are taken into account. The discretisation is worked out here for a positive velocity, i.e. in positive x -direction. The time dependent and convection parts (first two terms) are approximated by

$$\frac{c^{n+1} - c^n}{\Delta t} + u \frac{c_i^{n+1} - c_{i-1}^{n+1}}{\Delta x} \quad (\text{G.2})$$

The superscripts n and $n+1$ indicate the time step. The subscripts i , $i-1$ and $i+1$ indicate the cell numbers in x -direction. Where the subscript has been omitted, i is meant.

The equation above is an approximation of the differential equation. Using a Taylor series approximation gives:

$$c^n = c^{n+1} - \Delta t c_t^{n+1} + \frac{\Delta t^2}{2} c_{tt}^{n+1} + \text{HOT}(3) \quad c_t = \frac{\partial c}{\partial t} \quad (\text{G.3})$$

$$c_{i-1}^{n+1} = c_i^{n+1} - \Delta x c_x^{n+1} + \frac{\Delta x^2}{2} c_{xx}^{n+1} + \text{HOT}(3) \quad c_x = \frac{\partial c}{\partial x} \quad (\text{G.4})$$

The Higher Order Terms (HOT) are assumed to be negligible. Filling in these equations results in:

$$\frac{c^{n+1} - (c^{n+1} - \Delta t c_t^{n+1} + \frac{\Delta t^2}{2} c_{tt}^{n+1})}{\Delta t} + u c_x^{n+1} - u \frac{\Delta x}{2} c_{xx}^{n+1} \quad (\text{G.5})$$

Hence, because of the discretisation, instead of the two first terms in the transport equation ($\partial c / \partial t + u \partial c / \partial x$) appear the terms:

$$c_t^{n+1} + u c_x^{n+1} - \frac{\Delta t c_{tt}^{n+1} + u \Delta x c_{xx}^{n+1}}{2} \quad (\text{G.6})$$

The last term is the error, which can be regarded as a kind of diffusion. Assuming $c_{tt} = u^2 c_{xx}$, the coefficient ν_N for the numerical diffusion is

$$\nu_{ND} = \frac{u}{2} (u \Delta t + \Delta x) \quad (\text{G.7})$$

which is always positive (for positive velocity).

The numerical diffusion should be sufficiently smaller than the real diffusion, which consists of a laminar and a turbulent part: $(\nu_l / \sigma_l + \nu_t / \sigma_t) c_{xx}$, with σ denoting the Prandtl or Schmidt number. This means that ν_N should be smaller than $\nu_l / \sigma_l + \nu_t / \sigma_t$. If this requirement is not met, the error can become large, unless the flux due to the numerical diffusion is unimportant in comparison to the other fluxes:

$$\nu_N c_{xx} \ll u c_x \quad \text{OR} \quad \nu_N c_{xx} \ll c_t$$

In this case, the transport due to turbulence will also be unimportant (Chapter 3 gives the numerical diffusion in the simulations of the flow in a storm water settling tank).

Diffusion

The second derivative of the concentration to space can be derived in a similar way as the convective terms from the Taylor series. This results in:

$$c_{i+1} - 2c_i + c_{i-1} = \Delta x^2 c_{xx} + \frac{\Delta x^4}{12} c_{xxxx} \quad (\text{G.8})$$

Neglecting the c_{xxxx} and higher terms gives:

$$\frac{\partial^2 c}{\partial x^2} = \frac{c_{i-1} - 2c_i + c_{i+1}}{\Delta x^2} \quad (\text{G.9})$$

Consequently, the following convection diffusion equation must be solved.

$$\frac{c^{n+1}-c^n}{\Delta t} + u \frac{c_i^{n+1}-c_{i-1}^{n+1}}{\Delta x} - \frac{D_{i-1}+D_i}{2} \frac{c_{i-1}^{n+1}-c_i^{n+1}}{\Delta x} - \frac{D_i+D_{i+1}}{2} \frac{c_i^{n+1}-c_{i+1}^{n+1}}{\Delta x} = 0 \quad (\text{G.10})$$

The error in the discretisation of the diffusion term (i.e. neglecting the c_{xxxx} terms) is much smaller than that in the time dependent and convective terms (Chapter 3 compares the numerical diffusion to the turbulent diffusion).

The resulting concentrations computed with the described equations should always be positive. Furthermore, these equations should not result in concentrations higher than the values in the surrounding cells. To demonstrate that c is always positive, but not larger than the concentration in the surrounding cells, D is assumed to be constant. This results in:

$$\frac{c^{n+1}-c^n}{\Delta t} + u \frac{c_i^n - c_{i-1}^n}{\Delta x} - D \frac{c_{i-1}^n - 2c_i^n + c_{i+1}^n}{\Delta x^2} = 0 \quad (\text{G.11})$$

which can be rewritten as:

$$c_i^{n+1} = \frac{c_i^n + (\sigma+q)c_{i-1}^{n+1} + qc_{i+1}^{n+1}}{1+\sigma+2q}, \quad \text{with } \sigma = u \frac{\Delta t}{\Delta x} \quad \text{and } q = D \frac{\Delta t}{\Delta x^2} \quad (\text{G.12})$$

Because both σ and q are positive, this means that c_i^{n+1} is always positive for positive values of c_i^n , c_{i+1}^{n+1} and c_{i-1}^{n+1} . Furthermore, for c_i^n , c_{i-1}^{n+1} and c_{i+1}^{n+1} smaller than or equal to 1.0 also c_i^{n+1} will not be larger than 1.0.

In the computations D will vary, but it will be positive. Consequently, c_i^{n+1} will still be between 0.0 and 1.0. The discretisation is quick and robust, but results in an important numerical diffusion.

The equations presented above are valid for positive velocities (in x -direction). When the flow direction is opposite, the convective term depends on c_i^{n+1} and c_{i+1}^{n+1} . It is possible that water enters from both the left and the right side (or up and down).

Other discretisation schemes than the implicit fully upwind discretisation scheme are available within PHOENICS and can be selected. The more accurate the approximation is, the more complex will be the equations, and therefore, the longer will be the computation time. Also, the possibility of divergence or impossible values (such as negative concentrations) are important.

Hybrid upwind scheme

PHOENICS by default applies a hybrid upwind scheme. When the diffusion is expected to be small compared to the convective term, the diffusion term is neglected, otherwise the diffusion term is taken into account in combination with a correction for the numerical diffusion. To explain how this is effectuated, the following 1-dimensional steady state convection diffusion equation is observed. To prevent the following from becoming unnecessarily complicated the diffusion coefficient D and the horizontal velocity u have been assumed to be constant.

Fully upwind discretisation gives for a horizontal velocity in the x -direction:

PHOENICS solves the following equation to solve the differential equation.

$$u \frac{\partial c}{\partial x} - D \frac{\partial^2 c}{\partial x^2} = 0 \quad (\text{G.13})$$

$$u \frac{c_i^{n+1} - c_{i-1}^{n+1}}{\Delta x} - D \frac{c_{i-1}^{n+1} - 2c_i^{n+1} + c_{i+1}^{n+1}}{\Delta x^2} = 0 \quad (\text{G.14})$$

$$c = \frac{a_{i+1} c_{i+1} + a_{i-1} c_{i-1}}{a_{i+1} - a_{i-1}} \quad (\text{G.15})$$

With $a_{i-1} = \text{Max}(0, D/\Delta x - \alpha |u|) + \text{max}(0, u)$

and $a_{i+1} = \text{Max}(0, D/\Delta x - \alpha |u|) + \text{max}(0, -u)$

For a positive horizontal velocity, this results in:

$$u(c - c_{i-1}) + \text{max}\left(0, \frac{D}{\Delta x} - \alpha u\right)(c_{i-1} - 2c + c_{i+1}) = 0 \quad (\text{G.16})$$

By default α equals 0.5 which means that the diffusion term is omitted when the cell Péclet number ($u\Delta x/D$) is above 2.0. In that case the equation reduces to

$$u \frac{c_i^{n+1} - c_{i-1}^{n+1}}{\Delta x} = 0 \quad (\text{G.17})$$

When the cell Péclet number is below 2.0, the diffusion term is taken into account, together with the term αu :

$$u \frac{c_i^{n+1} - c_{i-1}^{n+1}}{\Delta x} - D \frac{c_{i-1}^{n+1} - 2c_i^{n+1} + c_{i+1}^{n+1}}{\Delta x^2} + \frac{u\Delta x}{2} \frac{c_{i-1}^{n+1} - 2c_i^{n+1} + c_{i+1}^{n+1}}{\Delta x^2} = 0 \quad (\text{G.18})$$

The last term on the left hand side compensates for the numerical diffusion. In fact equation G.18 can also be considered as central differencing.

This interpolation scheme which makes the fact whether the diffusion term is taken into account dependent on the cell Péclet number is called the hybrid upwind scheme.

Curriculum Vitae

Jeroen Kluck werd op 7 mei in Maastricht geboren. Na het gymnasium-6 in Eindhoven (1985) heeft hij eerst een half jaar voor verstandelijk gehandicapten in Frankrijk gezorgd, en daarna een cursus Engels gevolgd in Engeland. In 1986 begon hij met de studie Civiele Techniek aan de Technische Universiteit van Delft. In oktober 1992 studeerde hij bij prof. ir J.B.M. Wiggers (Vakgroep Gezondheidstechniek en Waterbeheersing) af op een project over regenwaterafvoer in een stad in Yemen. Op basis van een stage in Indonesie en extra vakken haalde hij een aanvullend examen waterbeheersing.

Vanaf februari 1992 tot juni 1993 heeft hij in het kader van zijn vervangende dienstplicht bij de sectie Gezondheidstechniek onderzoek verricht naar de bestaande ontwerpmethoden van bergbezinkbassins. In november 1993 kwam hij als toegevoegd onderzoeker daar in dienst om te promoveren op dat onderwerp. Op 6 mei 1997 verdedigt hij zijn proefschrift. Sinds oktober 1996 is hij in dienst bij het adviesbureau TauwMabeg civiel en bouw.